LANDSLIDE HAZARD MAPPING
PART 1: ESTIMATING PIEZOMETRIC LEVELS

By

Tien H. Wu
Carolyn J. Merry
Christopher P. Benosky
Mohamed Abdel-Latif

June 1993

FINAL REPORT

LANDSLIDE HAZARD MAPPING

1. ESTIMATING PIEZOMETRIC LEVELS

TIEN H. WU, CAROLYN J. MERRY,

MOHAMED ABDEL-LATIF, CHRISTOPHER P. BENOSKY

JANUARY, 1993

revised, JUNE, 1993

CIVIL ENGINEERING DEPARTMENT

THE OHIO STATE UNIVERSITY

COLUMBUS, OHIO

ACKNOWLEDGMENTS

The work reported here was done as part of a project on landslide hazard mapping, with support from NASA's Center for Commercial Development of Space, at Ohio State University, and the CMER Committee of the Washington Tiiber/Fiih/Wildlife Agreement. The writers wish to thank members of the SHAMW Technical Steering Committee for their contributions to this study. We are especially grateful to M. J. Brunengo, who provided us with the statistics on rainfall and snow depth, and the preliminary findings of his landslide inventory in the focus township.

ABSTRACT

This project concentrated on mapping the piezometric levels following rain-on-snow events. This report begins with a review of available methods for computing infiltration and groundwater changes (the hydrology model), for computing slope stability (stability model), and for estimating failure probability. The results obtained will be used to produce landslide hazard maps.

The lumped-parameter model of Reddi and Wu (1991) was used for the hydrology model. A sensitivity analysis was made, and it was found that the important input variables were rainfall, soil thickness, soil porosity, and soil permeability; the piezometric level was found to be insensitive to slope dimensions. Effects of variations in topography, uncertainties about soil properties and geologic anomalies, and rainfall and snow depth were evaluated.

A plot of piezometric level versus return period was constructed for the average site condition, representative of the focus township. Maps of piezometric level for a 10-year period were constructed for Glenoma and Mineral quadrangles. A preliminary landslide hazard map was constructed for Glenoma quadrangle.

TABLE **OF CONTENTS**

ACKNOWLEDGMENTS ii

ABSTRACT iii

LIST OF FIGURES vi

LIST OF TABLES ix

CHAPTER

I. INTRODUCTION 1

1.1 Problem Statement 1
1.2 Objective and Scope 3
1.3 Literature Review.. 4

II. METHODS.. 8

2.1 General Principles 8
2.2 The Hydrology Component 8
2.3 Site Conditions.. 11
2.3.1 Average Site Conditions 11
2.3.2 Spatial Variations 12
2.3.3 Geologic Anomalies 12

III. RESULTS 18

3.1 Sensitivity Analysis 18
3.2 Variation within a Catchment 24
3.3 Spatial Variations 24
3.4 Flow Through Fractures and Previous Inclusions 34
3.5 Prediction and Mapping of Piezometric Levels 41
3.6 Uncertainties about Piezometric Levels.. 51
3.7 Probability of Failure 52

IV. SUMMARY 53

APPENDICES

A. THE LUMPED PARAMETER MODEL.. 58

B. FLOW THROUGH FRACTURES IN BEDROCK 61

C. EFFECT OF STORM CHARACTERISTICS 67

C.1 Storm Precipitation 67

C.2 Storm Duration 68

C.3 Model of Snowmelt 71

C.4 Total Amount of Infiltration.. 73

C.5 Effect of Sequence of Storms..... 76

C.5.1 Storm Sequence.. 76

C5.2 Variation of groundwater Due to the Sequence of Storms 79

C.5.2.1 Effect of Number of Storms Per Season 79

C.5.2.2 Effect of the Time Interval Between Storms 84

D. DISTRIBUTION OF EXTREME STORM 89

E. REFERENCE.. 95

F. NOTATIONS 100

LIST OF FIGURES

Figure 1.1 Components of (a) landslide hazard assessment system (b) groundwater flow. 2

Figure 2.1 Slope parameters. 9

Figure 2.2 Spatial variations in bedrock profile and soil thickness. 13

Figure 2.3 Seepage through joints. 15

Figure 2.4 Groundwater profile on two sides of a ridge 15

Figure 2.5 Pervious inclusions in the soil layer (a) profile (b) section 1-1. 16

Figure 3.1 Effect of (a) precipitation, R, (b) soil depth, H, on he/H. Mean values of all other parameters were used. 21

Figure 3.2. Effect of (a) drainable porosity, θ_d, (b) permeability, K_s, on h_o/H. Mean values of all other parameters were used. 22

Figure 3.3 Effect of (a) slope length, L, (b) parameter, B, (c) suction at saturation, ψ_s, on h_o/H. Mean values of all other parameters were used. 23

Figure 3.4 Variation of groundwater level within a catchment. 26

Figure 3.5 Zones of piezometric level. To obtain values of h_w/H for mapping, multiply h_o/H from Reddi's model by the fraction shown in Table 3.3. 27

Figure 3.6 Kennel Creek watershed. 29

Figure 3.7 Values of (a) K_s, (b) C, and, (c) H, for Kennel Creek watershed. 31

Figure 3.8: Effect of spatial variations in K_s, C, and H on h_w/H for a plane slope. .32

Figure 3.9 Model for flow through a fracture or joint, b = width of joint, B = width of slope. 33

Figure 3.10 Variation of h_w/H within a slope with flow through fracture $a = L/3$, $b = 10$ m. 36

Figure 3.11 Change of hw / H at exit point with time. 37

Figure 3.12 Sensitivity of fracture flow to input parameters a/L, b/B, c/L, and K_f/K_s. 38

Figure 3.13 Flow through porous inclusion. (a) Model for flow through porous inclusion (b) Variation of h_w/Hwithin a slope. a = L/3 b = 20 m. 40

Figure 3.14 Mean piezometric level for storms of various return periods..... 42

Figure 3.15 Catchment boundaries, Glenoma quadrangle, Washington 44

Figure 3.16 Catchment boundaries, Mineral quadrangle, Washington..... 45

Figure 3.17 Piezometric level map for Glenoma quadrangle, a) cleared slope, b) forested slope. 47

Figure 3.18 Piezometric level map for Mineral Quadrangle, (a) cleared slope, b) forested slope. 49

Figure 3.19 Preliminary landslide hazard map, a) Glenoma quadrangle, b) zone A enlarged. 56

Figure A.1 Kinematic storage model,(a) saturated zone (b) unsaturated zone..... 62

Figure B.1 Geometric parameters of two-dimensional model (Lee, 1986), (a) slope geometry, (b) dimensions of element.. 65

Figure C.l (a) Effect of precipitation, R, on h_0/H, (b) Scatter graph of storm duration vs. precipitation (Brunengo, 1989). 69

Figure C.2 Effect of storm duration, D, on groundwater level h_w/H for R = 5.04 in 70

Figure C.3 Probability density function of (a) snowmelt and snow-water equivalent, (b) potential snowmelt 72

Figure C.4 Probability density function and distribution function of (a) storm precipitation, (b) total amount of water available for infiltration = snowmelt plus precipitation 74

Figure C.5 Probability function of (a) number of storms per season, (b) duration between storms in a 2-storm season and between the last two storms in a 3-storm season 77

Figure C.6 (a) Frequency function of days with a given range in precipitation, (b) simulated small rain events, (c) he/H, θ_1, θ_2 for a sequence of storms 82

Figure C.7 (a) Initial moisture conditions for different number of storms, (b) frequency of h_o/H for different number of storms 83

Figure C.8 Groundwater for l-storm season and 2-storm season. Moisture content and ho/H vs. time for (a) l-storm, and (b) 2-storms. 85

Figure C.9 Groundwater for 3-storm season and 4-storm season. Moisture ..... content and h_o/H vs. time for (a) 3-storm, and (b) 4-storms.. 86

Figure C.10 Effect of initial moisture conditions on ground water for 2-storm and 3-storm seasons (a) average $(\theta)_i$, and (b) $\left(\frac{h_{oi}}{H_i}\right)$ 88

Figure D.l Asymptotic probability distribution function 93

Figure D.2 Asymptotic probability density function. 94

LIST OF TABLES

Table 1.1 Relation between component models, supporting data and input-output. 4

Table 3.1 Parameters used in computations of infiltration and drainage. 19

Table 3.2 Effect of topographic parameters on groundwater. 25

Table 3.3 Correction factors for h_o/H 28

Table 3.4 Soil properties for Kennel Creek watershed. 30

Table 3.5 Distribution of parameters for jointed rock.. 39

Table 3.6 Uncertainties about input to the hydrologic model. 53

Table 3.7 Proposed mapping scales.. 54

Table C.1 Precipitation data 80

Table D.1 Means and variances of amount of precipitation. 92

CHAPTER 1

INTRODUCTION

1.1 Problem Statement

The transient snow zone is an area where landslides occur frequently as a result of rain-on-snow events, when rain plus snowmelt infiltrate into the soil on hillside slopes (Berris and Harr, 1987, Coffin and Harr, 1992). Snow accumulation prior to such an event and snowmelt during such event are believed to be influenced by logging on the slopes. Accordingly, the hazard of landslides in the transient snow zone should be considered in the management of forested watersheds. The overall objective of this project is to assess and map landslide hazard and to provide information for use by land managers and foresters who plan and conduct timber harvest and related operations.

The physical components of a landslide hazard assessment system are shown in Fig 1.1a. The atmospheric conditions that accompany a "rain-on-snow" event induce melting of the snowpack and the rain plus snowmelt constitute a source for infiltration into the soil. A part of the water that infiltrates the soil is retained in the unsaturated zone; the remainder reaches the saturated zone as recharge, and causes a rise in the piezometric level, h,. Water in the saturated zone drains downslope by gravity, and this drainage causes a drop in h_w. Hence, the change in the piezometric level is the recharge minus the drainage. A rise in the piezometric level reduces the shear strength of the soil and increases the seepage force on the soil; the net result is a reduction in the factor of safety with respect to slope failure. These three components will be called rain-on-snow, hydrology, and slope stability, respectively. It follows that development of the technology for predicting all three components is required for a prediction of

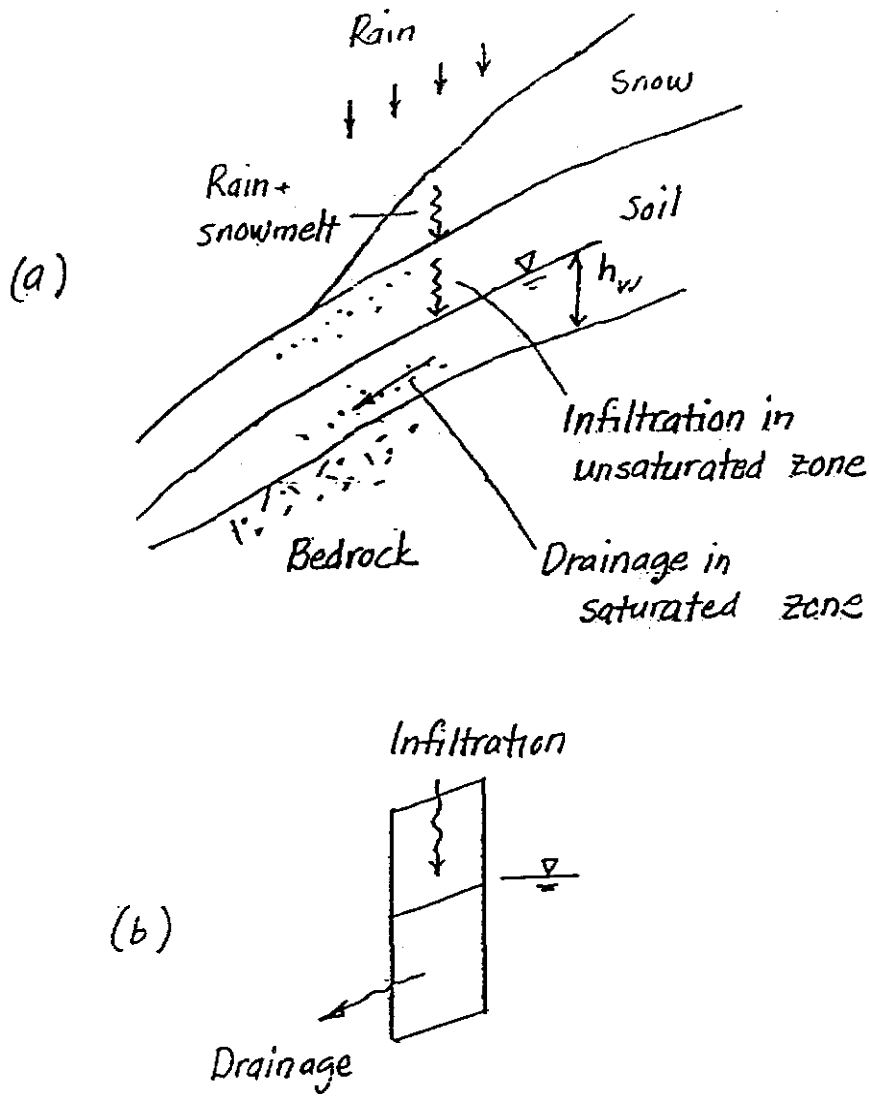

Figure 1.1: Components of (a) landslide hazard assessment system (b) groundwater flow.

landslide hazard, which is defined as the probability of slope failure. In this report we describe the appropriate models for components B and C, and the use of the models to predict landslide hazard.

The relationship of this work with respect to Timber/Fish/Wildlife Agreement's (TFW) overall goal of landslide hazard mapping is shown in Table 1.1. The rainfall model (Brunengo, 1989), the statistical snow depth model based on weather records (Brunengo, 1989), and the snowmelt model constitute component A. The output of this model is available water at the surface, the source for infiltration into the soil. The hydrology model takes the water and calculates the rate at which it will infiltrate into the slope, and the consequent changes in the piezometric level.

1.2 Objective and Scope

The objective of this research is to develop the methodology for predicting and mapping the groundwater response and landslide hazard of hillside slopes in the lower and middle elevations of mountains in Washington. The results are intended to be used by land managers and foresters for evaluation of slope stability under forested and clear-cut conditions. The method is rational, with components that account for precipitation, snowmelt, infiltration, drainage, and stability. The method is applied first to a township in Lewis Co., (hereafter referred to as focus township) which is the location of the landslide inventory being conducted by M. J. Brunengo and J.D. Dregovich. Two types of groundwater response were computed: the sensitivity of the peak piezometric level to catchment characteristics, and the peak piezometric level for a given set of catchment characteristics. An example the landslide hazard map computed from the piezometric levels is given. Landslide hazard maps may be used in level 1 of Washington's watershed analysis process, and the results of level 2 watershed analysis may be used for updating landslide hazard maps.

Table 1.1

Relation between component models, supporting data, and input-output.

Model	Data	output
A. Ram-on-snow Snow depth Brunengo) **Snowmelt** (Corps. of Engrs., USGS)	**Weather records** **Snowmelt** experiments **(Harr)**	Rain plus **snowmelt**
B. Hydrology	Measured piezometric level	Piezometric level map
C. Slope stability	Field landslide survey (Brunengo **&** Dragovich)	Landslide hazard map

1.3 Literature Review

The problems in components B, hydrology, and C, slope stability, require the solution of equations describing groundwater flow and shear failure in soil, respectively. Solutions of these problems are available in various forms, and a brief review of the important features of the solutions and their relevance to the proposed work is given below.

The governing differential equation for flow in unsaturated soil is Richards' equation (Richards, 1931). If the soil is saturated, the equation simplifies to Laplace's equation. The most sophisticated solution of infiltration and drainage in a slope is the finite difference formulation of Richards' equation by Freeze (1971). It solves for the flow in both the unsaturated and saturated zones, with permeability and storage expressed as functions of soil suction.

Most simplified solutions compute the flows in the unsaturated and saturated zones separately. The flow in the unsaturated zone is primarily in the vertical direction, and a simplification is to compute this as one-dimensional flow (Fig. 1.1b). The equation of Green and Ampt (1911) assumes plug flow with velocity equal to the saturated permeability and is the simplest one-dimensional solution. Numerical integration of the one-dimensional form of Richards' equation is the most sophisticated form. An intermediate solution is the method of Reddi and Wu (1991), in which the unsaturated zone is separated into three zones: a surface zone where flow is controlled by soil moisture, a middle zone where flow is controlled by gravity, and a bottom zone where flow is controlled by capillarity (Eagleson, 1978). Several methods are also available for solving the drainage in the saturated zone. The most sophisticated is to solve the three-dimensional flow by finite difference method. Simplified solutions have been proposed by Beven (1981) and Sloan and Moore (1984). Various combinations of

methods have been used to solve the deterministic problem, in which the source and soil properties are assumed to be known with no uncertainties. Comparatively simple solutions for flow in hillside slopes using combinations of these methods have been obtained by Lumb (1975), Beven (1981), Wu and Swanston(1980), and Reddi and Wu (1991).

For the purpose of hazard prediction and mapping, a probabilistic solution is required because the sources (or input for models) are stochastic. In addition, estimates of soil properties and slope geometries involve uncertainties. Probabilistic solutions also can have a range of sophistication. A rational choice of methods should consider not only the accuracy of the results, but also the quality of the available data. The simplest is the first-order second-moment (FOSM) method, in which the mean and variance of the output are determined from the means and variances of the input variables; the forms of the probability distributions must be assumed (Ang and Tang, 1980). Because of its simplicity, FOSM methods are widely used for large systems. FOSM solutions of flow in slopes have been given by Hachich and Vanmarcke (1983), Sitar et al. (1987), Reddi and Wu (1991). The lack of accuracy may be balanced by calibration against observed data. Use of Bayesian updating (Ang and Tang, 1980) makes it possible to calibrate the model parameters with observed data. This has been done for hydrologic systems by Wilson et al. (1978), Hachich and Vanmarcke (1983), and Reddi and Wu (1991). The most sophisticated probabilistic solution is the derived distribution, in which the probability distribution function is derived mathematically (Ang and Tang, 1980). Because of the complicated relations in the components, derived distributions are not attainable for a large system such as the one under consideration. One alternative is Monte Carlo simulation. For large systems, Monte Carlo simulation may be impractical because of the large volume of computations. However, the Monte

Carlo method may be applied to individual components and used to derive approximate distribution functions.

In the slope stability problem, failure is considered to occur when the shear stress due to the applied loads equals the shear strength of the soil. Deterministic solutions of slope stability have been available for some time. These range from the simple solution for the infinite slope (e.g., Taylor, 1948) to three-dimensional solutions (Baligh and Azzouz, 1975). Probabilistic solutions for stability have mostly been obtained by FOSM method (Cornell, 1971; Tang et al., 1976; Wu *et* al. , 1986), and derived distributions are usually not attainable except for simple geometries such as the infinite slope. Despite the approximate nature of the FOSM method, it is a very useful tool which can be used to assess the relative safety or hazard of different site conditions and constructions. In many stability problems, this is sufficient for management decisions. This is particularly relevant because in many stability problems, we are concerned with events that occur infrequently, such as 20-year storms. Data for such events are scarce because of the nature of these events. It follows that we do not know very much about the tails of the probability distributions, even when probability distribution functions are fitted to the data. The approximate nature of probability estimates can be improved by calibration of the predicted hazard with field observations and past experience, such as those being obtained by Brunengo and Dragovich in a related project. Bayesian updating provides a formal procedure for this step. Calibration and updating of probability estimates has been used for management and decision-making in design and construction operations, such as planning of transportation routes (Einstein, 1988) and offshore construction (Wu *et al., 1986).*

CHARTER II

METHODS

2.1 General Principles

In order to produce hydrologic-frequency maps and landslide-hazard maps for a range of site conditions and scales, we need to evaluate available techniques for solving flow and slope stability problems with respect to their suitability for the site conditions and scales encountered in this project. Past experience indicates that, in general, approximate methods are most suitable for evaluating average conditions over a large area on small-scale maps. More precise methods can be used to study the departures from the average over smaller zones within a large area. Maps of different scales are useful for a variety of purposes. Small-scale maps over large areas may be used by land use planners as preliminary information to identify areas where landslide hazards should be considered. Detailed maps at larger scales will alert planners and managers to take specific actions, which may include field investigation prior to logging or construction, special design, or control. A range in map scales, to meet the needs of land managers, is considered in this project.

2.2 The Hydrology Component

The lumped kinematic storage model of Reddi and Wu (1991) (Appendix A), predicts the piezometric level at specific points in a watershed. It has performed well when compared with piezometric levels measured by Pierson (1977) in the Perkins Creek basin in Oregon. This model uses the average properties in a watershed, represented either as a plane or a bowl (Fig. 2.1), and calculates the piezometric response h_o at the exit point. Flow through unsaturated and saturated zones are computed separately and

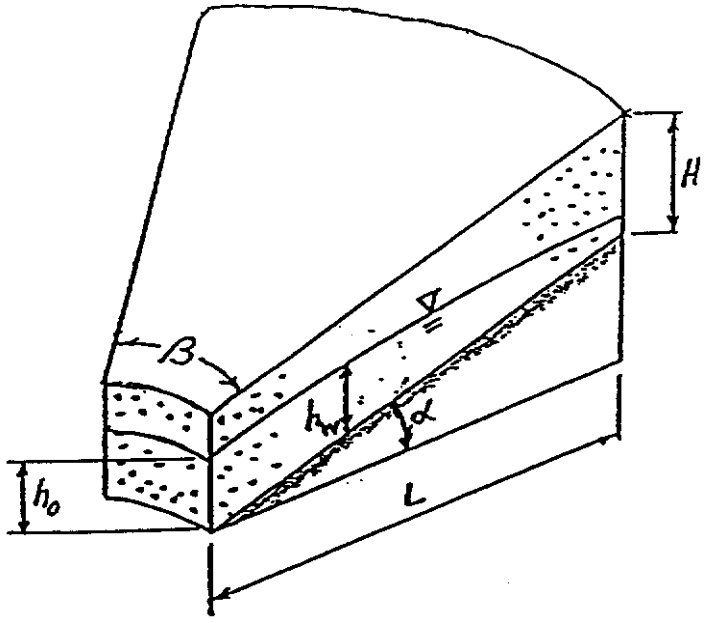

Figure 2.1 Slope parameters.

then combined. It represents a relatively simple model that does not require excessive computer time, can solve probabilistic problems, and perform updating.

The approach adopted was to use the lumped kinematic storage model of Reddi and Wu (1991) and Lee's (1986) finite difference solution to compute the groundwater response. In the first phase, we used Reddi and Wu's model to calculate the sensitivity of the groundwater response to the site conditions. Results of the sensitivity analysis allowed us to limit our attention to the input parameters that have the highest sensitivities.

In the second phase, we calculated groundwater response for two conditions. Reddi's procedure was used to calculate the groundwater response of a slope under average site conditions (Fig. 2.1): average values of slope α, soil thickness (H), and soil properties (C= storage coefficient and K_s = permeability) (see Sec. 2.3.1). These characteristics were obtained from topographic maps and estimated from information given in soil survey reports, and represented the best estimates available, in the absence of a site investigation. These calculations may be considered as a preliminary investigation, and the results serve as an indicator of the piezometric level in a given slope. Because the lumped parameter solution assumed a simplified groundwater profile, a better estimate of the groundwater levels at points within individual catchments were obtained by the 2-dimensional finite difference solution (Lee, 1986). This was used to identify the zones of high piezometric level within individual catchments.

The third phase is an investigation of the effect of spatial variations in site conditions on the groundwater response. Spatial variations in bedrock slope, soil thickness, and soil properties were introduced into a 2-dimensional finite difference analysis (Lee, 1986). The measures of spatial variations were estimated from available

data from other sites, plus observations in the region under study. The effects were added to the average state.

In the fourth phase, the effect of geologic anomalies on groundwater response was investigated by the finite difference method. This required input specific to the site under consideration. The specific site conditions were derived from observations of geology, slope, and soil characteristics made by Brunengo and Dragovich in the course of the landslide inventory. The values of h_w calculated in phases 3 and 4 were used to estimate random departures from the average.

The following formulation of landslide hazard is used to present the results. The failure probability is defined as

$$P_f = P(h_w > h,) \tag{2.1}$$

where h_w = height of groundwater level (Fig. 2.1), h_c = critical **groundwater** level required to produce a slope failure. The effect of uncertainties is represented as a model error, denoted by N_i for the *ith* source (Tang *et* al., 1976). Each N_i is a random variable with mean $E(N_i)$, which represents our best judgment, and a coefficient of variation, $\Omega(N_i)$, which represents our uncertainty about N_i . Then

$$P_f = P(Nh_w > h,) \tag{2.2}$$

where $N = \prod N_i$.

2.3 Site Conditions

2.3.1 Average Site Conditions.

The average site conditions were determined from USGS topographic maps and county soil survey report (Soil Conservation Service, 1987). The soil series and/or

associations that are found on slopes in the focus twp. are Pheeney-Jonas, and Stahl-Reichel. The soil depth is 20 to 60 in (0.5-1.5m) and the saturated permeability (K_s) is 0.6 to 2.0 in/hr (1.5-5.0 cm/hr). The average soil depth is taken as lm. The geometric mean of the permeability, 2.8 cm/hr, is used in the calculations. The range in permeability is the same for all of the soils in this area. The average condition is considered to be applicable to the entire area. The area can be subdivided according to the detailed soils map, and each subdivision assigned different soil depth and soil properties, at a later stage (sec. 3.5).

2.3.2 Spatial Variations

Spatial variations denote the natural variations in soil properties from one point to another and may be shown as random departures from the mean **value,** E (.). The magnitude of the departures can be expressed as a variance, Var(.), and a correlation distance, δ (Vanmarcke, 1983). Variances and correlation distances of natural soils have been reviewed by Wu (1989) and Freeze (1980). Observations by Brunengo (pers. comm., 1991) in the focus twp. indicate that variations of K within $\pm$ 0.5 E(K) can occur within distance of 3-7 m. However, variations of an order of magnitude are considered unlikely within a distance of 70m. Spatial variations in bedrock slope and soil thickness are illustrated in Fig. 2.2. Observations in the focus twp. indicate that irregularities in the bedrock profile are not likely to exceed that shown in Fig. 2.2 (Brunengo, pers. comm., 1991).

2.3.3 Geologic Anomalies

Geologic anomalies include all geologic features in the region that depart from the average state. These were identified by Brunengo (pers. comm. 1991) based on observations in the focus twp. The principal anomalies are: a weathered zone in the bedrock, joints in the bedrock, pervious inclusions in the soil layer, and spatial trends in

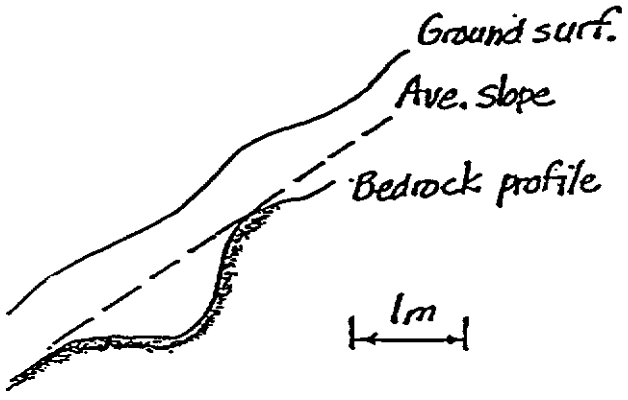

Figure 2.2 Spatial variations in bedrock profile and soil thickness

soil properties. These features are not described in soil reports and geologic maps and are not included in the average site conditions. The following paragraphs summarize Brunengo's field observations that are pertinent to the infiltration and drainage problem.

As with many rock types in the Cascades, the volcanic rooks in the central Cascades have a weathered layer, up to ~2.5m in thick, composed of coarse-grained particles (up to boulders of 0.3 m in diameter within a finer matrix). The weathered layer is less commonly observed in sandstones in the central and North Cascades. Within the bedrock, joints and bedding planes provide avenues of seepage. A simplified model of seepage through joints is illustrated in Fig. 2.3. The controlling parameter is the length of interconnected joints. The maximum dimension of interconnected joints is shown in Fig. 2.3. Seepage through joints can also lead to different groundwater profiles on two sides of a ridge (Fig. 2.4): the groundwater level at a is higher than that at b, because of seepage through joints from one side to the other.

Pervious inclusions in the soil layer serve as zones of high seepage velocity. In the focus twp. the most important type of pervious inclusion is a widespread layer of pumice, 5–30cm thick and composed of particles of 1-2 cm. in diameter. A hypothetical profile and cross-section is shown in Fig. 2.5. A pumice layer may be broken or interrupted, as shown in Fig. 2.5a. However, the width of the break in the Y direction is expected to be less than 2 m and therefore its influence on the flow is ignored. Lenses of sand and gravel have also been observed in the soil layer; their length or width is less than 0.5 m. Tubular voids left by decay of roots are also present, is usually less than 5 cm diameter and less than 1m long. Sand and gravel lenses and tubular voids are considered to be randomly distributed in the soil layer and to increase its average

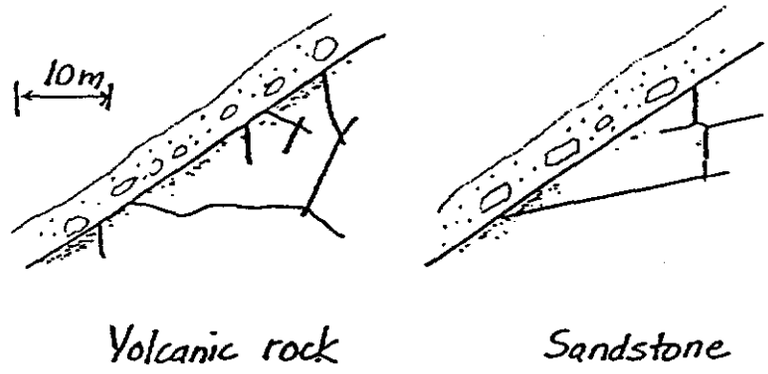

Figure 2.3 Seepage through joints

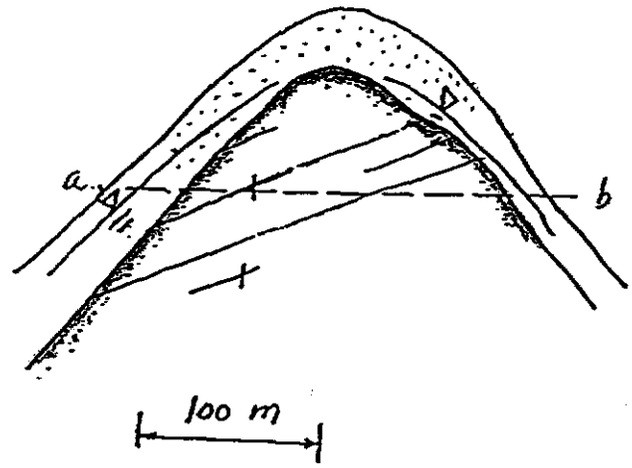

Figure 2.4 Groundwater profile on two sides of a ridge.

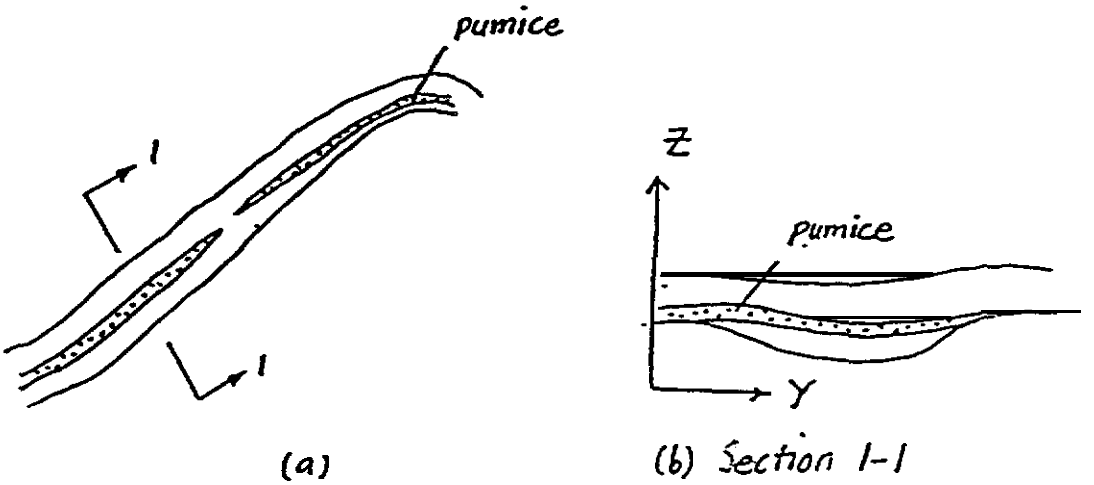

Figure 2.5 Pervious inclusions in the soil layer (a) profile (b) section 1-1

permeability. Because of their relatively small dimensions, their effect on groundwater levels is ignored.

The observed spatial trend in soil thickness is that it is greater at the foot of slopes than at the ridges. The trend is that H = 0 ▪ 0.6 m at ridges and increases to 1.3 ▪ 2.6 m at foot of slopes. There is also a trend of increasing proportion of boulders and gravel with depth in the soils that overly volcanic rock. The percentage increases from about 15% near the surface, to 65% near the bottom. This phenomenon is considered to reflect the weathered zone in the volcanic rock, and is treated accordingly.

CHAPTER III

RESULTS

3.1 Sensitivity Analysis

Examination of the governing equations of the lumped parameter model (Appendix A) indicate that the change in the water level $(h_o^1 - h_o^o)/H$ (Eqs. A.8 and A.9), depends on the relative rates of infiltration and drainage, expressed as a ratio $\kappa = \frac{i\,\Delta t}{H\theta_d}$, which is the ratio of the infiltration during time t to the volume of water that can be stored in the soil; and λ (Eq. A.7), which is a dimensionless drainage rate, equal to the ratio of the rate of drainage in the saturated zone to the volume of water in the saturated zone. The ratio κ/λ is the ratio of infiltration to drainage and is equivalent to the parameter (TM/q) in O'Loughlin (1986). If the velocity of drainage, v, is small, or λ is small, Eq. A.11 shows that $(h_o^1 - h_o^o)/H$ depends only on κ. If we are interested in the maximum rise in the water level for a given storm, then $i\Delta t$ can be used to represent the rainfall, R, of the storm. Eq. A.11 also shows that the time At required to reach a given $(h_o^1 - h_o^o)/H$ is proportional to $H\theta_d / 2i$. This is why, at a given site with given H and θ_d, the value of At and i required to trigger a failure can be correlated (Wieczorek, 1987; Wilson, 1989).

The average material properties are summarized in Table 3.1. In addition to the properties H and K_S described in Sec. 2.3.1, the drainable and saturated volumetric water contents, θ_d and θ_s, and the parameters B and ψ_s that describe the unsaturated permeability were estimated from Clapp and Hornberger (1978), Black (1979), and Schroeder (1983). For the values given in Table 3.1, v and λ are small and Eq. (A.ll) may be used. The controlling parameter is κ (or $i\Delta t$ = R, H, and θ_d). To evaluate the sensitivity of h_O/H to the different parameters, peak h_O/H were computed for a range of values for a given parameter, while all other parameters were kept at their mean

Table 3.1

Parameters used in computations of infiltration and drainage

soil Parameter	Range	Mean	Variance of Mean	Sensitivity
K_s (cm/hr)	0.5 – 15 (cm/hr)	2.8 (cm/hr)	5.29 (cm^2/hr^2)	0.0263 (hr/cm)
H	0.5 – 1.5 (m)	1.0 (m)	.0816 m^2	-0.436 m^{-1}
θ_d	0.29 – 0.35	0.32	0.00034	-0.818
θ_s	0.4 – 0.5	0.45	0.0005	-1.6
B	4.0 – 5.0	4.38	0.75	-0.05
ψ_s	5.0-30.0 (cm)	17.5(cm)	52 (cm^2)	-0.006 (cm^{-1})

values (Table 3.1). The peak h_o/H is critical to initiation of landslides; for brevity, all subsequent references to h_o/H imply the peak value. Values of h_o/H computed for a plane slope are shown in Fig. 3.1. The variables are R (Fig. 3.1a), H (Fig. 3.1b), and θ_d (Fig. 3.2a). In addition, h_o/H. also depends on K_s, because the ratio R/K_s controls the flow through the unsaturated zone, as expressed in Eq.(A.1). Fig. 3.2b shows the effect of K_s. Variables whose influence on h_o/H are comparatively small include slope length, L (Fig. 3.3a), and the parameters B and ψ_s, which describe the unsaturated permeability (Fig. 3.3b and c).

The results of this sensitivity study allows us to identify the variables that do not have a strong influence on h_o/H. For the site conditions under consideration, $\frac{h_o}{H}$ is sensitive to R, H, θ_d and K but not to L, B, and ψ_s. Hence, mean values of L, B, and ψ_s are used in subsequent calculations of h_o/H. The slope of each of the curves in Figs 3.1 to 3.3 is the sensitivity or the rate of change of h_o/H with respect to the independent random variable R, H, . . The sensitivity can also be expressed as $\frac{\partial \frac{h_o}{H}}{\partial X_i}$, where X_i is the random variable. This sensitivity study allows us to identify the variables that do not have a strong influence on h_o/H. The values of $\frac{\partial \frac{h_o}{H}}{\partial X_i}$ are used in Sec. 3.6 to calculate the variance of h_o/H, which is a measure of uncertainty about h_o/H. It should be noted that R represents not only rainfall but rain-plus-snowmelt in case of a rain-on-snow event. In addition, R also depends on storm sequence. These factors are considered in the evaluation of the variance of h_o/H (Sec. 3.6).

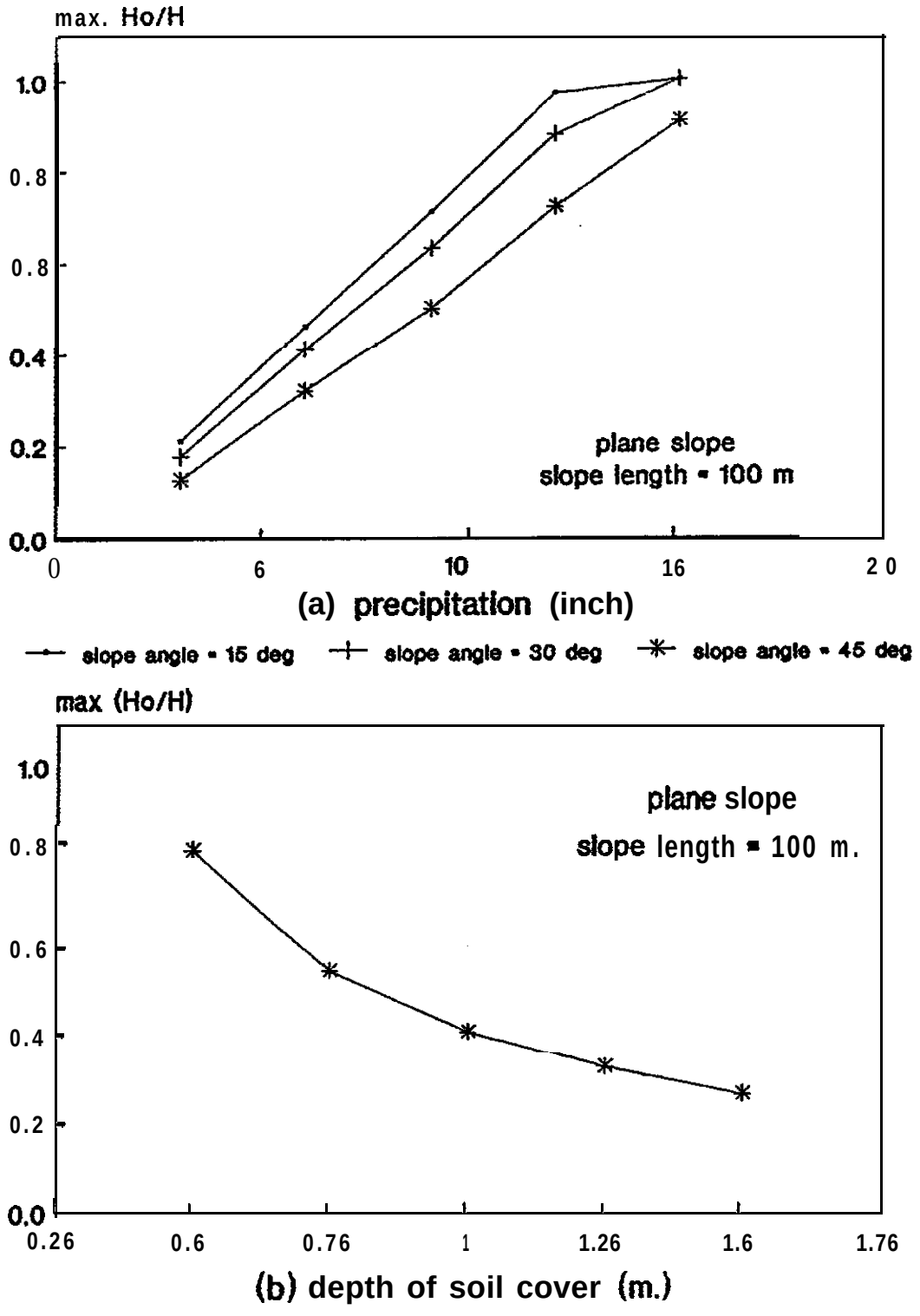

Figure 3.1 Effect of (a) precipitation, R, (b) soil depth, H, on h_o/H. Mean values of all other parameters were used.

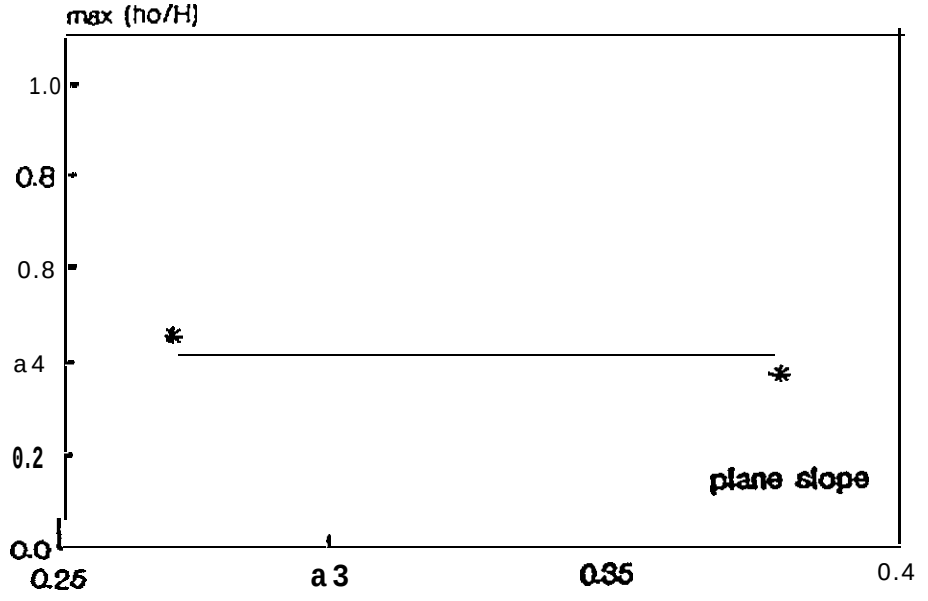

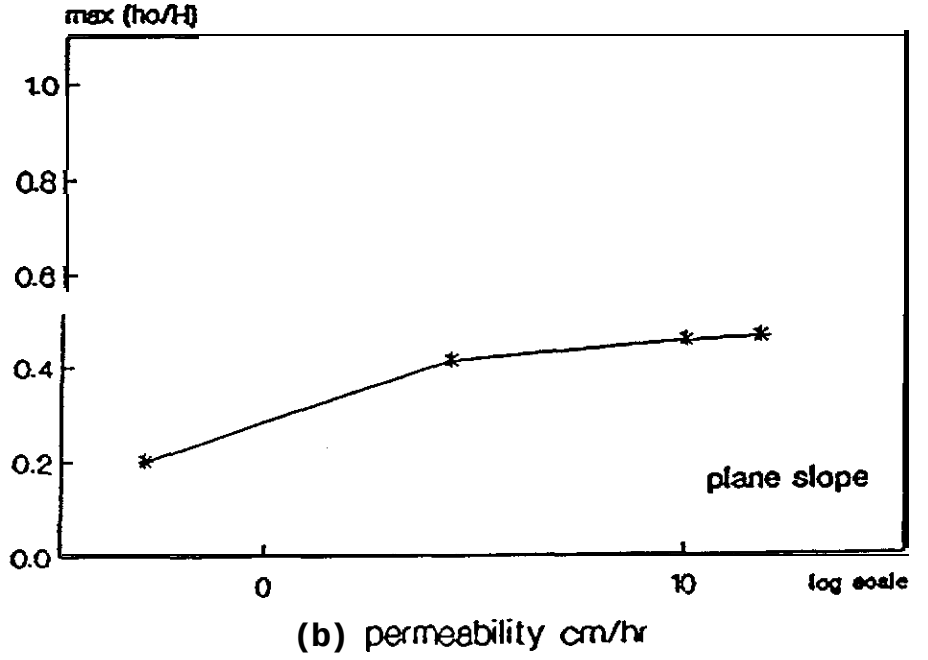

Figure 3.2. Effect of (a) drainable porosity, θ_d, (b) permeability, K_s, on h_o/H. Mean values of all other parameters were used.

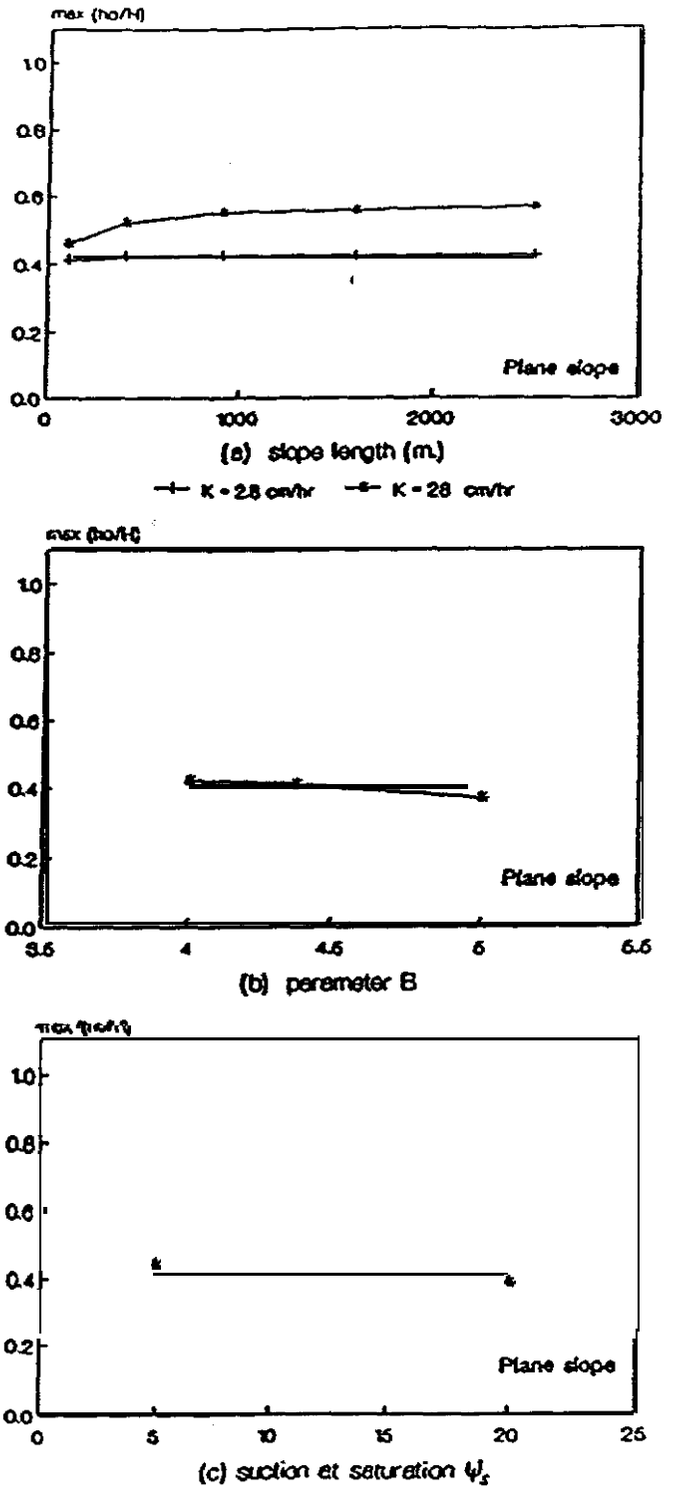

Figure 3.3 Effect of (a) slope length, L, (b) parameter, B, (c)suction at saturation, ψ_s, on h_o/H. Mean values of all other parameters were used.

3.2 Variation within a Catchment.

The 2-dimensional finite difference program (Lee, 1986) was used to study the effects of topography within a catchment. The groundwater levels were calculated for catchments of different length-to-width ratios; Table 3.2 gives the variables that were studied. An example is given in Fig. 3.4. The results show that, for the variables studied, the maximum value of h_w/H, which occurs in the valley floor of a catchment, is close to the value of h_o/H calculated by Reddi's lumped parameter model. The results are similar to those calculated by O'Loughlin's (1986) method. Values of h_w/H within different parts of a catchment, shown in Fig. 3.5, may be estimated by using the predicted h_o/H from Reddi's lumped model, multiplied by a correction factor as given in Table 3.3.

3.3 Spatial Variations

Random spatial variations introduce errors in the predicted h_w/H. As summarized in Sec. 2.3.2, only general observations of spatial variations in K_s and H available. These are in general agreement with measurements of permeability and depth made in the Kennel Creek watershed by Swanston (pers. comm., 1985; see Reddi and Wu, 1991). Hence, we use the data from Kennel Creek to evaluate the effect of spatial variations. The Kennel Creek watershed on Chichagof Island, Alaska, is shown in Fig. 3.6. The measured values of K_s and H and the X, Y coordinates of the sampling points are shown in Table 3.4. These values are used to illustrate the effect of spatial variations on h_o/H. The values of K_s and H at unobserved points were estimated by kriging (see Lee, 1986) and are shown in Fig 3.7. The 2-dimensional finite difference analysis of Lee (1986) was used to calculate the water level h_w/H for a plane slope; the results are shown in Fig. 3.8. The departures from the h_w/H calculated with the average values were used to calculate the variance of h_w/H due to spatial variations;

Table 3.2

Effect of Topographic Parameters on Groundwater

Slope length, L (m)	Width, B (m)	β (°)	h_o/H
100	20	30°	0.42
	40		0.43
	60		0.44
	80		0.46
	100		0.46
100	20	90°	0.39
	40		0.40
	60		0.404
	80		0.408
	100		0.413
400	80	90°	0.398
	160		0.401
	240		0.405
	320		0.409
	400		0.422

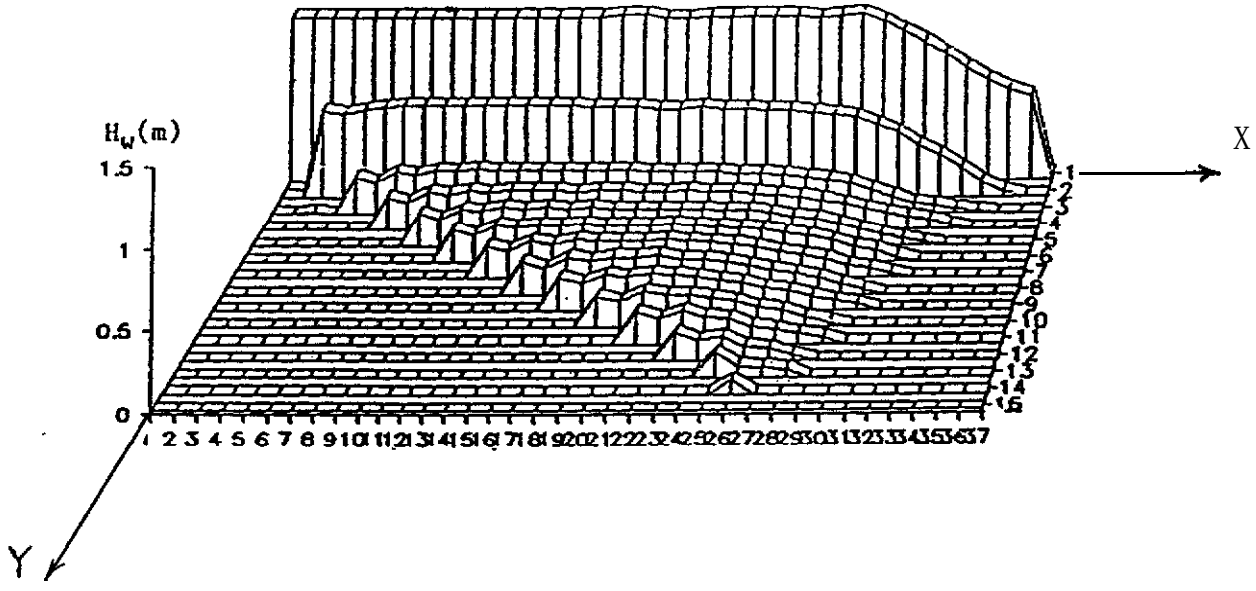

Figure 3.4 Variation of groundwater level within a catchment. K = 2.8cm/hr, R = 5.04 in, a= 30°, β = 90°, and L = 300 m.

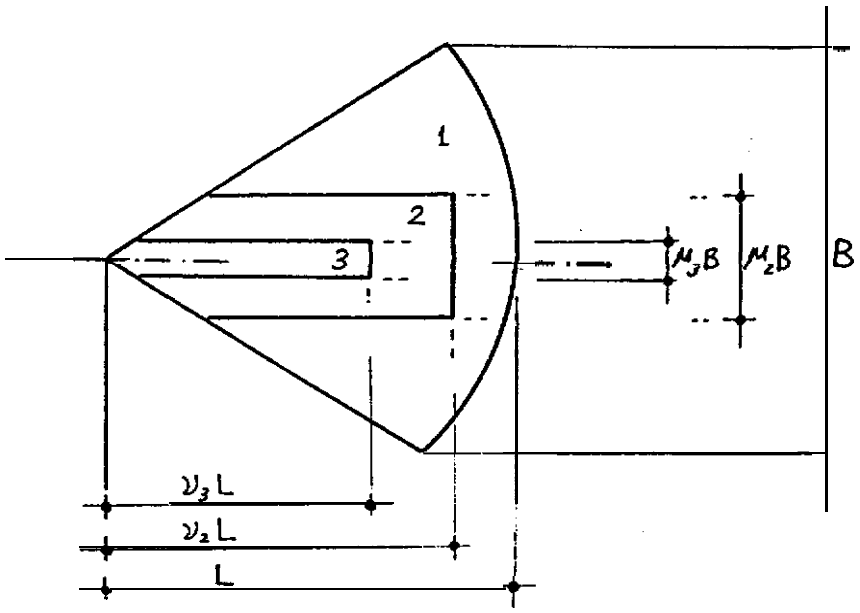

Figure 3.5 **Zones of piezometric level. To obtain values of h_w/H for mapping, multiply h_o/H from Reddi's model by the fraction shown in Table 3.3**

Table 3.3

Correction factors for h_w/H

	Convergent slope, no pumice	Convergent slope, pumice	Plane slope, no pumice	Plane slope, pumice
Zone 1				
η_1	0.5	0.3	0.5	1.0
Zone 2				
μ_2	1/15	4/15	2/15	4/15
ν_2	0.8	0.8	1.0	1.0
η_2	1.0	1.2	1.0	3.0
Zone 3				
μ_3	1/15	1/15	1/15	1/15
ν_3	0.6	0.6	1.0	1.0
η_3	Saturated	Saturated	Saturated	Saturated

NOTE: For each zone (see Fig 3.5), the dimensions are given by μb and νL and $h_w/H = \eta\, h_o/H$, where ho/H is calculated by the lumped parameter model.

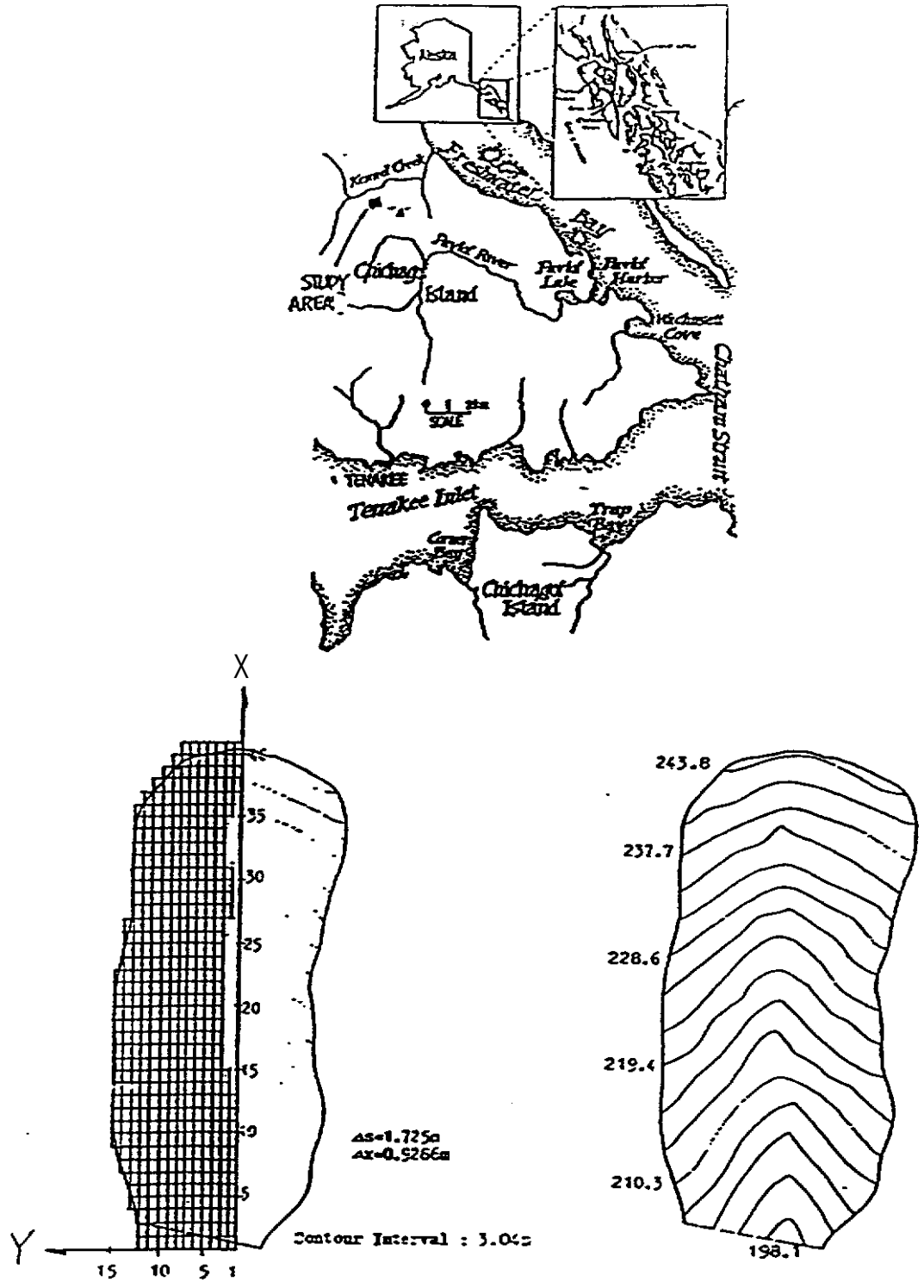

Figure 3.6 Kennel Creek watershed

Table 3.4

Soil Properties for Kennel Creek Watershed (Swanston, pers. comm. 1985)

variable	No. of data points	ralue	X (m).	Y (m.)	5 (m.)	nean	var
Permeability	9	.705	7.54	11.20	1.5	.964	1.254
m/day		.657	10.27	15.53		n/day	m/day2
		.657	10.27	15.53			
		3.740	1.04	24.15			
		.290	10.48	33.93			
		1.272	1.26	43.70			
		.408	9.89	54.05			
		.194	7.54	55.78			
		.165	1.34	60.95			
		.246	4.19	64.40			
Specific	9	.18	7.54	11.20	1.5	.178	.0042
Yield		.17	10.27	15.53			
		.32	1.04	24.15			
		.14	10.48	33.93			
		.20	1.26	43.70			
		.16	9.89	54.05			
		.12	7.54	55.78			
		.10	1.34	60.95			
		.22	4.19	64.40			
soil depth m	10	.71	-0.84	5.75	1.0	0.528 m	1.0144
		.61	1.68	7.48			m^2
		.40	2.10	13.22			
		.33	-0.63	14.38			
		.44	2.51	20.82			
		.51	0.00	21.28			
		.53	1.89	32.20			
		.61	10.00	40.25			
		.48	2.60	40.42			
		.66	0.84	54.63			

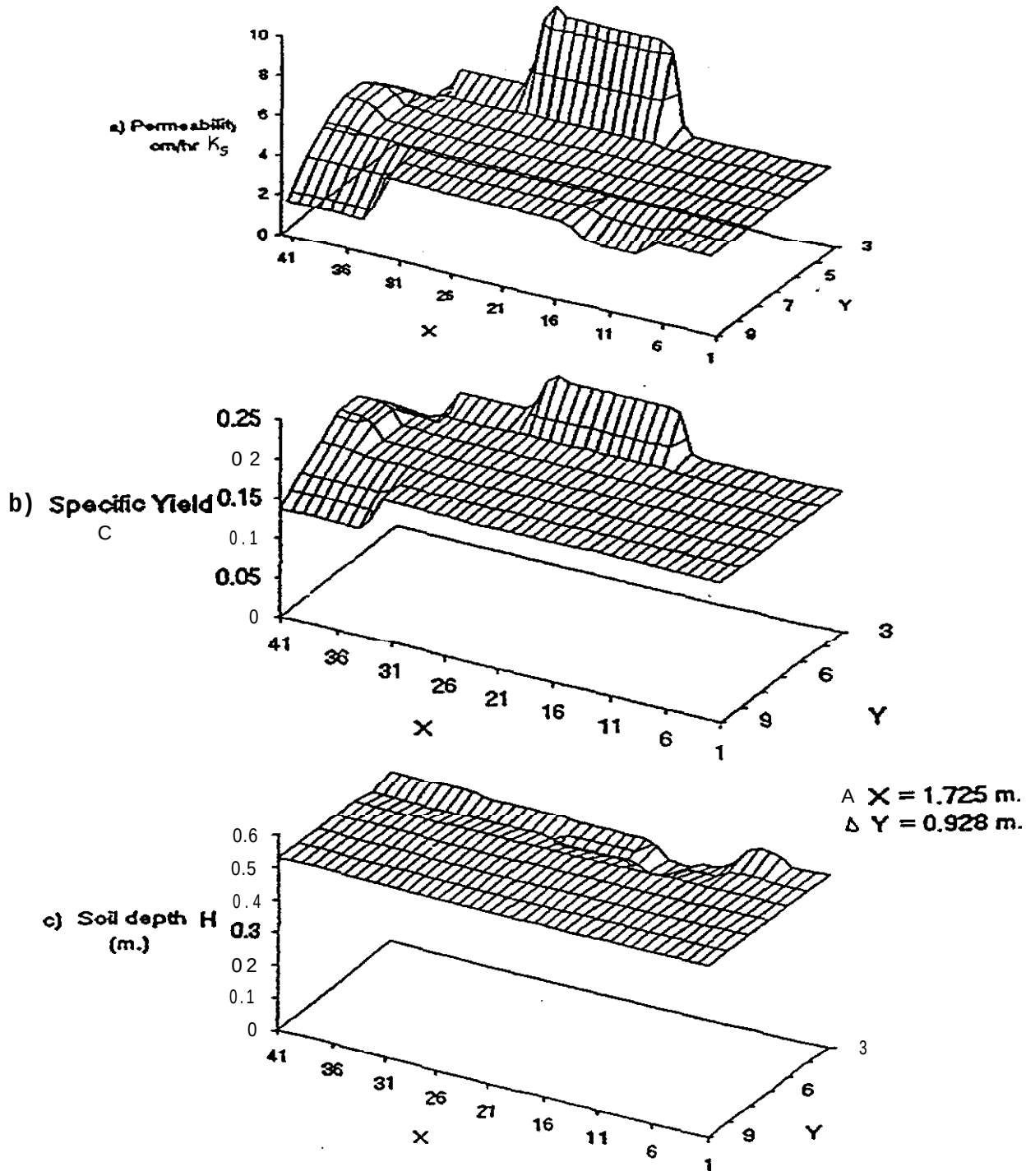

numbers in X. and Y directions are node numbers

Figure 3.7 Values of (a) K_s, (b) C, and, (c) H, for Kennel Creek watershed

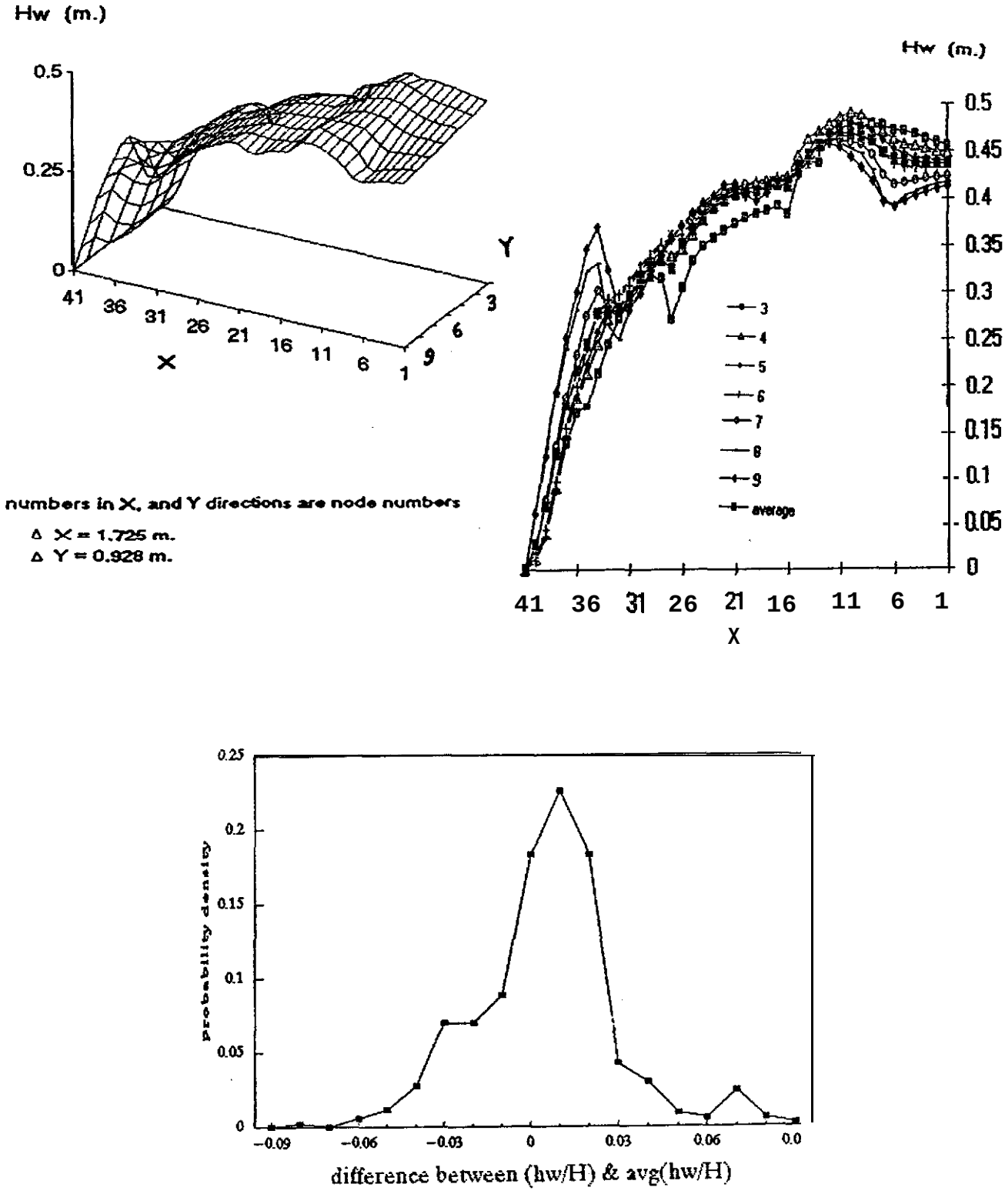

Figure 3.8 Effect of spatial variations in K_s, C, and H on h_w/H for a plane slope.

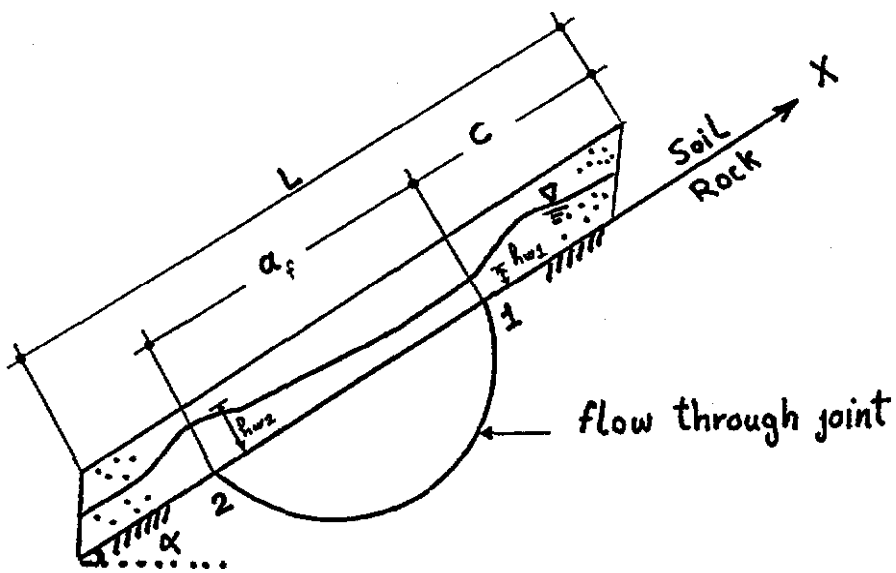

Figure 3.9 Model for flow through a fracture or joint, b = width of joint, B = width of slope.

the variance is $8x10^{-4}$. The variance represents the uncertainty about the ratio h_w/H due to spatial variations. It is a measure of local departures from the value of h_w/H, predicted using average properties, and is one of the compenents of uncertainties considered in Sec. 3.6. As pointed out earlier, the spatial variation in the focus township are of similar magnitude. Hence, the calculated variance of h_w/H is assumed to be applicable to focus township.

3.4 Flow Through Fractures and Pervious Inclusions.

To estimate the effect of flow through fractures, the 2-dimensional finite difference solution of Lee (1986) was modified. A flow path was added to represent the flow through a fracture, as shown in Fig. 3.9. The equations for flow are described in Appendix B. The transmissibility of the fracture or joint can be estimated by several methods. Values of equivalent permeability for fractured rock reported by Huitt (1956) and Hoek and Bray (1981) range between $10^{-2}cm/sec$ for joints filled with clay, to $10^{2}cm/sec$ for heavily fractured rock. The equivalent permeability can also be expressed as (Louis, 1969)

$$K_f = \frac{ge^3}{12\eta b} \qquad (3.1)$$

where g = gravitational acceleration, e = opening of the fracture, b = joint spacing, and η = kinematic viscosity. For a spacing of 1 fracture/meter and e between 0.1 and 1 mm, the calculated K_f ranges from $10^{-4} - 10^{-1}cm/sec$. The lower limit of these values is approximately equal to Ks, while the upper limit is several orders of magnitude larger. Without actual measurement of the transmissibility, we evaluated the effects with values of K_f/K_s of 0.1, 1, 10, and 100.

The calculated results for a fracture of b/B =0.1 are shown in Fig. 3.10; Y = 7 denotes the centerline of the fracture. The change in h_w/H at the exit, as a function of time, is shown in Fig. 3.11. For all cases, the water level at the exit point is greater than 0 after the end of storm, which corresponds to the delayed response described by Johnson and Sitar (1989). Calculations with K_f/K_s > 100 are not meaningful because flow through the fracture exceeds the supply at the entrance point.

Calculations were made to evaluate the sensitivity of the water level at the exit to the joint dimensions a, b, and c (Fig. 3.9). The results in Fig. 3.12 show that h_w/H is sensitive only to b/B, Without detailed field data on the continuity of the joints, we assumed that probability is 1 that a continuous joint exists and the distributions of b/B and K_f/K_s are as given in Table 3.5. The flow through joints changes h_w/H and this change is represented as a model error N, so that N h_w/H is the change in h_w/H. The model error N has a mean of 0 because it increases h_w/H at the exit but reduces it at the entrance point. The variance of the model error is, according to FOSM,

$$\text{Var } N = \text{Var } (K_f/K_s) \left(\frac{\partial N}{\partial (K_f/K_s)} \right)^2 + \text{Var}(b/B) \left(\frac{\partial N}{\partial (b/B)} \right)^2 \qquad (3.2)$$

The variances are given in Table 3.4 and the sensitivities or derivatives are equal to the slope in Fig. 3.12. These were used to obtain Var (N) = .039. This is the uncertainty about N, and about h_w/H, due to the uncertainties about K_f/K_s and b/B

The effect of flow through porous inclusions is treated by replacing a section of the soil with a permeability that represents the porous inclusion. The equivalent permeability of a two-layered system, Fig. 3.13 is

$$K_p = \frac{K_i H_i + K_s (H - H_i)}{H} \qquad (3.3)$$

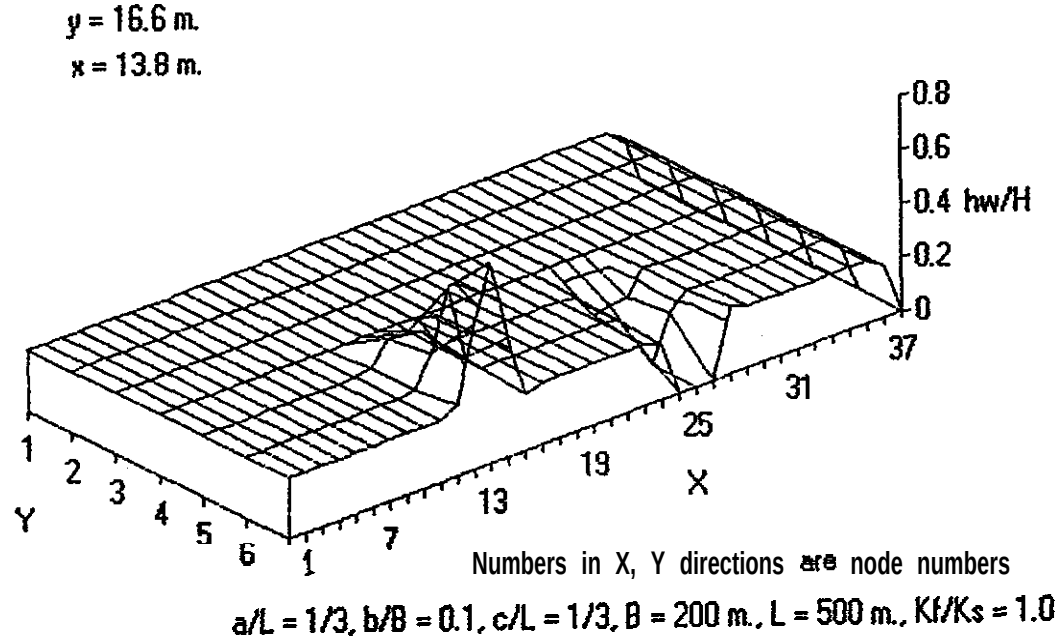

Figure 3.10 Variation of h_w/H within a slope with flow through fracture, a = L/3, b = 10 m.

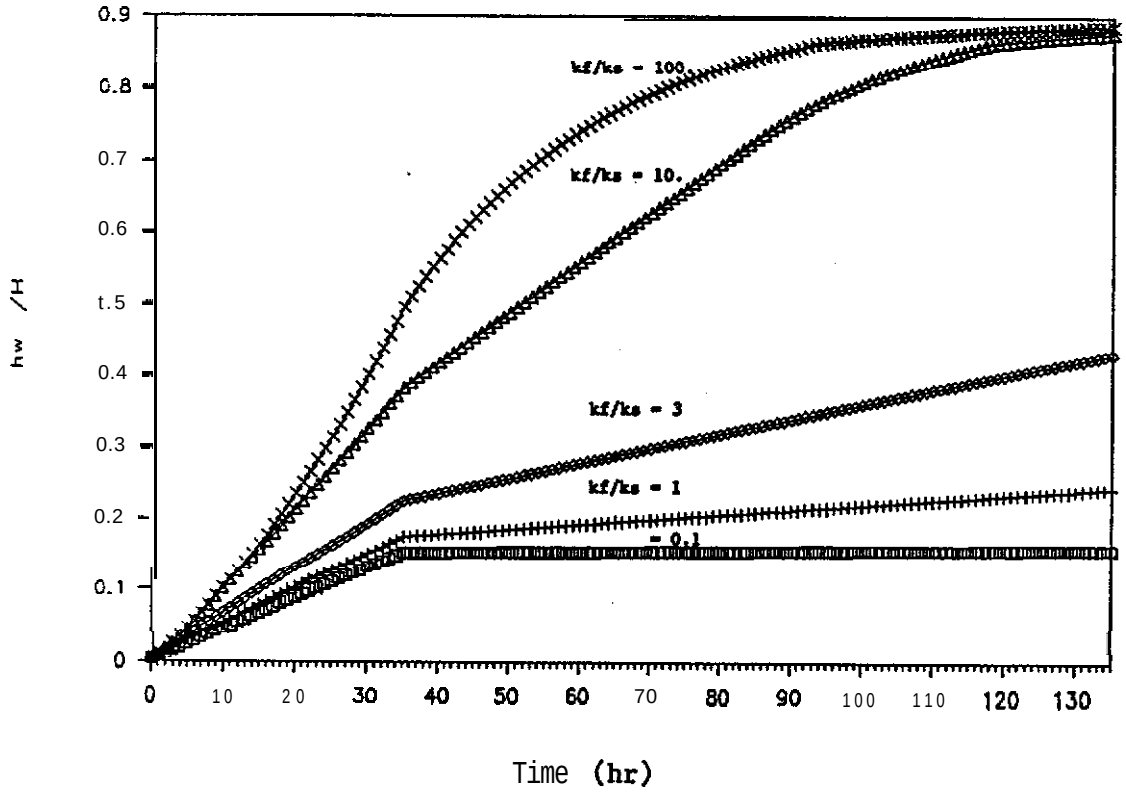

Figure 3.11 Change of hw / H at exit point with time.

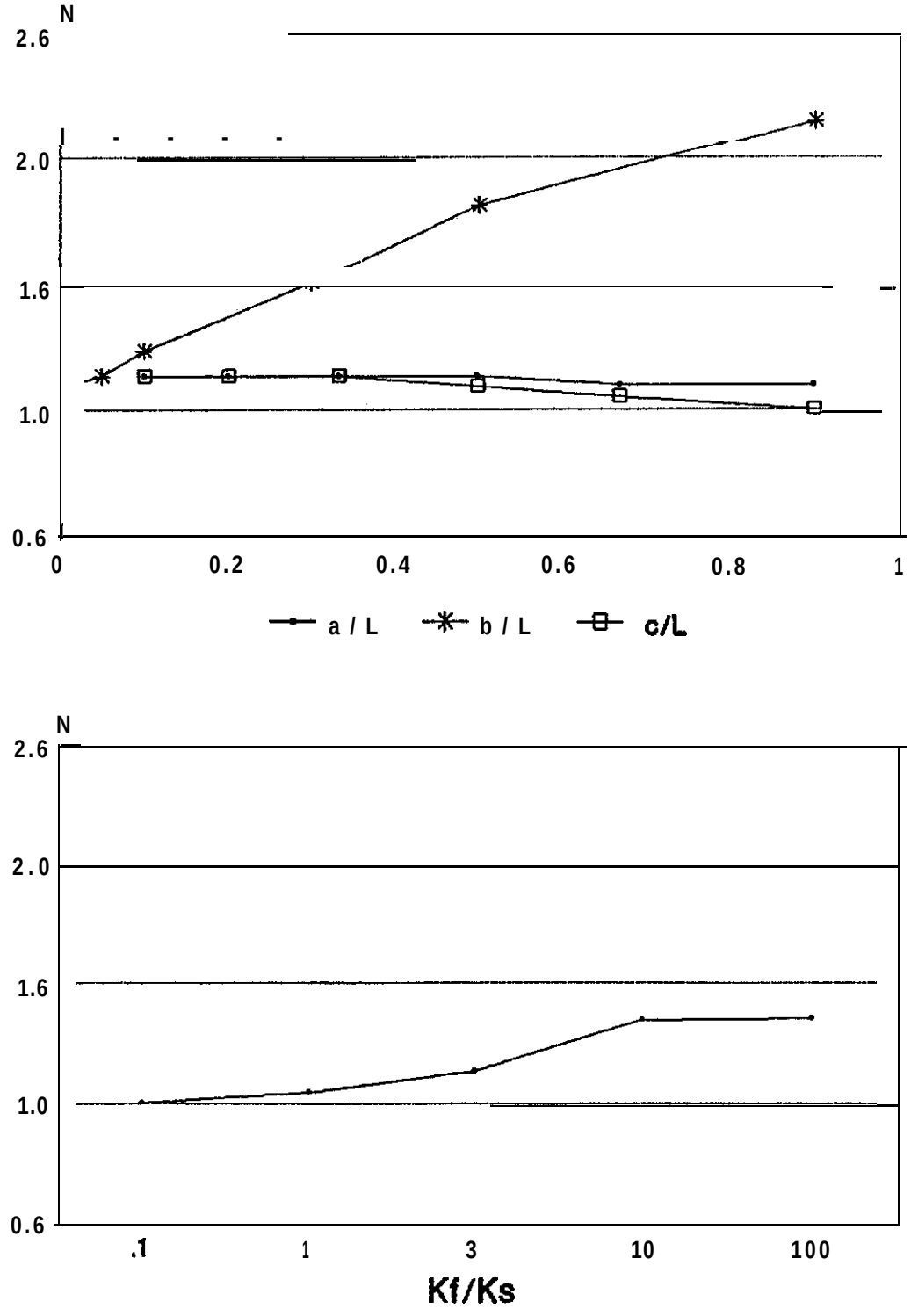

Figure 3.12 Sensitivity of fracture flow to input parameters a/L, b/B, c/L, and K_f/K_s.

Table 3.5

Distribution of parameters for jointed rock

variable	distribution	range	mean	variance	sensitivity
K_f/K_s	log normal	.1 - 100	3.0	23.26	0.0334
α/L	uniform	.1 - .67	0.333	0.037	-0.0564
b/L	log normal	.01 - .9	0.1	5.61×10^{-3}	1.508
c/L	uniform	.1 - .67	0.333	0.037	-0.06

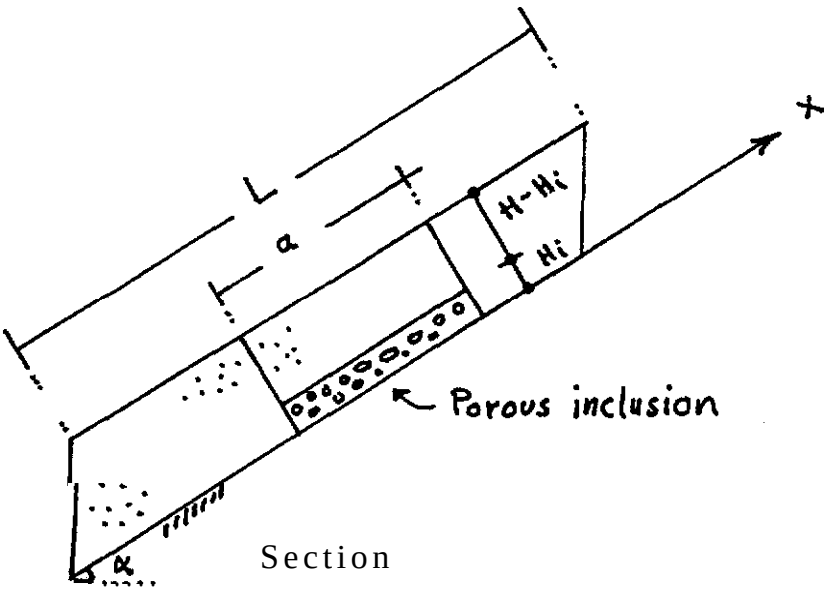

Section

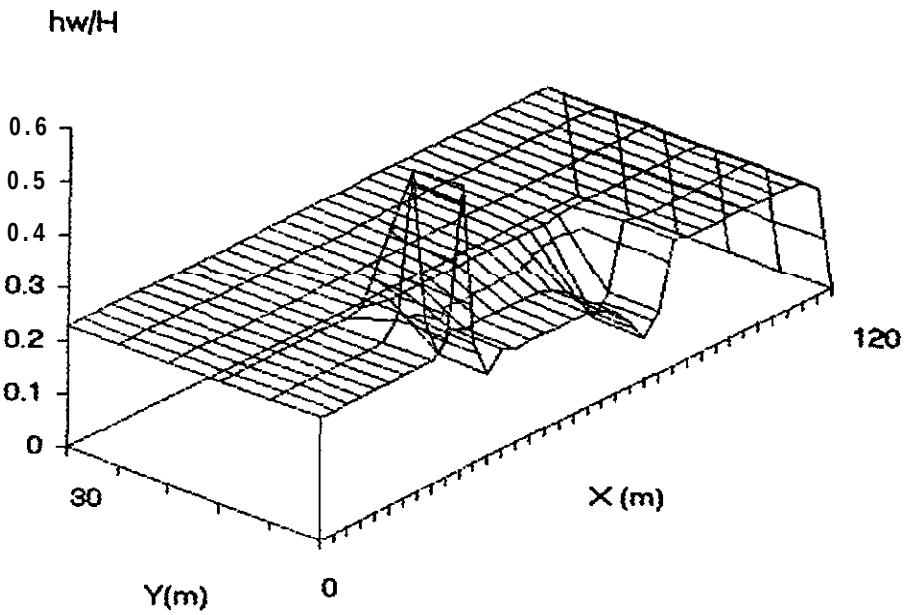

Figure 3.13 Flow through porous inclusion. (a) Model for flow through porous inclusion (b) Variation of h_w/Hwithin a slope. a = L/3 b = 20 m.

where K_i = permeability of the inclusion, and Hi = depth of inclusion. In the present case, the pumice layer is the porous inclusion, and K_i may be close to that of gravel, or as large as 3.6 x 10^4 cm/hr. Based on observations (Sec. 2.3.3), the pumice layer is considered to be continuous over the entire slope. Then K_P is used for K_s in the drainage submodel wherever the pumice layer is considered to exist. It is assumed that the pumice layer has an exit at the foot of the slope and drains freely. Hence, its net effect is to increase the downhill flow and drainage in the saturated zone. This reduces the value of h_o/H estimated with the lumped parameter model by about 20%. No uncertainties are assigned to this factor.

3.5 Prediction and Mapping of Piezometric Levels.

Prediction of piezometric levels can be made at several levels, with various degrees of refinement. In this report, we present two prediction levels that can be used later for landslide hazard mapping. The first prediction is for different storm intensities and for soil properties that represent the average condition (Sec. 2.3.1 and Table 3.1) throughout a large area, such as the focus township. This is the simplest approach. The precipitation for a given return period and mean snow depth were taken from the weather statistics compiled by Brunengo (1989), and a simplified snowmelt model (U.S. Army Corps of Engineers, 1956) was used to calculate the snowmelt on a cleared slope. Weather data for elev.2500 ft. and Dec 18 were used in the calculations because the elevation is about the middle of the transient snow zone and Dec 18 is about the midpoint of the winter storm season. A plane slope was assumed. The results of calculations with Reddi's model are shown in Fig. 3.14 as a plot of h_o/H versus the return period of the storm. It can be used as a first approximation of the piezometric level for input into a stability analysis, such as LISA (Hammond et al. 1991), which in turn, can be used to produce an approximate landslide hazard map. The plot is

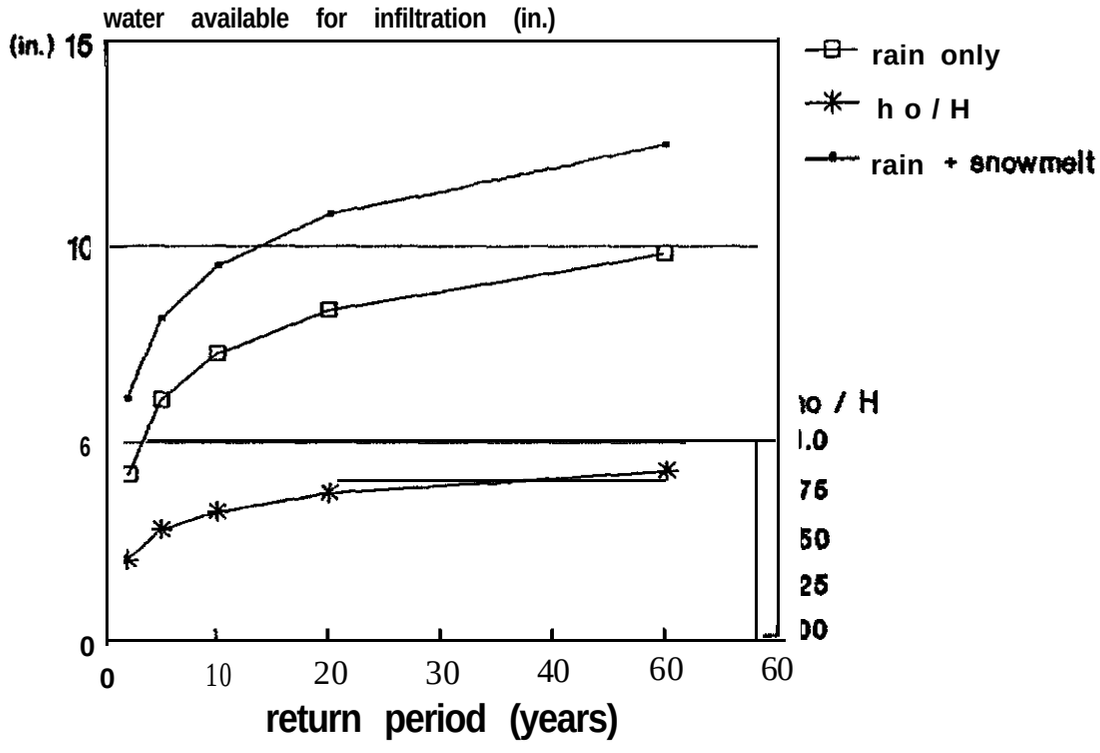

Figure 3.14 Mean piezometric level for storms of various return periods, cleared slope, elevation = 2500 ft., and weather data for December 18.

representative of the average site condition for the focus township and accounts for the uncertainty about the magnitude of the storm, but do not account for the various uncertainties discussed in the prededing sections.

A more detailed prediction can be made for the specific conditions at different locations within a broader region. The detailed calculations consider catchment shape (β, b, L), variation of h_w/H within a catchment (Sec. 3.2), and use soil properties for the specific locations. The results can be used to plot a map of the piezometric level. The following steps were employed to make such a map:

(1) The digital elevation model (DEM, from the U.S. Geological Survey) was read into the geographic information system (GIS) and used to determine the physical characteristics of catchments (Benosky, 1992). Micro Image's Map and Image Processing System (MIPS) and the Spatial Manipulating Language (SML) were used to identify the catchment boundaries and extract the catchment or watershed features, which are: perimeter, width, and flow path. This procedure is an outgrowth of the model developed by Jenson and Dominique (1988) and Marks et al. (1984). Specific software used in this project was written by Benosky (1992). The minimum size of a catchment was specified as 500 pixels ($0.45 km^2$). Clearly, the smaller the minimum size, the more detailed the map. In this case, we consider 500 pixels to be a reasonable compromise between level of detail and volume of computation. Further refinement is probably not justifiable considering the limitations in the available data on site conditions data. Fig 3.15 and 3.16 show the boundaries of the individual catchments in Glenoma quadrangle.

(2) The soil survey data provided by Washington Department of Natural Resources were read into the GIS using Arc/Info format. For each catchment, the average soil property was the area1 average of the properties of the soils in the

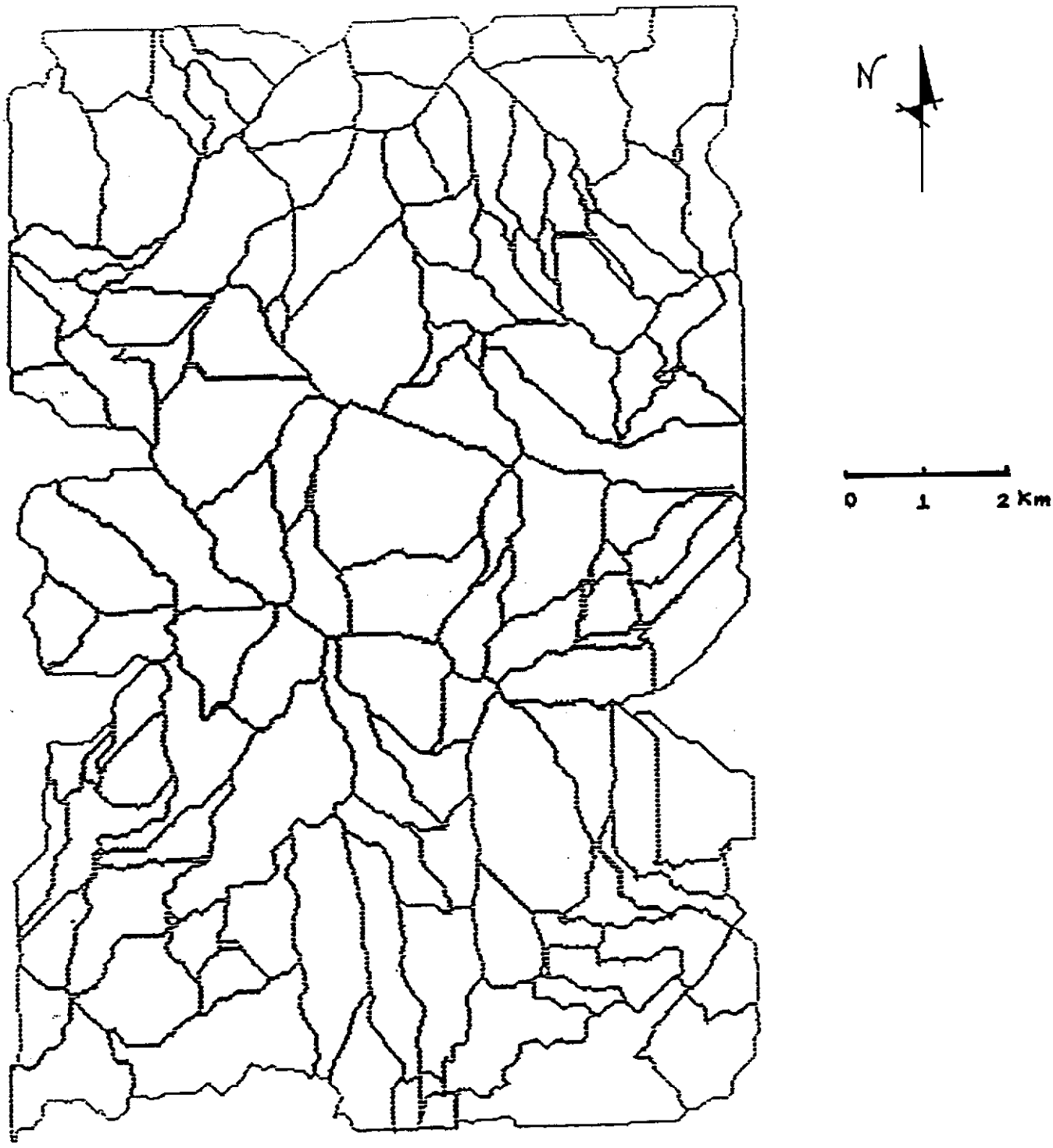

Figure 3.15 **Catchment** boundaries, Glenoma quadrangle, Washington. Blank areas are valley floors.

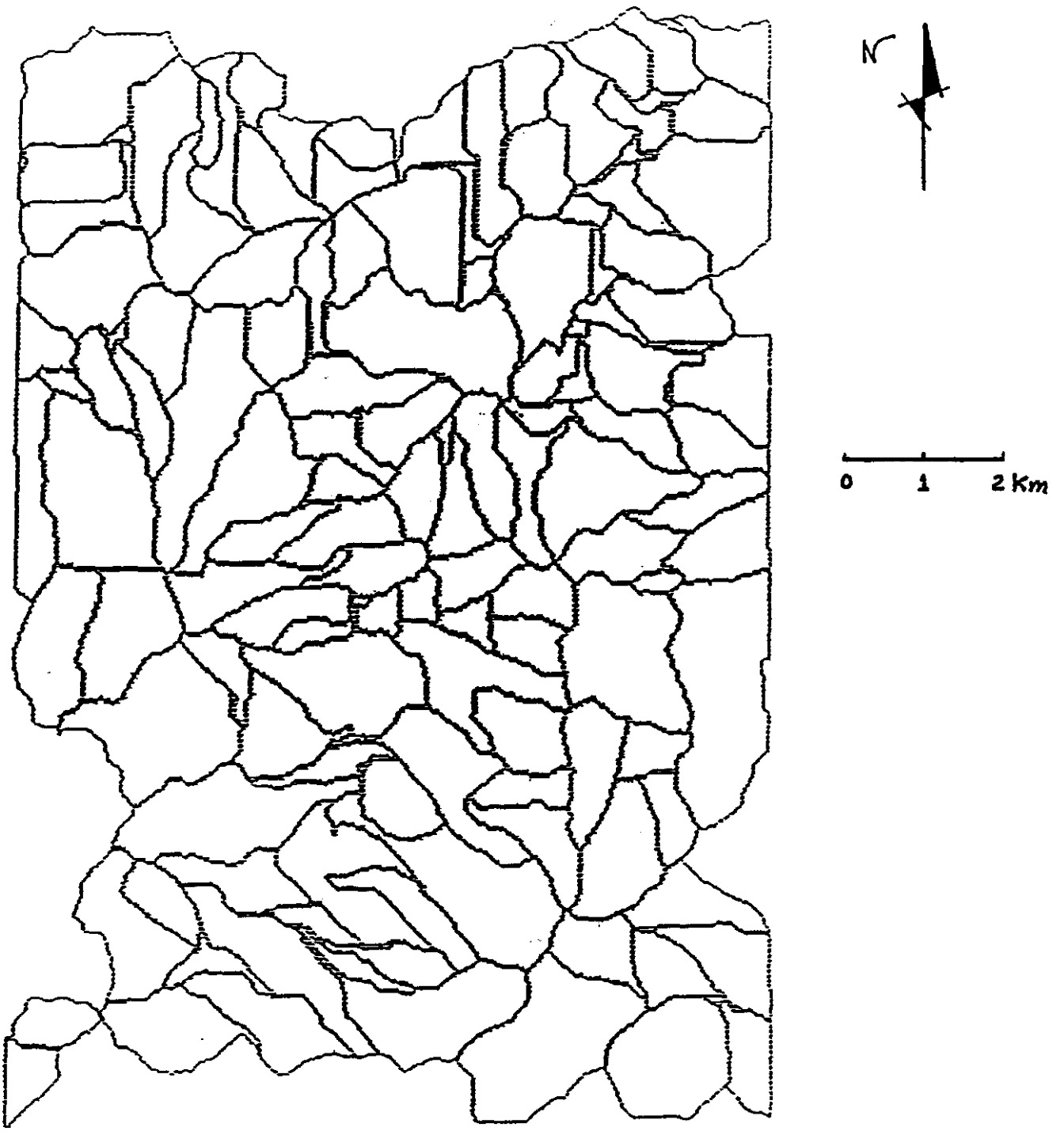

Figure 3.16 Catchment boundaries, Mineral quadrangle, Washington. Blank areas are valley floors.

catchment. The pumice layer was assumed to be present when "pumice" was mentioned in the soil profile. Then the permeability was calculated with Eq 3.3. We note that field observations (Sec. 2.4) and Brunengo (pers. comm., 1991) indicate that the pumice is widespread in the area. However, we have based the calculations on the soil reports for consistency in the procedure. The results of field observations can logically be incorporated in the updating process, as outlined in Wu and Merry (1992). For the same reason, these maps do not include the effects of flow through rock joints.

(3) The largest storm within a period of 10 years (design life) was assumed to fall on a cleared slope. The mean and variance of the storm precipitation were calculated (Appendix D) and the U. S. Army's (1956) snowmelt model was used to compute the melt. As before, weather data for elev. 2500 ft. and Dec 18 were used in the calculations. The value of h_o/H was calculated for each catchment by Reddi's model. The values of h_w/H at different points within a catchment were calculated through the use of the correction factors in Table 3.3. The computed piezometric levels for cleared slopes were plotted as maps for Glenoma and Mineral quadrangles, as given in Fig 3.17 and 3.18

(4) The rain-plus-snow melt on forested slopes was estimated empirically, because data on temperature and wind speed under forest canopy are not available and the snowmelt model can not be used. Based on the observations Coffin and Harr (1992) that rain-plus-snowmelt on clear-cut slopes may be 20-50 % higher than that on forested slopes, we used a rain-plus-snowmelt equal to 0.8 times that calculated in part (3). The remaining procedures were the same as described in (3). The computed piezometric levels for forested slopes are also shown in Figs 3.17 and 3.18. We note that these are computed for average conditions. In the FOSM approach the piezometric levels are the expected maximum values in a 10 year period.

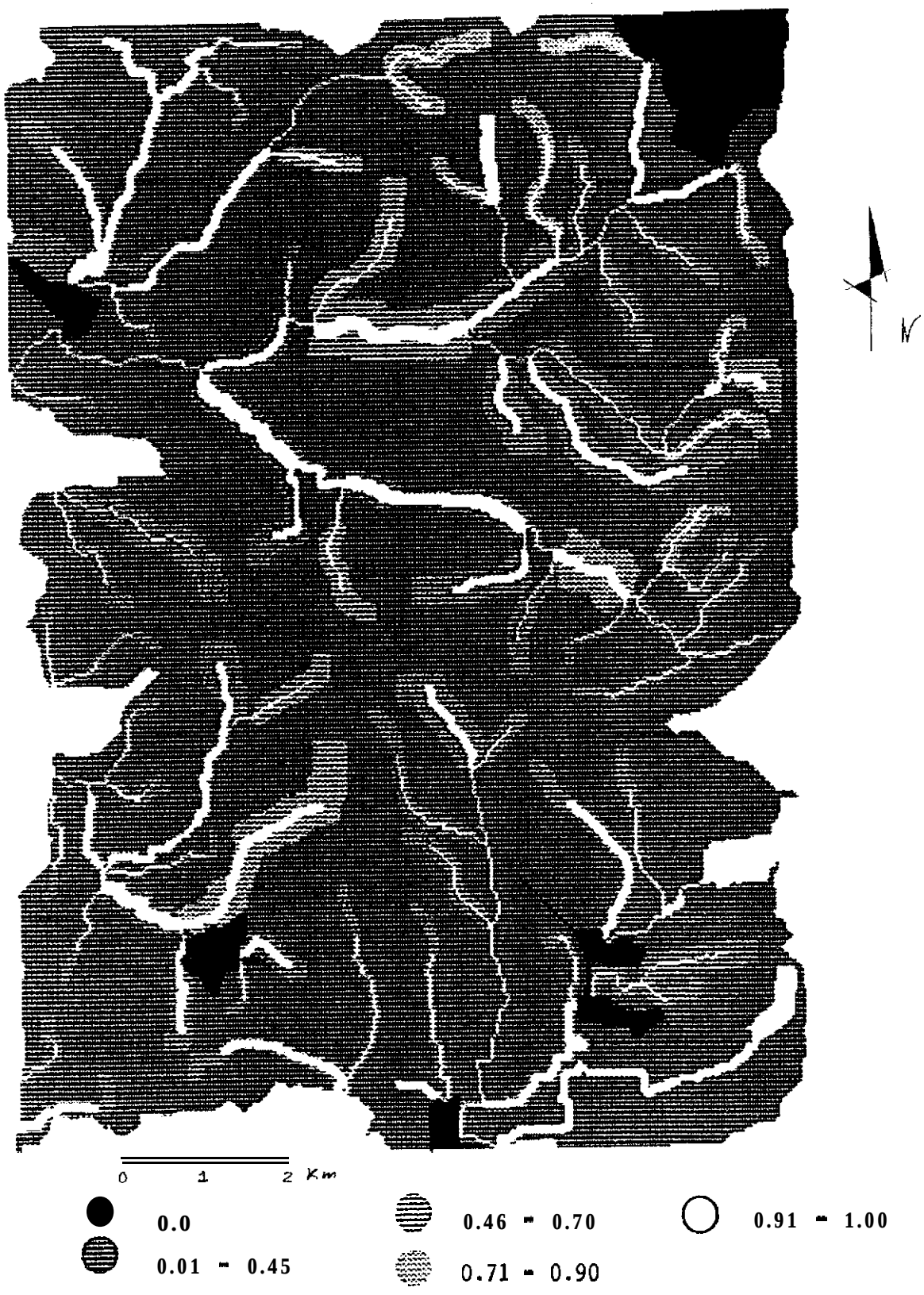

Figure 3.17a Piezometric level map for Glenoma quadrangle, cleared slopes. Catchment boundries are shown in Fig. 3.15.

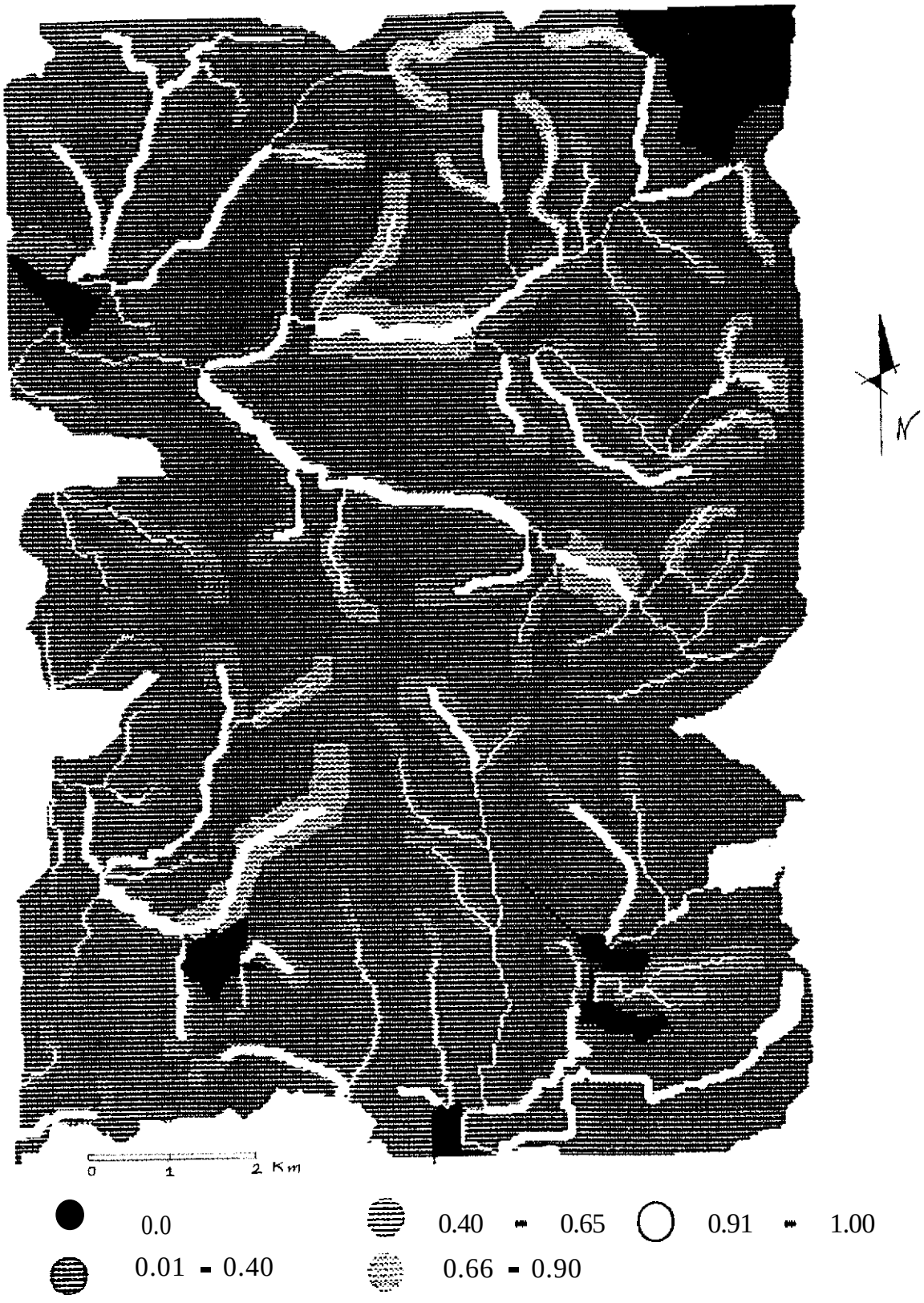

Figure 3.17b Piezometric level map for Glenoma quadrangle, forested Slopes. Catchment boundries are shown in Fig. 3.15.

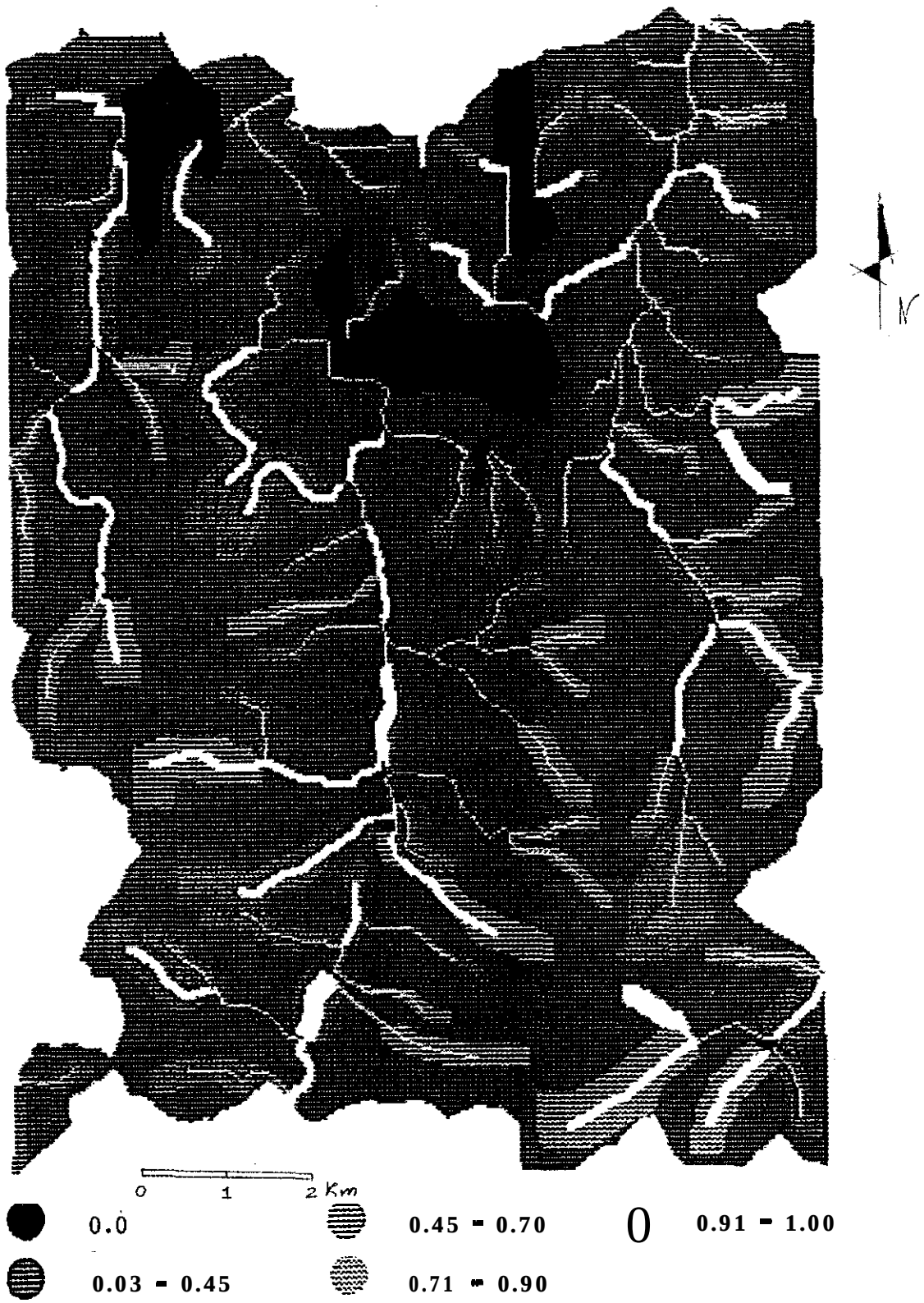

Figure 3.18a Piezometric level map for Mineral Quadrangle, cleared slopes. Catchment boundries are shown in Fig. 3.16.

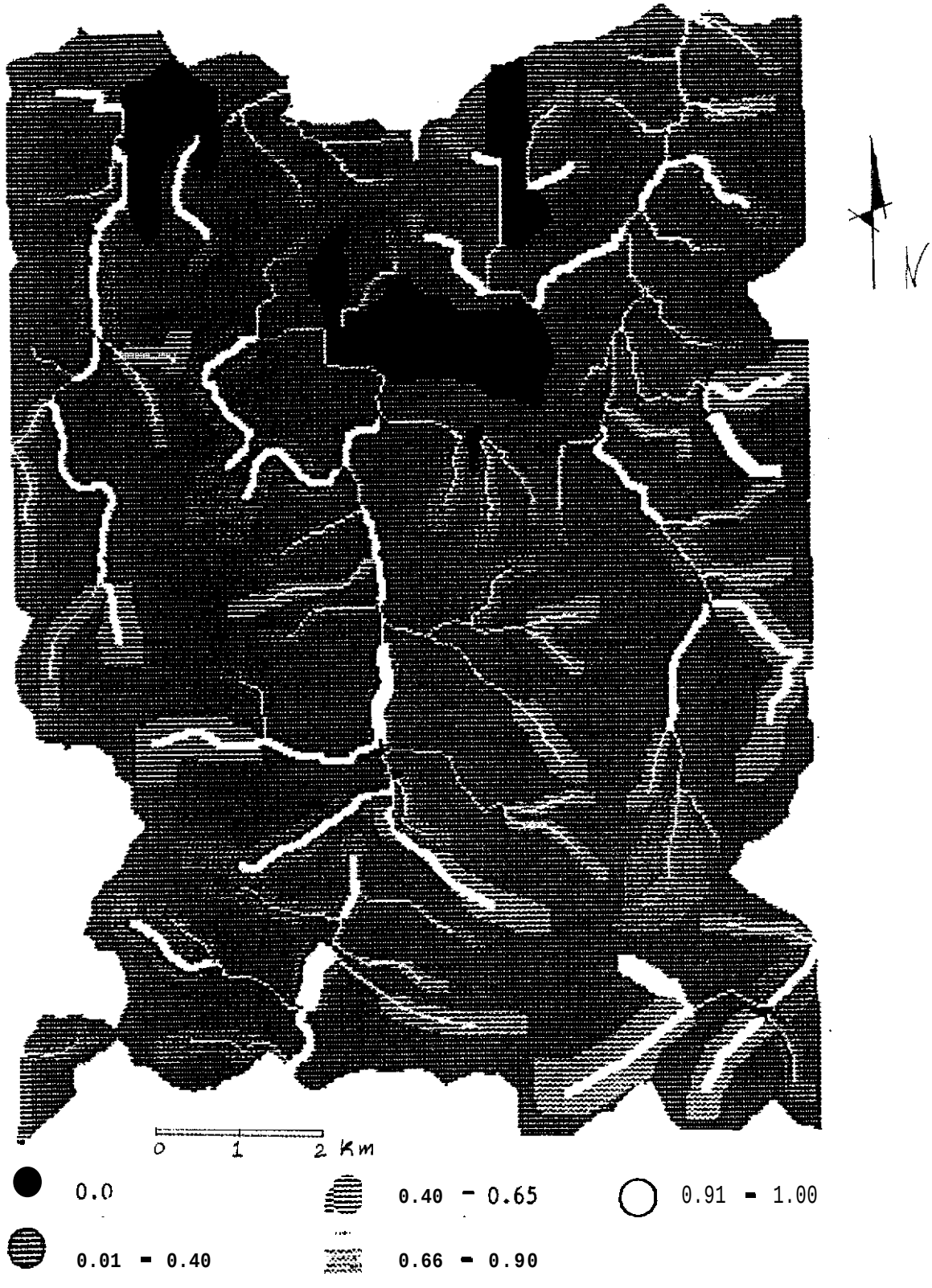

Figure 3.18b Pieometric level map for Mineral quadrangle, forested slopes. Catchment boundries are shown in Fig. 3.16.

3.6 Uncertainties about Piezometric Levels

The uncertainties about the predicted piezometric levels are the result of uncertainties about rainfall and snowmelt, soil properties, and slope geometry. The uncertainties about rainfall are caused by the uncertainty about the maximum precipitation and the antecedent moisture in the soil, which in turn depends on the number of storms and the interval between storms. This problem and the probability of a given rainstorm falling on a particular snow depth, is analyzed in Appendix C. The results are the mean and variance of the maximum annual rainfall plus snowmelt.

Within a large region or watershed, uncertainties about the average site conditions arise because of insufficient data or observations used to compile the soils report. The range in soil properties (Table 3.1) represents the uncertainties. It was assumed that the distribution was uniform and this distribution was used to calculate the variance. Figures 3.1 – 3.3 show the sensitivity to the soil parameters, which are listed in Table 3.1. The computed sensitivities of h_o/H to the input variables and the variances of the input were used in the FOSM formulation to calculate the variance of h_o/H

$$\mathrm{Var}\left(\frac{h_o}{H}\right) = \left(\frac{\partial \frac{h_o}{H}}{\partial K}\right)^2 \mathrm{Var}(K) + \left(\frac{\partial \frac{h_o}{H}}{\partial B}\right)^2 \mathrm{Var}(B) + \left(\frac{\partial \frac{h_o}{H}}{\partial \psi}\right)^2 \mathrm{Var}(\psi) + \left(\frac{\partial \frac{h_o}{H}}{\partial \theta_d}\right)^2 \mathrm{Var}(\theta_d)$$

$$+ \left|\frac{\partial \frac{h_o}{H}}{\partial \theta_s}\right|^2 \mathrm{Var}(\theta_s) + \left|\frac{\partial \frac{h_o}{H}}{\partial H}\right|^2 \mathrm{Var}(H) + \left(\frac{\partial \frac{h_o}{H}}{\partial K}\right)\left(\frac{\partial \frac{h_o}{H}}{\partial \theta_d}\right) \mathrm{COV}(K, \theta_d)$$

$$+ \left(\frac{\partial \frac{h_o}{H}}{\partial \theta_s}\right)\left(\frac{\partial \frac{h_o}{H}}{\partial \theta_d}\right) \mathrm{Cov}(\theta_s, \theta_d) \qquad (3.4)$$

In this study positive correlation is assumed between drainable porosity, θ_d and permeability, K, and also between saturated water content, θ_s and porosity, 8,. The computed variance of h_o/H due to uncertainty about the mean soil properties is given in Table 3.6.

In addition, the values of h_w/H within a catchment contain uncertainties due to spatial variation of soil and rock properties (Sec. 3.3), such as flow through fractures (Sec. 3.4). The variances of h_o/H are given in Table 3.6 as spatial variation of soil properties and rock fractures, respectively. The topographic maps and DEM were assumed to be correct and the uncertainty about the slope geometry was assumed to be zero. The value of h_w/H also depends on the storm characteristics: the precipitation and snowmelt associated with the largest storm, the number of storms per season, and the antecedent moisture content θ_i, which depends on the number of storms and the time interval between storms. The effects of these uncertainties on h_w/H were calculated (Appendix C). All the uncertainties are summarized in Table 3.6. The total variance is a measure of the uncertainty about h_w/H, or its probable deviation from the mean h_w/H, calculated with the average conditions. The variance is used in Sec 3.7 to calculate the probability of h_w/H exceeding h_{wc}/H, which is the critical value that would initiate a landslide.

3.7 Probability of Failure

For landslide hazard mapping, we need the probability that the critical piezometric level, h,,, may be exceeded. The uncertainties in Table 3.6 were used to calculate the coefficient of variation of h_w/H and the probability $P[h_w/H \geq h_{wc}/I\text{-}I]$. We propose to produce landslide hazard maps at three different scales or levels, as shown in Table 3.7 (Wu and Merry, 1992). The macro-map would show the hazard for an area of approximately 10 km x 10 km, such as Glenoma quadrangle. It would identify all areas

Table 3.6

Uncertainties about input to the hydrologic model

Source of Uncertainty	Variance of h_o/H
number of storms per season	0.0279
duration and amount of infiltration	0.0493
interval between storms	0.0000
uncertainty about mean	0.0337
Spatial variation	0.0008
fractures in rock	0.0388
Total	**0.1505**

Table 3.7

Proposed mapping scales

Level	Site Conditions	Area (km^2)	Resolution (m^2)
1. Macro-map	average	100	$10^4 - 10^6$
2. Refined macro-map	spatial variation	100	$10^4 - 10^6$
3. Micro-map	spatial variation geologic anomalies catchment shape	10	1000

with a failure probability, P_f, exceeding a specified threshold value, P_{fo}, in a storm with a given return period T_o, or a design life T_L. The values of P_f and T_L are to be defined by knowledgeable scientists or managers. As an illustration we made a trial calculation for a IO-year period or lifetime with the mean of the largest storm (Appendix D) falling on mean snow depth for December and average site condition. The uncertainties are those about the average soil properties (Table 3.1) and the storm characteristics (Table 3.6). The results are shown in Fig. 3.19, in which the shaded portions represent areas with an annual failure probability $P_f > 0.1$. This is admittedly a very approximate map because of the simplified input. More refined macro-maps can be made, and incorporation of the landslide inventory into the hazard map has been proposed by Wu and Merry (1992).

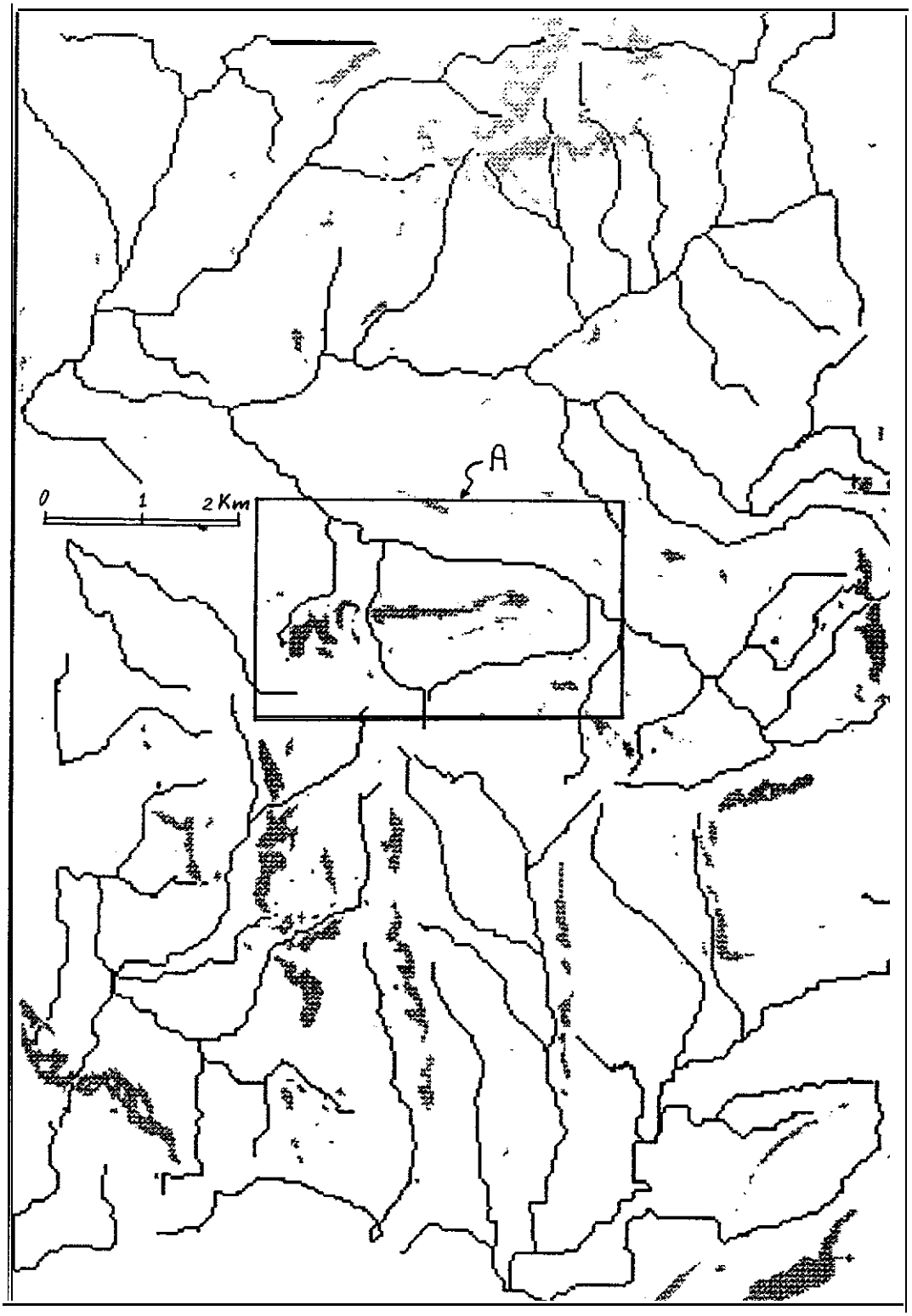

Figure 3.19 Preliminary landslide hazard map (a) Glenoma quadrangle.

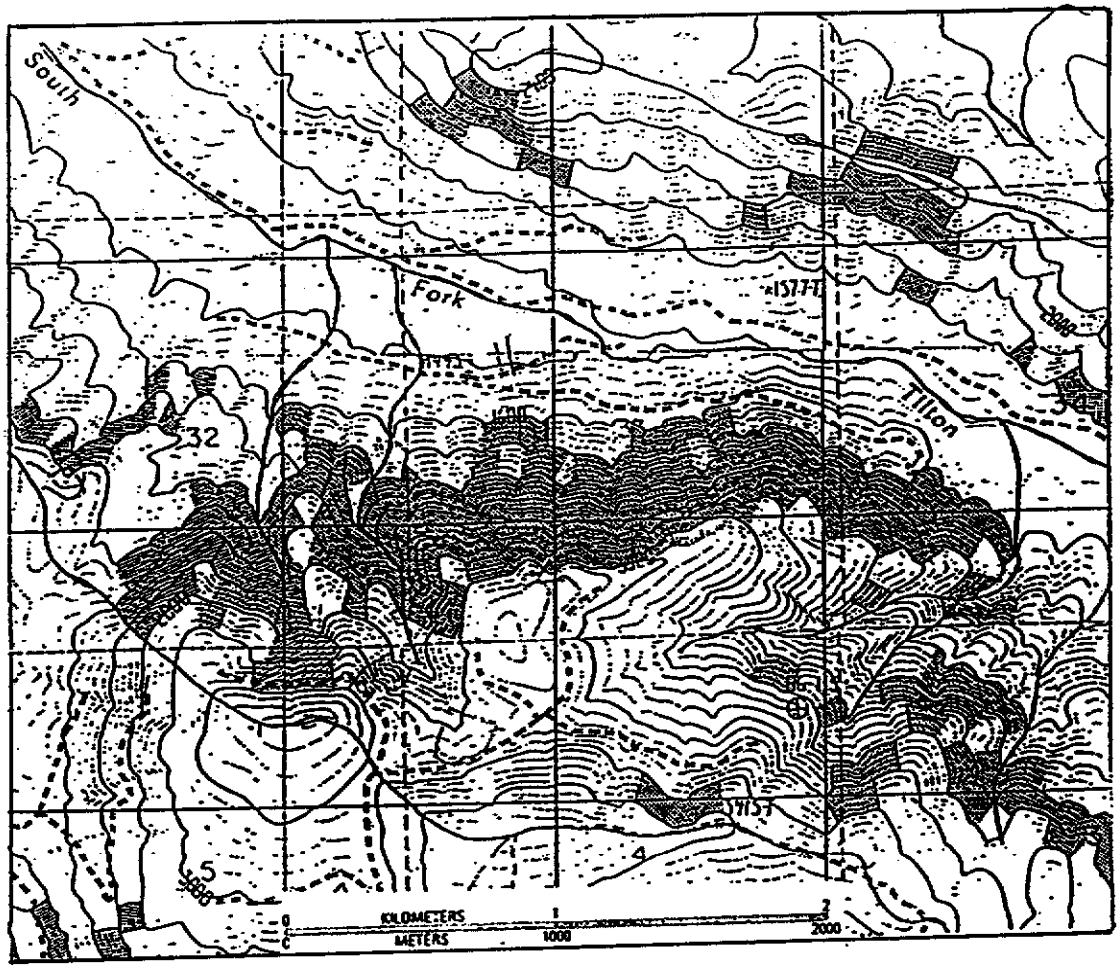

Figure 3.19 Preliminary landslide map (b) zoneA enlarged.

CHAPTER IV

SUMMARY

The results obtained to date show that comparatively simple calculations using Reddi's lumped parameter model can be used to predict changes in piezometric level due to infiltration of rain or rain-plus-snowmelt. A senssitivity analysis showed that, for the site conditions in the focus township, the pieaometric level (h_o/H) is sensitive to rainfall (R) and soil depth (H), less sensitive to drainable porosity (θ_d) and saturated permeability (K_s), and not sensitive to slope length (L) and unsaturated permeability (B and ψ_s). The important physical parameters R, H, and θ_d can be combined into one dimensionless parameter $\kappa = R/H\theta_d$, which is the ratio of rainfall (equal to infiltration in this case) to the pore volume.

Methods have been developed to account for variations in groundwater water level within a catchment due to catchment shape, flow through fractures in bedrock, and flow through porous inclusions. Catchment shape, has an important influence on the piezometric level. A converging slope, that represents a catchment, concentrates the flow in the valley floor and increases the piezometric level (h_w/H) in the valley floor. In most cases, h_w/H in the valley floor of a catchment is equal to h_o/H at the exit point of the slope. Spatial variations in permeability may increase the local piezometric level (h_w/H) to twice the value for uniform permeability. The presence of a pumice layer reduces the piezometric level to $2/3$ of that when there is no pumice layer. Flow through fractures in bedrock may raise the piezometric level h_w/H at the exit point of the flow path to twice the value of h_w/H when there is no flow through fractures. It should be noted that the catchment shape and presence of pumice layer are assumed to be known from topographic maps and soils report, respectively. These are treated as deterministic inputs used to calculate the mean piezometric levels. On the other hand

spatial variations and flow through fractures are probabilistic because their presence is not known with certainty. They contribute to the uncertainty about predicted piezometric levels and their effect is included in the variance of the predicted piezometric level.

Two types of predictions were made for piezometric levels. The average site condition was used to produce a chart that shows the piezometric level in a plane slope as a function of the return period (Fig. 3.14). It can be used as a first approximation of the piezometric level for input into a stability analysis, such as LISA (Hammond et al. 1991), which in turn, can be used to produce an approximate landslide hazard map. The plot is representative of the average site condition for the focus township and accounts for the uncertainty about the magnitude of the storm, but does not account for the various uncertainties discussed in the preceding sections. Maps of piezometric-level were made for parts of Glenoma and Mineral quadrangles (Fig. 3.17 and 3.18) by using local site conditions and accounting for individual catchments, which were delineated by MIPS operating on data in the GIS. The maps provide more detail than the plot in Fig. 3.14 and identify the variations in piezometric level within a quadrangle and within individual catchments. It shows where piezometric levels are likely to be highest. Those maps could be used as input into a stability analysis to produce a detailed landslide hazard map. In the meantime the piezometric levels, expressed as a ratio h_w/H, can be used as a rough guide on the likelihood of landslides.

In preparation for landslide hazard mapping, we have evaluated the uncertainty about the predicted piezometric levels. We have evaluated the probability distributions of precipitation, and the probabilities of material properties, which include those of the soil, rock fracture, and porous inclusions. These will be used as input to the slope stability model to estimate probabilities of slope failure. We have also made preliminary calculations of the failure probability and show a preliminary landslide hazard map of

Glenoma Quadrangle as illustration (Fig. 3.19). This map was constructed with average site conditions and the IO-year storm (Fig. 3.14). Such a map can be used for preliminary planning. Detailed landslide hazard maps can be produced using the maps of piezometric levels (Fig. 3.17 and 3.18). These will be done in the as Part 2 of landslide hazard mapping.

APPENDIX A

THE LUMPED PARAMETER MODEL

The lumped parameter model of Reddi and Wu (1991) considers infiltration through the unsaturated zone (Fig. A.1a), and the drainage by gravity flow in the saturated zone (Fig. A.2b). The governing equations for infiltration are:

$$v_j = 0.5K(\theta)\left(\frac{\psi_j - \psi_{j-1}}{Z_j} + 1\right) + \left(\frac{\psi_{j-1} - \psi_j}{Z_{j+1}} + 1\right) \tag{A.1}$$

$$v_o = (i - \alpha_e E_e) \tag{A.2}$$

$$q = v_2 - \Delta\theta_3 Z_3 \tag{A.3}$$

v_{j-1}, v_j = velocity at the top and bottom of the j th layer (Fig. A.1), i = rainfall intensity, E_e = equilibrium evapotranspiration, α_e = evapotranspiration coefficient, K = permeability coefficient, θ = volumetric moisture content, θ_d = drainable volumetric water content, ψ = potential, q = infiltration into the saturated zone. The unsaturated permeability is

$$K(\theta) = K_s\left(\frac{\theta}{\theta_2}\right)^{2B+3} \tag{A.4}$$

and

$$\psi(\theta) = \psi_s\left(\frac{\theta}{\theta_s}\right)^{-B} \tag{A.5}$$

where θ_s = volumetric water content at saturation; ψ_s and B are soil properties

(a)

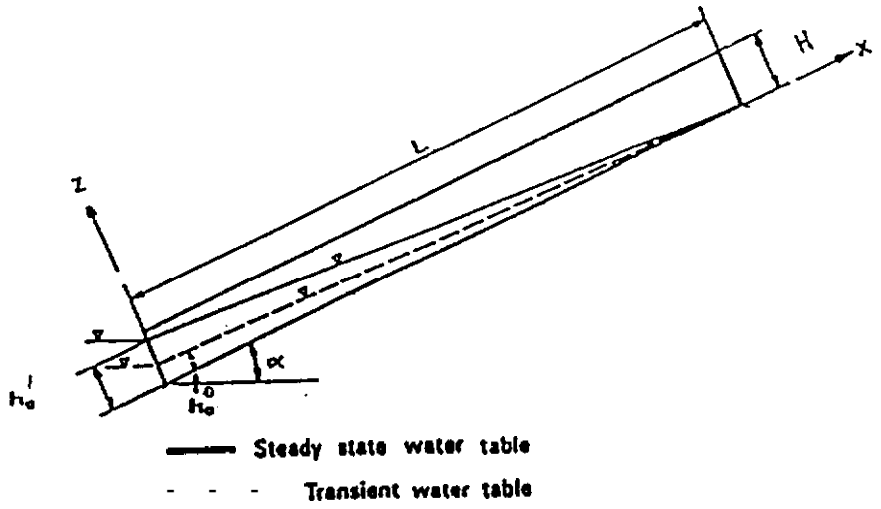

(b)

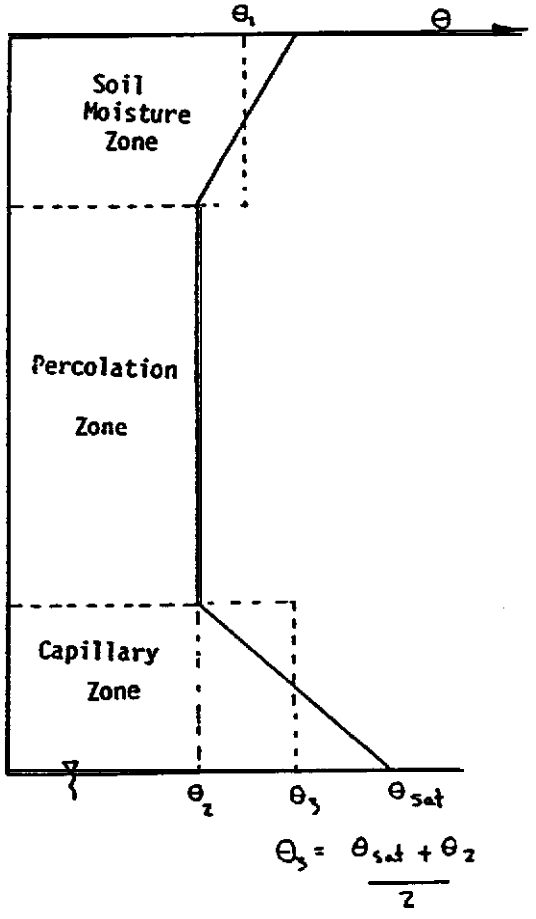

Figure A. Kinematic storage model, (a) saturated zone, (b) unsaturated zone (Reddi and Wu, 1991).

The drainage rate is

$$v = K_s \sin \alpha \tag{A.6}$$

where K_S = saturated permeability. The groundwater level at time t = 1 is

$$h_o^1 - \frac{h_o^o(L\theta_d - v\Delta t) - 2L\ i\Delta t}{L\theta_d + v\Delta t \quad L\theta_d - vAt} \tag{A.7}$$

From this,

$$h_o^1 - h_o^o \frac{1-\lambda}{1+\lambda} = \frac{2\ i\Delta t}{\theta_d(1-\lambda)} \tag{A.8}$$

where

$$\lambda = \frac{v\Delta t}{L\theta_d} \tag{A.9}$$

For purposes of stability analyses, the ratio ho/H is significant. From Eq. (A.8), we obtain

$$\frac{h_o^1 - h_o^o \frac{1-\lambda}{1+\lambda}}{H} = \frac{2i\Delta t}{\theta_d H(1-\lambda)} \tag{A.10}$$

From thii, we see that if v is small, or λ is small, which means that the drainage rate is insignificant. Then

$$\frac{h_o^1 - h_o^o}{H} \rightarrow \frac{2i\Delta t}{H\theta_d} \tag{A.11}$$

Then the change in ho is directly proportional to the precipitation $i\Delta t$.

Appendix B

FLOW THROUGH FRACTURES IN BEDROCK

A 2-dimensional finite difference analysis was used to investigate the effects on the groundwater level caused by flow through fractures in bedrock. Fig. B.1 illustrates the idealized problem. The following assumptions were adopted: (1) There is one continuous path through fractures in the bedrock. This means that the flow through fractures can be represented by a single hydraulic connection with an equivalent permeability. (2) The only potential for the flow in the hydraulic connection is the piezometric head in the soil layer. (3) The fracture is saturated with water and the flow obeys Darcy's law. (4) The geometry of the irregular flow path is represented by a circular arc. This has little effect on the accuracy of calculation since the head difference does not depend on the shape of the arc and the arc length is close to that of the irregular path. (5) The distance between the entrance and exit points (1 and 2 in Fig. 3.9) of the path is assumed to be at the one-third points of the plane slope; this assumption is in accordance with the site characteristics reported by Brunengo (pers. comm., 1991). A more detailed study can be done by varying the locations of the fractures, distances between the entrance and exit, as well as the coefficients of permeability.

The 2-dimensional finite difference model of Lee (1986), was modified to solve the problem. Following Lee's derivation, the governing equation for flow in isotropic porous media at node 1 is:

$$C\frac{\partial h_w}{\partial t} = Q_r \cos\alpha - Q_f + \frac{\partial}{\partial y}\left[K_s h_w\left\{\cos\alpha\left(\frac{\partial h_w}{\partial y} + \frac{\partial H_t}{\partial y} - \frac{\partial H_s}{\partial y}\right) + \tan\gamma\right\}\right]$$

$$+\frac{\partial}{\partial x}\left[K_s h_w\left\{\cos\alpha\left(\frac{\partial h_w}{\partial x} + \frac{\partial H_t}{\partial x} - \frac{\partial H_s}{\partial x}\right) + \sin\alpha\right\}\right] \qquad \text{(B.1)}$$

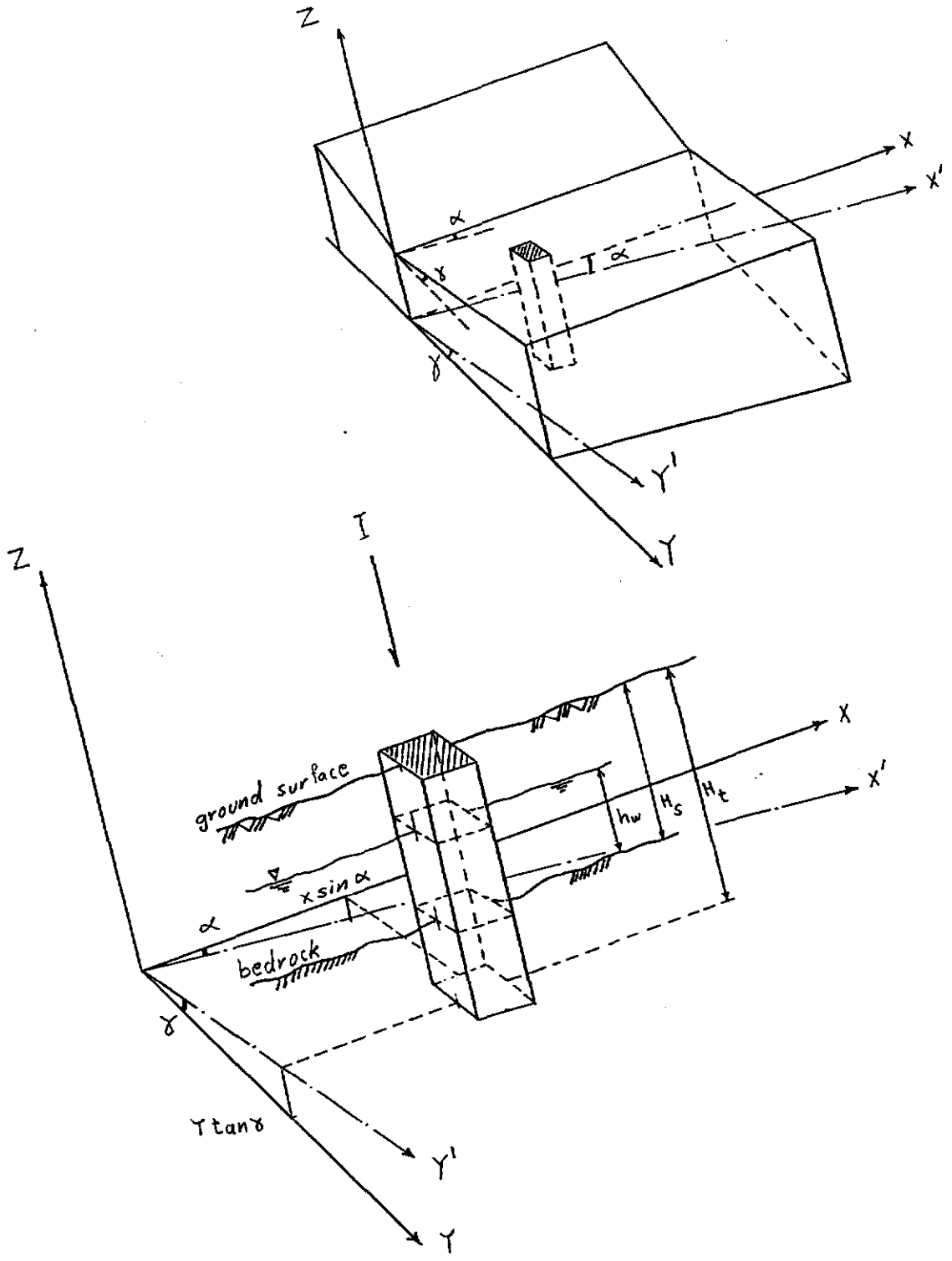

Figure B.l Geometric parameters of two-dimensional model (Lee, 1986), (a) slope geometry, (b) dimensions of **element**

At node 2, the governing equation is:

$$C\frac{\partial h_w}{\partial t} = Q_r \cos\alpha + Q_f + \frac{\partial}{\partial y}\left[K_s h_w\left\{\cos\alpha\left(\frac{\partial h_w}{\partial y} + \frac{\partial H_t}{\partial y} - \frac{\partial H_s}{\partial y}\right) + \tan\gamma\right\}\right]$$

$$+\frac{\partial}{\partial x}\left[K_s h_w\left\{\cos\alpha\left(\frac{\partial h_w}{\partial x} + \frac{\partial H_t}{\partial x} - \frac{\partial H_s}{\partial x}\right) + \sin\alpha\right\}\right] \qquad \text{(B.2)}$$

where C = specific yield, Qr = recharge to the saturated zone, and Q_f is given by Eq. B.3. Geometric variables used in Eqs B.l, and 8.2 are explained in Fig. B.l. For flow through fractures,

$$Q_f = I_g b_f K_f t \qquad \text{(B.3)}$$

$$I_g = \frac{x + (h_{w1} - h_{w2})\cos\alpha}{(\pi a_f)/2} \qquad \text{(B.4)}$$

where x = the difference in elevation between point 1 and 2 (Fig. 3.9), b_f = width of fracture, a_f = distance between entrance and exit points, K_f = permeability of the fracture, Q_f = flow through the fracture, t = time, h,,, h_{w2} = piezometric head at nodes 1 and 2, respectively, and I, = hydraulic gradient. The differential equations (B.l) and (B.2) are solved by the finite difference method for given dimensions of the slope and fracture to give the values of h_W, which were used to construct Fig. 3.10 and 3.11.

Appendix C

EFFECTS OF STORM CHARACTERISTICS

Cl Storm Precipitation

We consider the data on long continuous stormscompiled by Brunengo (1989). The amount of rainfall per storm is modeled by the EV-1 distribution, (Gumbel, 1958):

$$P(X \leq x) = \exp(-\exp(-y)) \tag{C.1}$$

$$y = a\,(x-u) \tag{C.2}$$

where u = location factor and a = a scale factor. The mean and standard deviation of the distribution are:

$$\mu = u + \frac{\varepsilon}{a} \tag{C.3}$$

$$\sigma = \frac{\pi}{a\sqrt{6}} \tag{C.4}$$

where ε = Euler's constant, approximately equal to 0.577. The parameters u and l/a can be estimated as a function of the mean $\bar{x}$ and standard deviation Sx:

$$\frac{1}{\alpha} = S_x \frac{\sqrt{6}}{\pi} \cong .78\, S_x \tag{C.5}$$

$$\mu = \bar{x} - S_x\, \varepsilon \frac{\sqrt{\bar{x}}}{\pi} \cong \bar{x} - 0.45\, S_x \tag{C.6}$$

The rainfall for a given exceedance probability, P, or return period, t_o, is calculated using Eqs. C.7 and C.8, respectively:

$$R_P = u - \frac{1}{a}\left[\ln \ln\left(\frac{1}{1-P}\right)\right] \tag{C.7}$$

$$R_P = u - \frac{1}{a}\left[\ln \ln\left(\frac{t_o}{t_o - 1}\right)\right] \qquad (C.8)$$

The values of u and l/a for long continuous storms are 4.02 and 1.78, respectively, which are the averages of the values given in Table 3.3 of Brunengo (1989). The corresponding mean μ is 5.04 inches and the standard deviation σ is 2.28 in. These values were used in the study of the sensitivity of hw against soil and topographic parameters. The probability of occurrence, P, of this 5.04 inch storm is 0.4, corresponding to a recurrence interval of 2.5 year.

Figure C.1a shows the effect of precipitation on maximum h_o/H. The sensitivity of maximum ho/H to rainfall, R, is equal to 7.58x10-2 in^{-1}.

C.2 Storm Duration

The distribution of storm duration is approximated as log-normal. The mean value for long continuous storms at all stations is 66.9 hr, and the standard deviation is 35.97 hr Brunengo, (1989). Fig. C.1b shows the plot of storm duration against precipitation for 168 recorded storms. The duration is correlated with the amount of precipitation by Eq. C.9.

$$R = 0.0729\ D \qquad (C.9)$$

where D is the duration in hours and R is the rainfall in inches. The correlation coefficient for Eq. C.9 is 0.748. If we apply this relation to the selected average precipitation of 5.04 in, the duration is 68.58 hr. The effect of storm duration on ho/H is shown in Fig. C.2 for R = 5.04 in.. The sensitivity of h_o/H is found to be 5.8 x 10^{-4} hr^{-1}

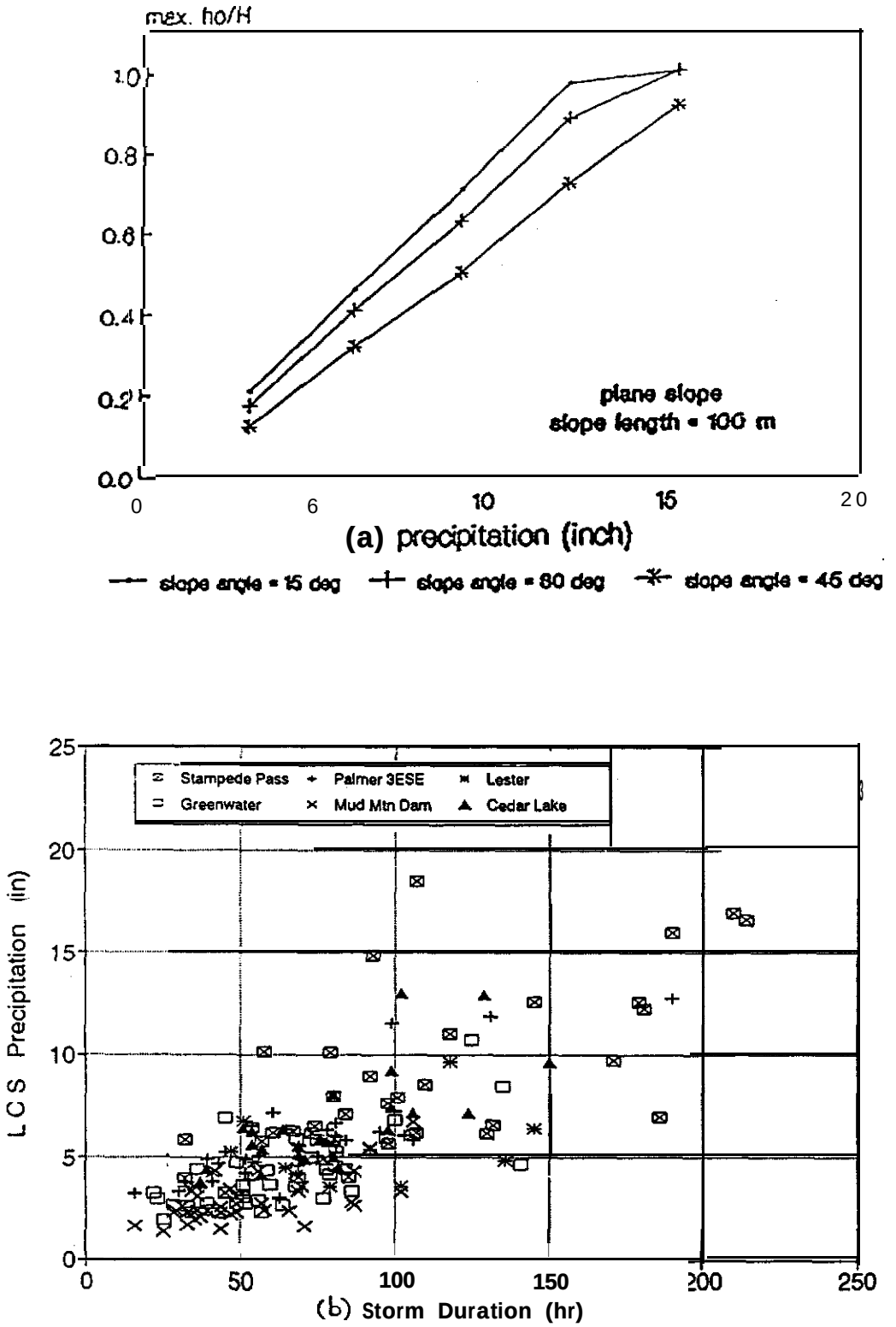

Figure C.1 (a) 'Effect of precipitation, R, on h_o/H, (b) Scatter graph of storm duration vs. precipitation (Brunengo, 1989).

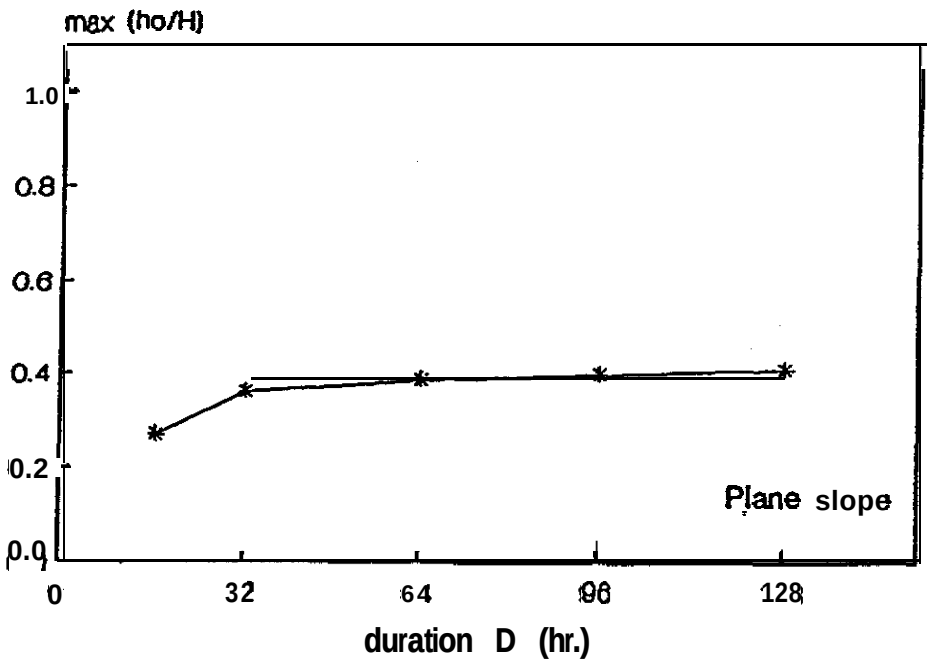

Figure C.2 Effect of storm duration, D, on groundwater level h_w/H for R = 5.04 in..

C.3 Model of Snowmelt

During rain-on-snow events, snow melts because of the combination of relatively warm temperatures and moderate winds that accompany the storm. Although most of the infiltration is due to rainfall, this melt represents a significant additional source of water. The total amount of infiltration is the sum of precipitation and snowmelt.

The main energy source for snowmelt is exchange by convection and condensation at the air-snow interface. Longwave radiation is also major source of snowmelt. Heat conduction from the ground and heat contributed by the precipitation increase snowmelt. Wiberg (1990) used the United States Army Corps of Engineers' (1956) snowmelt model to study the characteristics of snowmelt in the central Cascades of Washington. The total amount of potential snowmelt is

$$M_T = M_C + M_S + M_R = (0.029 + 0.0084\ kU)(T_\alpha - 32)\ D + 0.007\ (T_\alpha - 32)\ R \qquad (C.10)$$

where M_T = total amount of potential snowmelt, M_C = snowmelt due to convection - condensation and longwave radiation, M_S = snowmelt due to short-wave radiation and ground heat, M_R = snowmelt due to rainfall, k = exposure constant (equal to 1.0 in clearcut areas), D = the duration in days, U is wind velocity, T_α = air temperature, and R = rainfall. The parameters U, T, D, and R are all considered as random variables, and as a result, the snowmelt is also a random variable. The average values used in this study are k = 1, D = 2.5d, U = 13.4 m/h, T_α = 35.61°F, and R = 5 in.

The computed distribution of potential snowmelt is shown in Fig. C.3a. However, the actual melt is constrained by the available snow-water-equivalent on the ground. To account for that, two cases are possible. In the first case, the snow-water equivalent, S, is greater than the potential snowmelt ($M_T < S$). In this case, the water available for infiltration will be equal to the potential snowmelt. In the second case, the

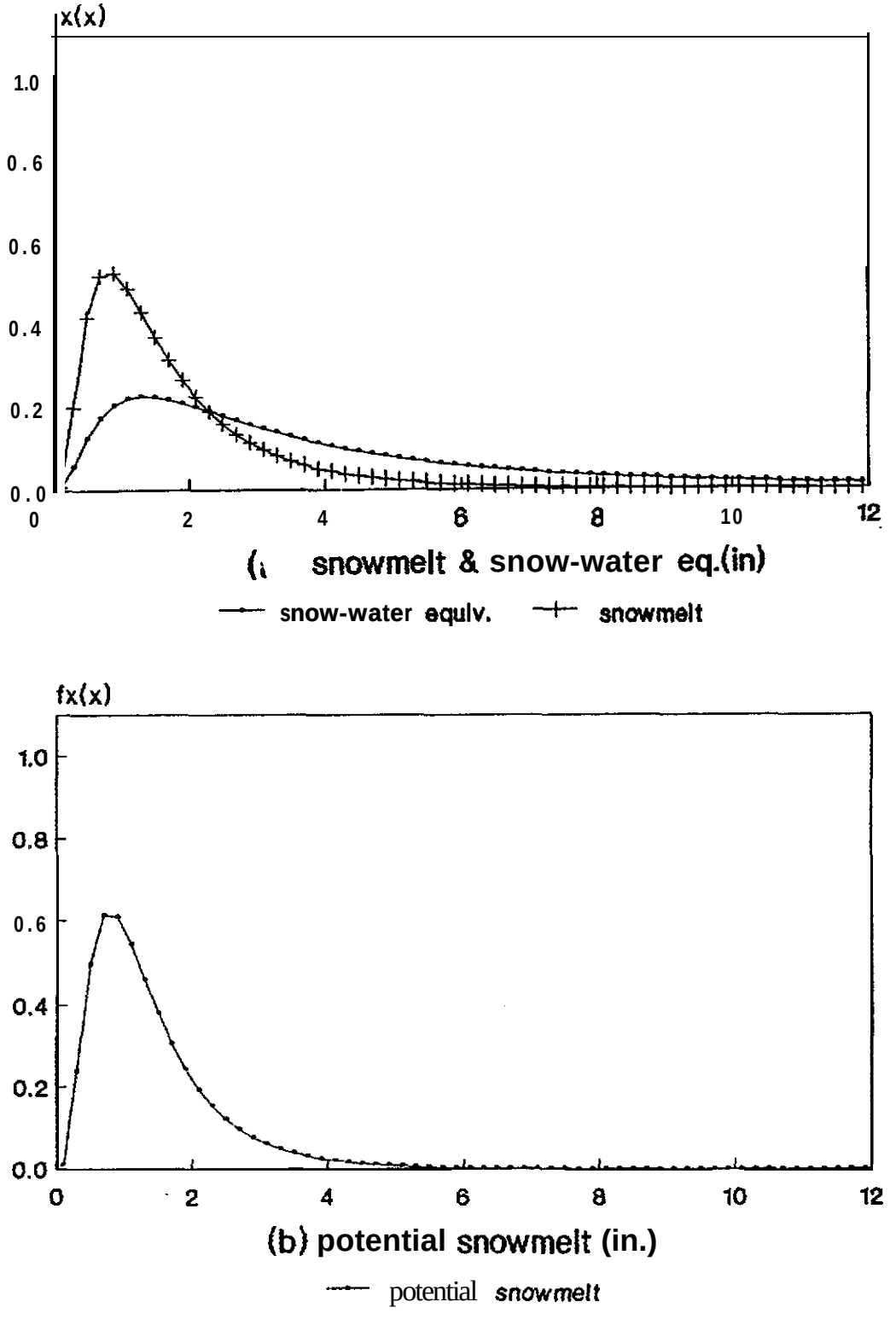

Figure C.3 Probability density function of (a) snowmelt and snow-water equivalent, (b) potential snowmelt.

snow-water equivalent is less than the potential snowmelt ($M_T < S$), and the actual melt in this case equals the snow-water equivalent. Both snow-water equivalent and potential snowmelt are random variables, and consequently so is the snowmelt. The distribution of snowmelt $f_M(m)$ is

$$f_M(m) = \int_{S=m}^{\infty} f(M_T = m, S)dS + \int_{M_T=m}^{\infty} f(M_T, S = m)dM_T \qquad (C.11)$$

The result of the integration is shown in Fig. C.3b; the mean value of available water for infiltration is 1.358 in, and the variance is 0.867 in^2

C.4 Total Amount of Infiltration

The water available for infiltration calculated with the snowmelt model is added to the precipitation to derive the distribution of total water for infiltration. The two possible events are rain-on-snow ($S > 0$), and rain-on-ground ($S = 0$). The probability density function of total infiltration I for all possible rain events is

$$f_I(i) = f(R = i \mid S = 0)\, P[S = 0] + f(M + R = i \mid S > 0)\, P[S > 0] \qquad (C.12)$$

The distribution of precipitation is given in section C.l and is shown in Fig. C.4a. The distribution of total water for infiltration (Eq. C.12) is computed numerically and the results are shown in Fig. C.4b The mean value of I is 6.5 in, and the variance is 8.5 in^2.

The variance of h_o/H can be computed from the variance of infiltration, I, and duration, D, as

$$\mathrm{Var}\left(\frac{h_o}{H}\right) = \left(\frac{\partial \frac{h_o}{H}}{\partial I}\right)^2 \mathrm{Var}(I) + \left(\frac{\partial \frac{h_o}{H}}{\partial D}\right)^2 \mathrm{Var}(D) + \left(\frac{\partial \frac{h_o}{H}}{\partial I}\right)\left(\frac{\partial \frac{h_o}{H}}{\partial D}\right) \mathrm{Cov}(I, D) \qquad (C.13)$$

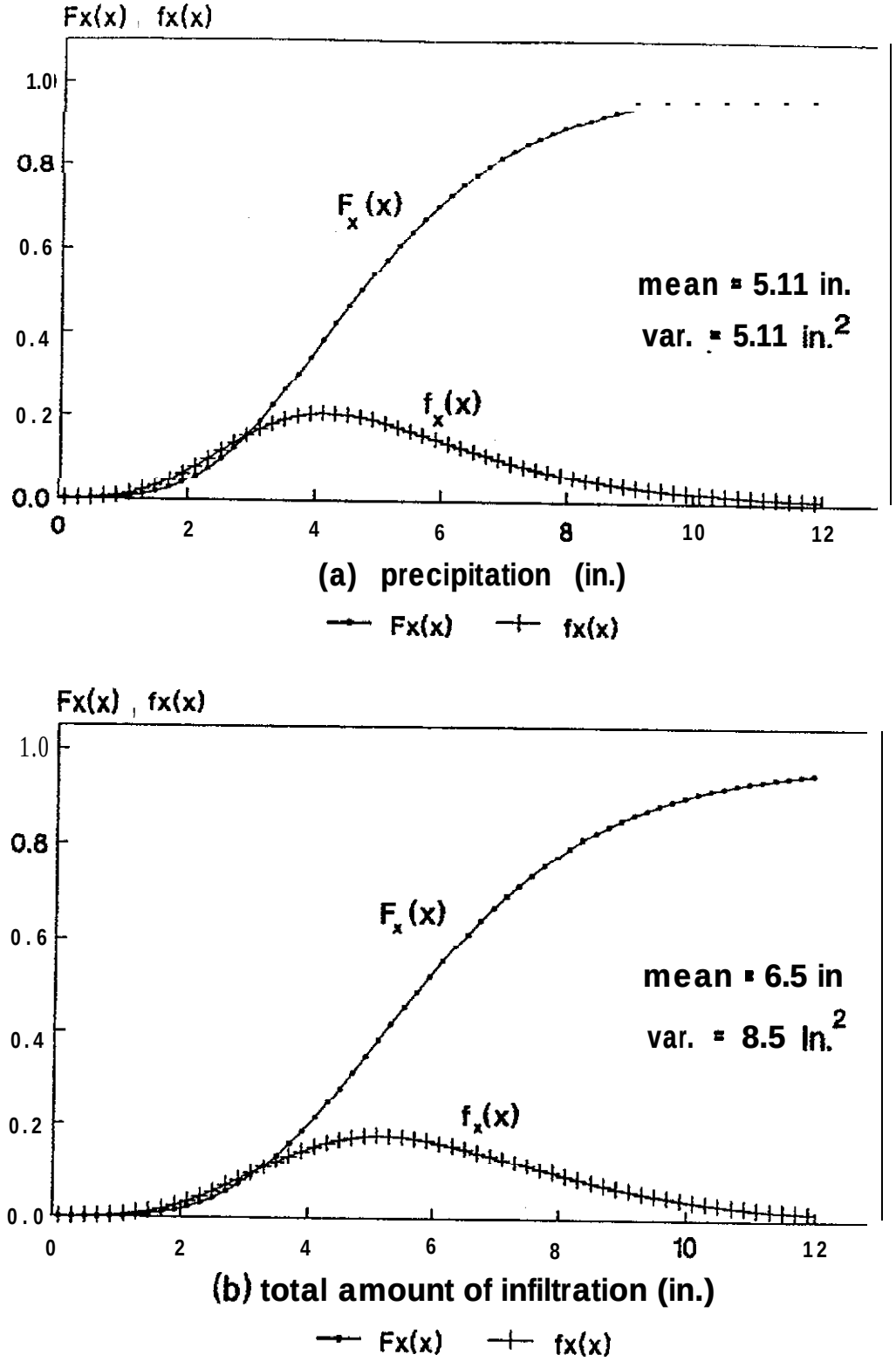

Figure C.4 Probability density function and distribution function of (a) storm precipitation, (b) total amount of water available for infiltration = snowmelt plus precipitation.

where $\frac{\partial \frac{h_o}{H}}{\partial i}$ and $\frac{\partial \frac{h_o}{H}}{\partial D}$ are the sensitivities of h_o/H to I and D. By using the lumped parameter model as described in Sec. 3.1 the sensitivities were evaluated in sections C.l, and C.2, and found to be 7.58x10-2 in^{-1} and $5.8x10^{-4}$ hr^{-1}.

The variance of I and D are 8.5 in^2 and 1296 hr^2, respectively. The covariance of I and D is 0.748. The variance of h_o/H because of storm characteristics and snowmelt is 0.0493. In fact, most of the variability of groundwater resulted from variability of the available amount of infiltration.

C.5 Effect of Sequence of Storms

Campbell (1975) reported that the amount of preceding rainfall is a limiting factor for debris flow initiation, he correlated antecedent rainfall of 10 inch with landslide occurrence in southern California. Wieczorek (1987) has shown that the threshold rainfall required to trigger debris flows in California is a function of the preceding rainfall. This preceding rainfall increases the moisture content in the soil mantle and is a major factor in the prediction of h_w. Both the coefficient of permeability K, and the suction, ψ, are functions of moisture content. The effect of antecedent moisture was evaluated by analyzing the results of a sequence of storms.

C5.1 Storm Sequence

Brunengo (1989) generated a sequence of long, continuous storms assuming independence between the dates of the sequence. First, the storm date was generated from normal distribution, which is the observed probability distribution function of storm date. The generation of storms for a season stopped when the last computed date was earlier than the previous one. The season was considered to have only one major storm if the second generated date was earlier than the first one. Using Monte Carlo simulation, the program was able to generate up to seven storms per season. Fig. C.5a shows the probability frequency function for number of storms per season.

The mean value of storm occurrence is two storms per season. The method of derived distribution (Ang and Tang, 1975) is used to investigate the characteristics of the interval between storms. For the case of a season with two storms, X and Y = the dates of first and second storms, respectively. The probability density function (pdf) of each storm is normal with mean = 120.4 days and standard deviation = 43.82 days (Brunengo, 1989). The joint distribution function for multivariate normal distribution of

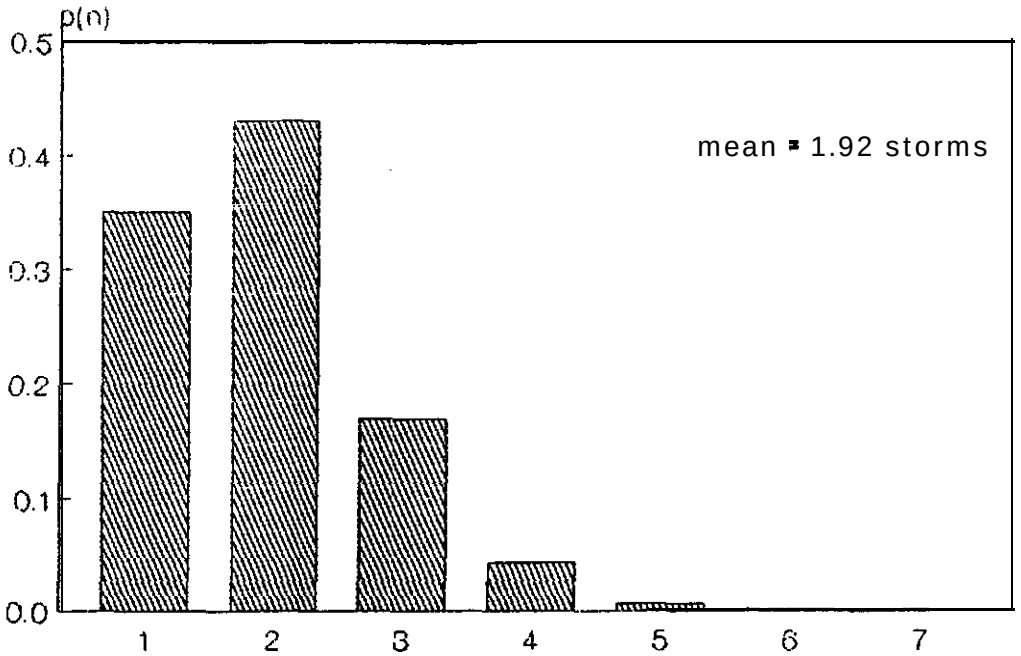

(a) number of storms per season

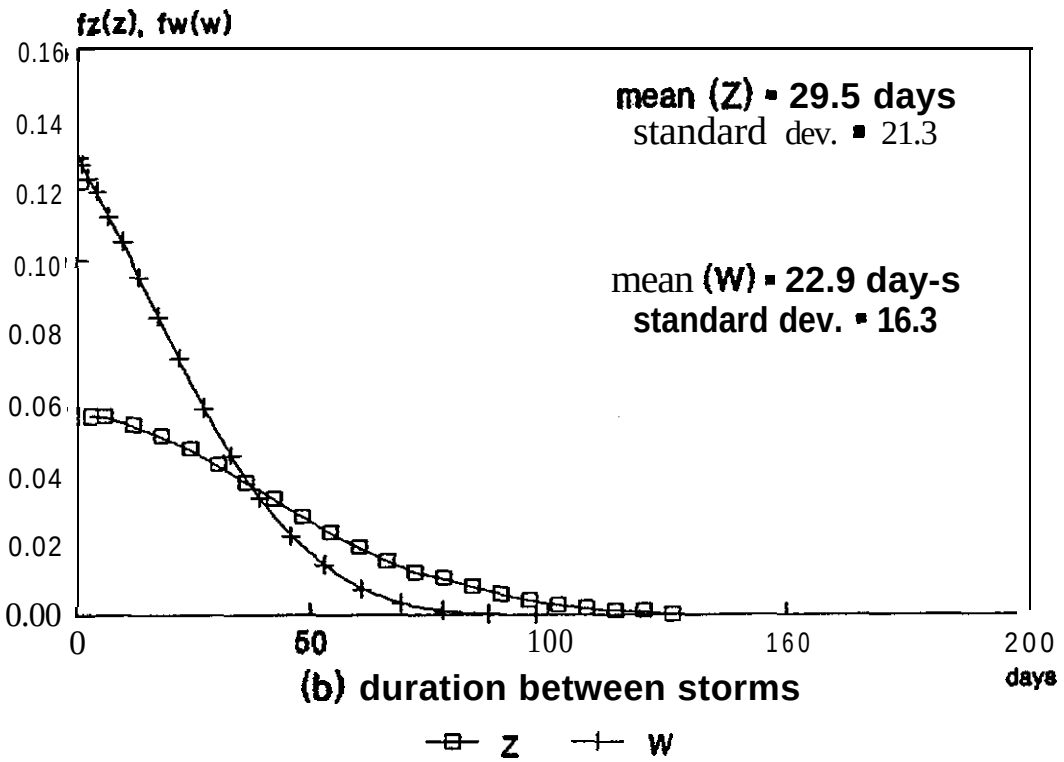

Figure C.5 Probability function of (a) number of storms per season, (b) duration between storms in a 2-storm season and between the last two storms in a 3-storm season.

two independent random variables with the same mean μ and the same standard deviation σ is :

$$f_{X,Y}(x,y) = \frac{-1}{2\pi\sigma^2} e^{\frac{-1}{2\sigma^2}\left((X-\mu)^2+(Y-\mu)^2\right)} \qquad \text{(C.14)}$$

The random variable Z, the time interval between two storms, is defined as:

$$Z = Y - x, \quad Y>X \qquad \text{(C.15)}$$

The probability distribution function of Z is

$$F_Z = \iint_R f_{X,Y}(x,y)dx\,dy = \int_{X=0}^{X=\infty}\int_{Y=x}^{Y=z+x} f_{X,Y}(x,y)dx\,dy \qquad \text{(C.16)}$$

Fig. C.5b shows the probability density function from Eq. C.16. The mean of the period between two storms is 29.5 days and the standard deviation is 21.3 days.

For a season with three storms, the previous procedure is used to derive the distribution of the period between the last two storms. A new random variable V is defined as the date of the third storm. The random variable W is the period between the second and the third storms. The pdf of V is normal, with the same mean and standard deviation as X and Y. The joint distribution function for the multivariate normal distribution for three independent random variables with the same mean μ and the same standard deviation σ is

$$f_{X,Y,V}(x,y,v) = \frac{-1}{\sqrt{2^3}\,\pi\sigma^2} e^{\frac{-1}{2\sigma^2}\left((X-\mu)^2+(Y-\mu)^2+(V-\mu)^2\right)} \qquad \text{(C.17)}$$

The random variable W, the period between the last two storms, is defined as

$$w = v - Y, \quad V > Y > X \qquad \text{(C.18)}$$

The probability distribution function of W is

$$F_w = \iiint_R f_{X,Y,V}(x,y,v)dx\ dy\,dv = \int_{X=0}^{X=\infty}\int_{Y=x}^{Y=\infty}\int_{V=y}^{V=w+y} f_{X,Y,V}(x,y,v)dx\,dy\,dv \qquad (C.19)$$

Fig. C.5b shows the probability density function from Eq. C.19. The mean of the period between the last two storms is 22.96 days with a standard deviation of 16.35 days.

C.5.2 Variation of Groundwater Due to the Sequence of Storms

The variation of h_w due to the sequence of storms consists of two parts. The first source of variation is the number of storm per season: the storm under consideration can be the only storm in a season, one storm in a season with two storms, etc. The mean antecedent moisture condition varies according to the number of storms per season and so does h_w. The second part is the effect of the variation of the time interval between storms. The variances of Z and W will affect the initial moisture conditions and consequently the h_w. In the next two sections, the two sources of variation will be discussed and the variation in h_w will be evaluated. The variability as a result of the time interval between storms will be assumed to be independent of the variability due to number of storms per season, although it is recognized that the time interval between storms is correlated to the number of storms.

C.5.2.1 Effect of Number of Storms per Season

Computations with the Reddi model were made for seasons with 1 - 4 long, continuous storms. For the computation of the mean values of h, the mean values of the input parameters for each category of storm number should be used.

In addition to the long, continuous storms, whose characteristics are described in C.l, C.2, and C5.1, we should consider small rain events that are not classified as long, continuous storms. Table C.l, (Brunengo 1989), shows the number of days with precipitation greater than specific values. It is clear that during the rain seaon

Table C.l

Precipitation data, Brunengo (1989)

Station	Annual Mean	September - Mav	Number days of predipitation		
			> 0.1"	>0.50"	>1.0"
Stampede Pass	92.57	84.32	148	65	29
Palmer	94.09	83.62	158	70	26
Cedar Lake	102.41	91.74	155	76	32

Appendix D

DISTRIBUTION OF EXTREME STORMS

Brunengo (1989) used the extreme-value distribution to describe the distribution of precipitation in the form of recurrence interval or exceedance probability (Eq. C.1). However, the largest storm to occur in a given period is a random variable with statistics related to the distribution of the initial variant (extreme value distribution). Let X be the amount of precipitation with the extreme value distribution given by Eq. C.l and let Y_n be:

$$Y_n = \max(X_1, X_2, \ldots, X_n) \tag{D.1}$$

where $X_1 \ldots . X_n$ are random samples. The cumulative distribution of X_n given by Ang and Tang (1984) is:

$$F_{Y_n}(y) = P(Y_n \le y) = (F_x(y))^n \tag{D.2}$$

The corresponding probability density function for Y_n is:

$$f_{Y_n}(y) = \frac{\partial F_{Y_n}(y)}{\partial y} = n\, F_x(y)^{n-1} f_x(y) \tag{D.3}$$

This means that the function $F_{Y_n}(y)$, $f_{Y_n}(y)$ will shift to the right with increasing n. The distribution of Y_n is generally difficult to obtain in analytical form. The usefulness of extreme value statistics is greatly enhanced by the theory of asymptotic extremal distribution. The analytical derivation of the appropriate extremal distribution, given the distribution of the initial variant, is facilitated by Cramer's (1946) method. Define the transformed random variable

$$\varsigma_n = n(1 - F_x(y_n)) = g(y) \tag{D.4}$$

then

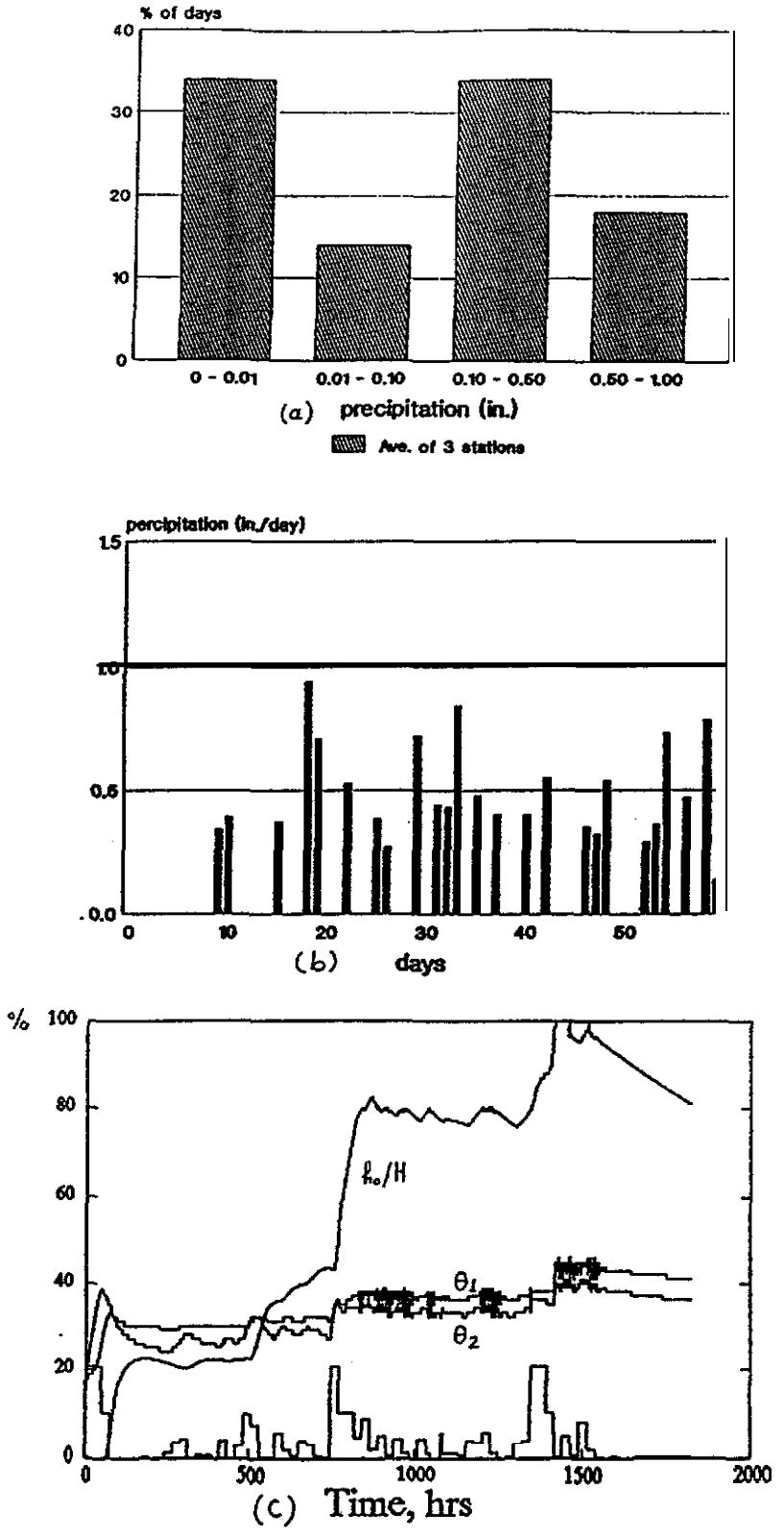

Figure C.6 (a) Frequency function of days with a given range in precipitation, (b) simulated small rain events, (c) h_0/H, θ_1, θ_2 for a sequence of storms

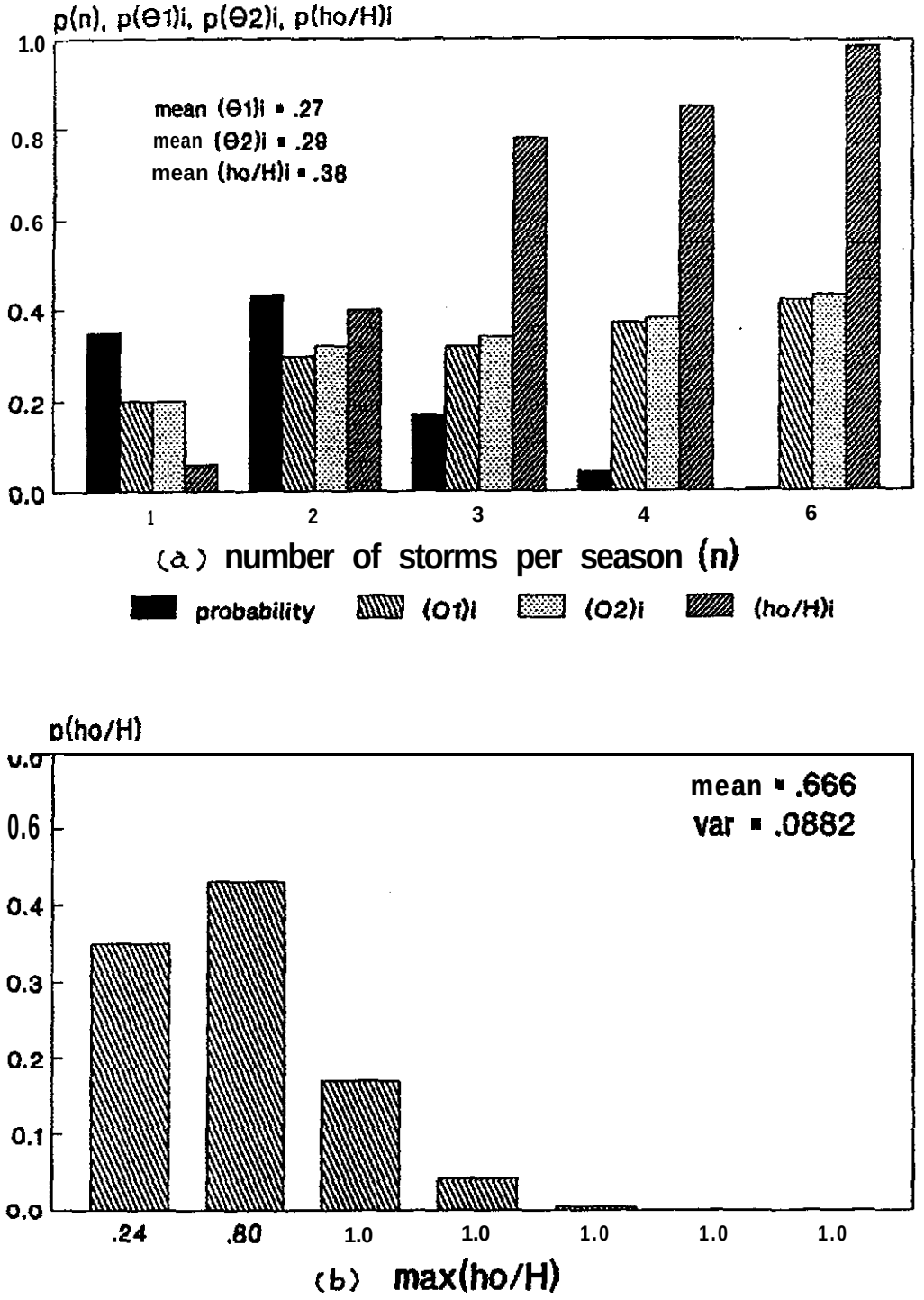

Figure C.7 (a) Initial moisture conditions for different number of storms, (b) frequency of h_o/H for different number of storms

C.5.2.2 Effect of the Time Interval Between Storms

In the above calculations mean values of θ_i and h_{oi}, for a given number of long, continuous storms per season, were used to calculate $P(h_O/H)$. It should be noted that even for a given number of storms per season, θ_i, hoi are random variables, depending on the time interval between storms. The interval between the storms affects hoi. To account for this, the FOSM procedure was used to calculate the variance of ho/H as a function of the variance of Z, W, etc. The time interval Z affects the initial moisture, which in turn affects ho/I-h

$$\mathrm{Var}(\theta_i) = \left(\frac{\partial \theta_i}{\partial Z}\right)^2 \mathrm{Var}(Z) \qquad \text{(C.20)}$$

$$\mathrm{Var}(h_{oi}) = \left(\frac{\partial h_{oi}}{\partial Z}\right)^2 \mathrm{Var}(Z) \qquad \text{(C.21)}$$

The derivative of θ_i and h_{oi} with respect to Z was derived from the relation between moisture parameters and time after the end of the first storm. For simplicity, only long, continuous storms were considered (Fig. C.8a). The procedure was repeated for different numbers of storms per season (Fig. C.9). Var(Z) was evaluated from Eq. C.16, then

$$\mathrm{Var}\left(\frac{h_o}{H}\right) = \left(\frac{\partial \frac{h_o}{H}}{\partial \theta_i}\right)^2 \mathrm{Var}(\theta_i) \qquad \text{(C.22)}$$

$$\mathrm{Var}\left(\frac{h_o}{H}\right) = \left(\frac{\partial \frac{h_o}{H}}{\partial h_{oi}}\right)^2 \mathrm{Var}(h_{oi}) \qquad \text{(C.23)}$$

The derivatives of ho/H with respect to θ_i and h_{oi} were computed from the sensitivity of ho/H to the initial moisture conditions (Fig C.10).

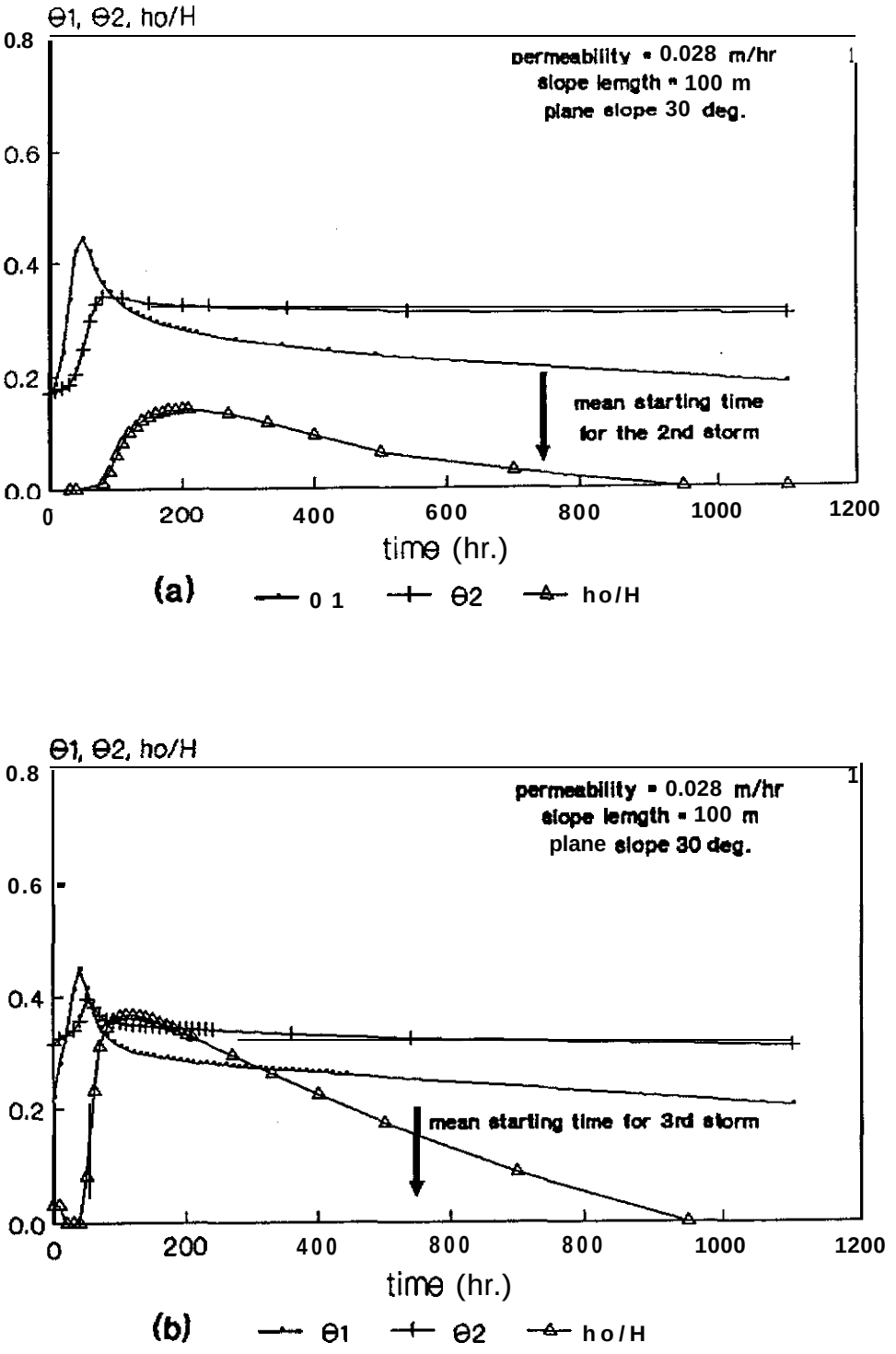

Figure C.8 Groundwater for l-storm season and Z-storm season. Moisture content and ho/H vs. time for (a) l-storm, and (b) 2-storms

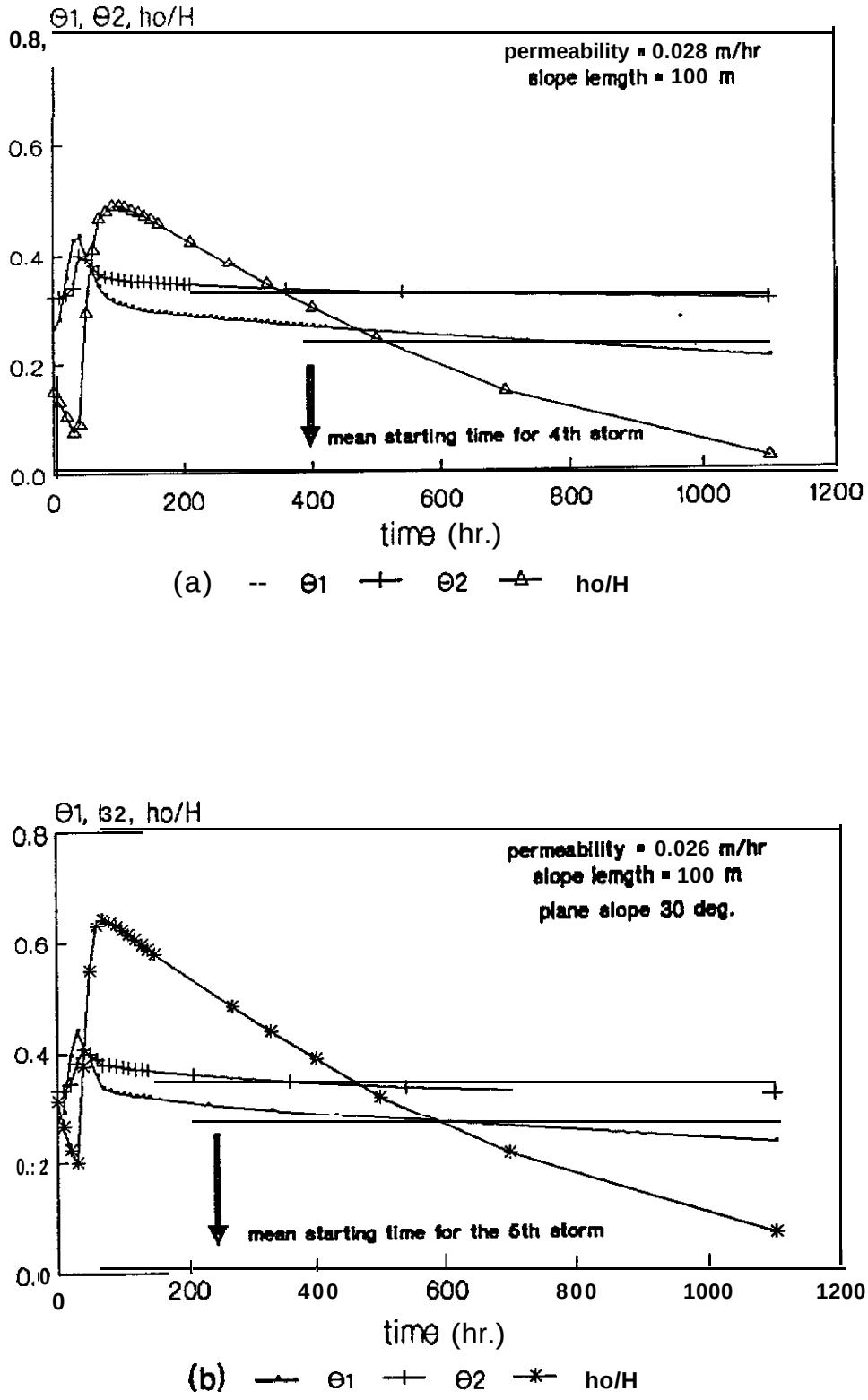

Figure C.9 Groundwater for 3-storm season and 4-storm season. Moisture content and h_o/H vs. time for (a) 3-storm, and (b) 4-storms

The variance of ho/H due to the variation of the time interval between storms was found to be 2 $\times 10^{-5}$. This is very small compared to the variance due to number of storms per season (.0279). It should be noted that θ_i and h_{oi} are correlated as it appears from Fig. C.8, and C.9. The number of storms and the time interval between storms are also correlated. The effect of the correlation may be ignored, because of the small variance due to variation of the time interval between storms.

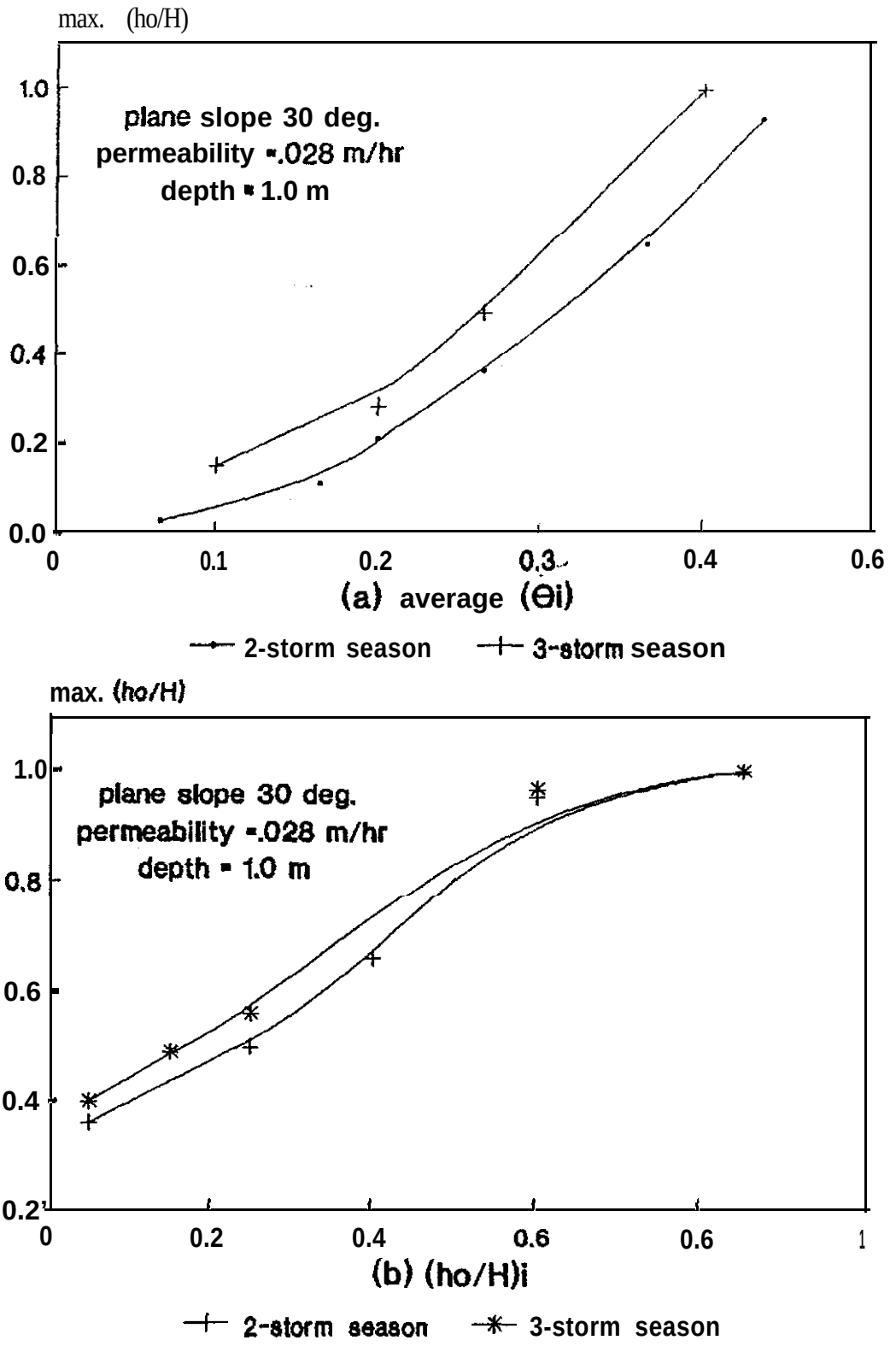

Figure C.10 Effect of initial moisture conditions on ground water for 2-storm and 3-storm seasons (a) average $(\theta)_i$, and (b) $\left(\frac{h_o}{H}\right)_i$

Appendix D

DISTRIBUTION OF EXTREME STORMS

Brunengo (1989) used the extreme-value distribution to describe the distribution of precipitation in the form of recurrence interval or exceedance probability (Eq. C.1). However, the largest storm to occur in a given period is a random variable with statistics related to the distribution of the initial variant (extreme value distribution). Let X be the amount of precipitation with the extreme value distribution given by Eq. C.l and let Y_n be:

$$Y_n = \max(X_1, X_2, \ldots, X_n) \tag{D.1}$$

where $X_1 \ldots . X_n$ are random samples. The cumulative distribution of X_n given by Ang and Tang (1984) is:

$$F_{Y_n}(y) = P(Y_n \le y) = (F_x(y))^n \tag{D.2}$$

The corresponding probability density function for Y_n is:

$$f_{Y_n}(y) = \frac{\partial F_{Y_n}(y)}{\partial y} = n\, F_x(y)^{n-1} f_x(y) \tag{D.3}$$

This means that the function $F_{Y_n}(y)$, $f_{Y_n}(y)$ will shift to the right with increasing n. The distribution of Y_n is generally difficult to obtain in analytical form. The usefulness of extreme value statistics is greatly enhanced by the theory of asymptotic extremal distribution. The analytical derivation of the appropriate extremal distribution, given the distribution of the initial variant, is facilitated by Cramer's (1946) method. Define the transformed random variable

$$\varsigma_n = n(1 - F_x(y_n)) = g(y) \tag{D.4}$$

then

$$F_{\varsigma_n}(\varsigma) = 1 - \left(1 - \frac{\varsigma}{n}\right)^n \tag{D.5}$$

As $n \to \infty$ we have

$$F_{\varsigma_n}(\varsigma) = 1 - e^{-\varsigma} \tag{D.6}$$

and the corresponding asymptotic probability density function is

$$f_{\varsigma_n}(\varsigma) = e^{-\varsigma} \tag{D.7}$$

Inverting Eq. D.4 for Y_n we have

$$Y_n = F_x^{-1}\left(1 - \frac{\varsigma_n}{n}\right) \tag{D.8}$$

Hence the cumulative distribution function Y_n can be obtained from that of ς_n as:

$$F_{Y_n} = \exp(-g(y)) \tag{D.9}$$

where g(y) is the right-hand side of Eq. D.4. The probability density function of Y_n is

$$f_{Y_n} = -\frac{\partial g(y)}{\partial y}\exp(-g(y)) \tag{D.10}$$

Applying this method to the distribution of the amount of precipitation given by Eq. C.1,

$$g(y) = n[1\text{-}\exp\{-\exp(-a(y_n - u))\}] \tag{D.11}$$

Then

$$F_{Y_n} = \exp\{-n\{1\text{-}\exp(-\exp(-a(Y_n - u)))\}] \tag{D.12}$$

and

$$f_{Y_n} = a\, n \exp\left[-n\left\{1-\exp\left(-\exp\left(-a\left(y_n - u\right)\right)\right)\right\}\right]$$

Random spatial variations introduce errors in the predicted h_w/H.

The plots of the pdfs and cdfs of Y_n are shown in Fig. D.l and D.2 for different values of n. A computer program using numerical integration was developed to compute the mean and the variance of asymptotic distributions shown in Fig. D.2. The results of integrations are listed in Table D.l for different values of n. It is clear that the variance does not change very much while the expected value of precipitation increases as n increases.

Table D.l

Means and variances of amount of precipitation

n (years)	Mean	Variance
5	7.72 in	6.94 in^2
10	9.11 in	5.68 in^2
20	10.4 in	5.46 in^2
50	12.08 in	5.35 in^2
100	13.33 in	5.32 in*
500	16.20 in	5.31 in*

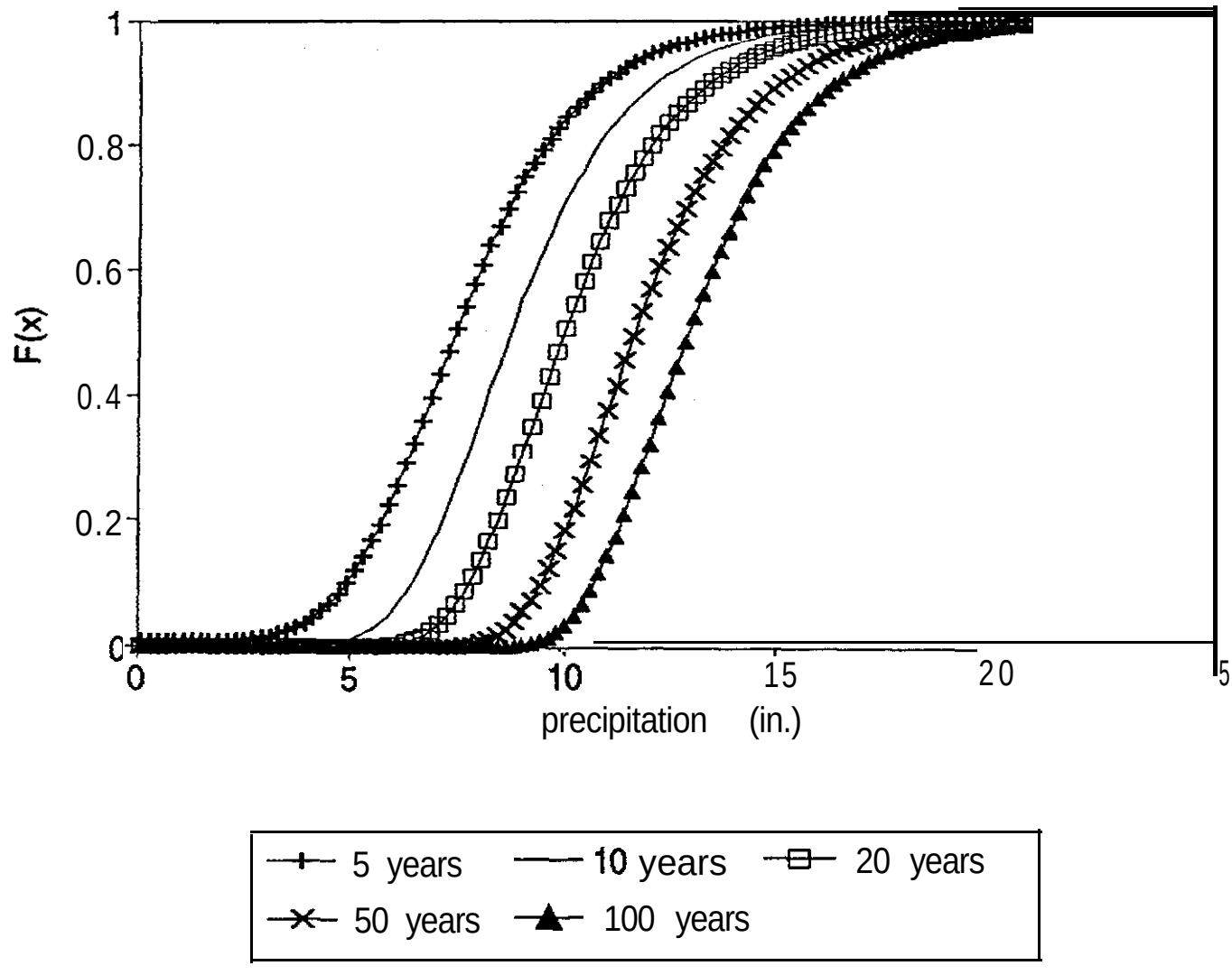

Figure D.l Asymptotic probability distribution function

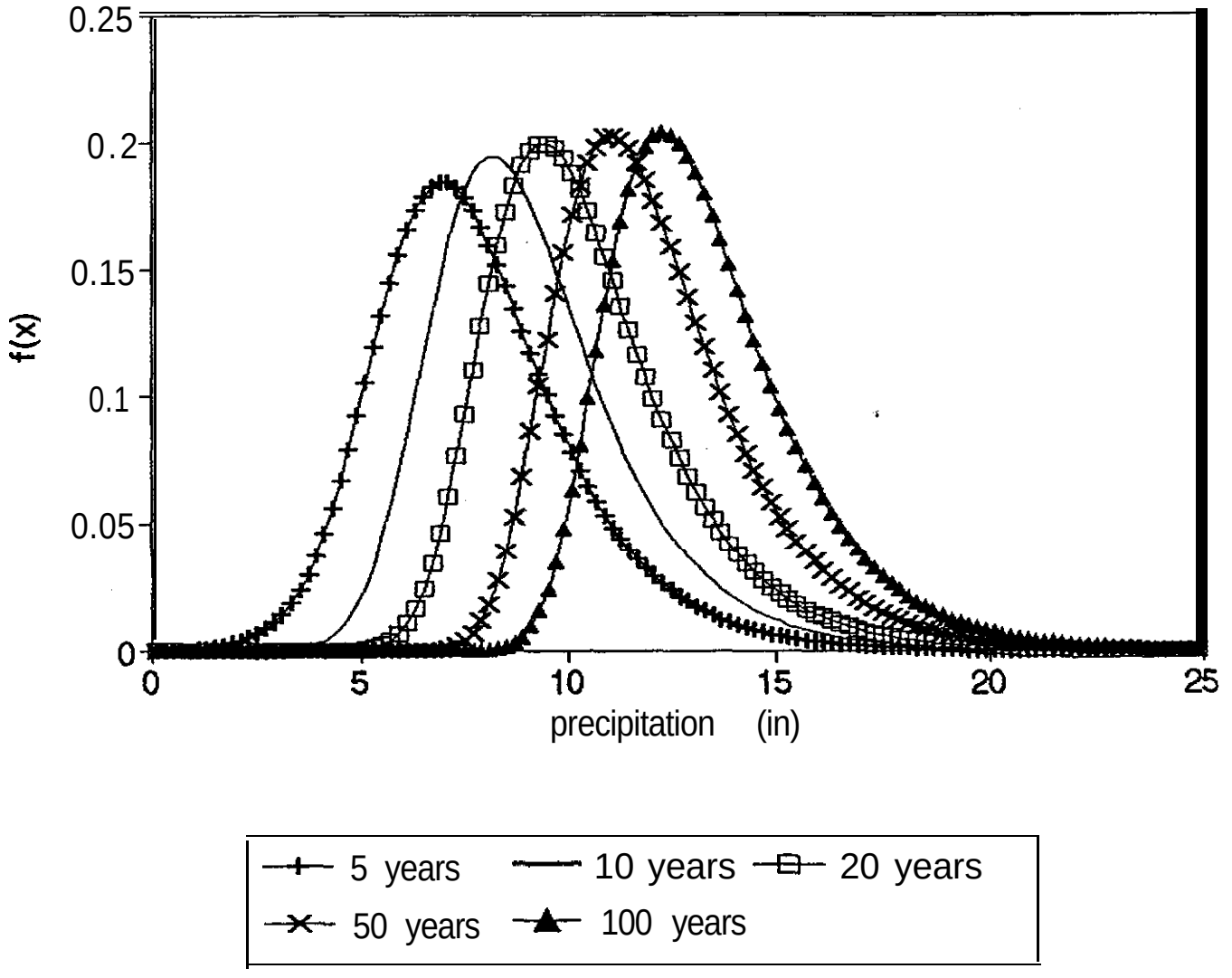

Figure D.2 Asymptotic probability density function

APPENDIX E

REFERENCES

Ang, A.H-S. and Tang, W.H. (1980) Probability Concepts in Engineering Planning and Design, John Wiley and Sons, New York.

Baligh, M. M., and Azzouz, AS. (1975) End effects on stability of cohesive slopes. Journal Geotechnical Division, ASCE, 101:1105- 1117.

Benosky, C.P. (1992) Spatial analysis techniques for the automated extraction of watershed characteristics. MS Thesis, Ohio State University, Columbus, OH.

Berris, S. N., and Harr, R.D. (1987) Comparative snow accumulation and melt during rainfall in forests and clear-cut plots in the western Cascades of Oregon. Water Resources Research, 23 (1): 135-141

Beven,K. (1981) Kinematic subsurface stormflow. Water Resources Research, 17:1419-1424.

Black, T. A. (1979) Evapotranspiration from Douglas fir stands exposed to soil water deficits. Water Resource. Res., 15, 164-170

Brunengo, M.J. (1989) Output data on precipitation, snow and storm weather, west central Cascade Range, Washington.

Box, G.E.P., and Jenkins, G.M. (1976) Time Series Analysis, Holder-Day, Oakland.

Campbell, R.H., (1975) Soil slips, debris flows, and rainstorms in the Santa Monica Mountains and vicinity, southern California, U.S. Geol. Survey Prof. Paper 851, 51 p.

Clapp, R. B., and Homberger, G. M. (1978) Emperical Equations for some soil hydraulic properties. Water Resource. Res., 14(4), 601-604.

Coffin B.A., and RD. Harr, (1992) Effects of forest cover on volume of water delivery to soil during rain-on-snow: final report, Project SH-1, submitted to CMER/SHAMW Committee, 118 p.

Cramer, H. (1946) Mathematical Methods of Statistics, Princeton Univ. Press, Princeton, NJ.

Cornell, C.A. (1971) First-order uncertainty analysis of soil deformation and stability. Proc. First International Conference on Applications of Statics and Probability to Soil and Structural Engineering, Hong Kong, 129-144.

Eagleson, P.S. (1978) Climate, soil, vegetation, Parts 3 and 4. Water Resources Research, 14:731-739, 741-748.

Einstein, H. (1988) Landslide risk assessment procedure. Fifth International Symposium on Landslides, Lausanne.

Freeze, R.A. (1971) Three-dimensional, transient, saturated-unsaturated flow in a groundwater basin. Water Resources Research, 7: 347-366.

Freeze, R.A. (1980) A stochastic conceptual analysis of rainfall-runoff processes on a hillslope. Water Resources Research, 16:391-408.

Green, W.H., and Ampt, G.A. (1911) Studies on soil physics: I. Flow of air and water through soils. Journal of Agricultural Science, 4: l-24.

Hachich, W., and Vanmarcke, E.H. (1983) Probabilistic updating of porepressure fields, Journal Geotechnical Engineering, 109 (12):373-387.

Hammond, C., Hall, D., Miller, S., and Swetik, Pl (1991) Level 1 stability analysis (LISA) General Tech. Rep. INT-000 Intermountain Research Sta., Forest Service, USDA, Moscow, ID.

Hoek, E., and Bray, J.W. (1981) Rock Slope Engineering. Institution of Mining and Metallurgy, London.

Huitt, J.L., (1956) Fluid flow in simulated fracture. Journal American Institute of Chemical Engineering, 2:259-264.

Jenson, S.K., and, Dominique, J.O. (1988) Extracting topographic structure from digital elevation model data for Geographic Information System analysis. Photogrammetric Engineering and Remote Sensing, Vol. 54, pp. 1593 - 1600

Johnson, K.A, and Sitar, N. (1989) Significance of transient porepressures and local slope conditions in debris flow initiation. Proc. 12 th International Conference Soil Mechanics and Foundations 3: X19-1622

Lee, I-M (1986) A probabilistic prediction of porewater conditions for unsteady groundwater flow on a sloping bed. Ph.D. Dissertation, Ohio State Univ. Columbus, OH.

Louis, C. (1969) A study of groundwater flow in jointed rock and its influence on the stability of rock masses. Doctorate Thesis, Univ. of Karlsruhe (in German), Rock Mechanics Research Report No. 10, Imperial College (English translation), 90p.

Lumb, P.(1975) Slope failures in Hong Kong. Quarterly Journal of Engineering Geology, 8:31-65.

Marks, D., Dozier, J., and Frew, J. (1984) Automated Basin Delineation from Digital Elevation Data Geo-Processing, Vol. 2, pp. 299 - 311.

O'Loughlin,E.M. (1986) Prediction of surface saturation zones in natural catchments by topographic analysis. Water Resources Research, 22:794-804.

Pierson,T.C. (1977) Factors controlling debris-flow initiation on forested hillslope in the Oregon Coast Range. Ph.D. Dissertation, Univ. of Washington, Seattle, WA.

Reddi, L.N. (1988) Probabilistic analysis of groundwater in hillside slopes, Ph.D. Dissertation, Ohio State Univ., Columbus, OH.

Reddi, L.N., and Wu. T.H. (1991) Probability analysis of groundwater levels in hillside slopes. J. Geotechnical Engineering, ASCE, 117:872-890.

Richards, L.A. (1931) Capillary conduction of liquids through porous mediums. Physics, 1:318-333.

Schroeder, W. L. (1983) Geotechnical properties of southeast Alaskan forest soils. USDA Forest Service Report, Civ. Engr. Dept., Oregon State University, Corvallis, Ore., Dec.

Sitar, N., Cawfield, J.D., and der Kiureghian, A. (1987) First-order reliability approach to stochastic analysis of subsurface flow and contaminant transport. Water Resources Research, 23 (5):794-804.

Sloan, P.G., and Moore, I.D.(1984) Modeling subsurface storm-flow on steeply sloping forested watersheds. Water Resources Research, 20: 1815-1822.

Soil Conservation Service (1987) Soil survey of Lewis County area, Washington. U.S. Dept. of Agriculture.

Tang, W.H., Yucemen, MS., and Ang, A.H-S.(1976) Probability based short term stability of slopes. Canadian Geotechnical Journal, 13 (3): 201-215.

Taylor, D.W. (1948) Fundamentals of Soil Mechanics, John Wiley and Sons, New York.

U.S. Army Corps of Engineers (1956) Snow Hydrology: Summary report of the snow investigations. North Pacific Div. Corps of Engineers, Portland, OR, 437p.

Vanmarcke, E.H. (1983) Random Fields. The MIT Press, 382 p..

Wiberg, E.J. (1990) The probability distribution of snowmelt in clearcuts from a rain-on-snow event in the central Cascades of Washington. M.S. Thesis, Ohio State Univ., Columbus, OH.

Wieczorek, G. F., (1987) Effect of rainfall intensity and duration on debris flows in central Santa Cruz Mountains, California. Geological Society of America, Reviews in Engineering Geology, Vol. VII.

Wilson, J., Kitanidis, P., and Dettinger, M. (1978) State and parameter estimation in groundwater models. in Application of Kalman Filter to Hydrology, Hydraulics and Water Resources, ed. C.L. Chiu. Univ. of Pittsburgh, p. 657-679.

Wilson, R. C. (1989) Rainstorms, pore pressures, and debris flows: a theoretical framework. Inland Geological Society Vol. 2:101-117

Wu, T.H., and Swanston, D.N.(1980) Risk of landslides in shallow soils and its relation to clearcutting in Southeastern Alaska. Forest Science, 26: 495-510.

Wu, T.H. (1989) Variability of geological materials, in The Art and Science of Geotechnical Engineering, E.J. Cording, W.J. Hall, J.D. Haltiwanger, A.L. Hendron Jr., G. Mesri, ed. Prentice Hall, Englewood Cliffs, NJ. 221-239.

Wu, T.H., Potter, J.C., and Kjekstad, 0. (1986) Site exploration for offshore structures. Journal Geotechnical Engineering, 112 (11):981-1000.

Wu, T. H., and, Merry C. J., (1992) Landslide Hazard Mapping, Part 2: Prediction of landslide hazard. Proposal to Timber /Fish / Wildlife. Coop. Monitoring, Elevation, and Research Committee (CMER).

APPENDIX F

NOTATIONS

a,b = dimensions
B = unsaturated flow parameter
C = storage coefficient
E(.) = expected value = mean
F = commutative distribution function
f = probability density function
H = soil thickness
H_s = soil thicknesses for the 2-D model
h_c = critical depth of groundwater
h_o = depth of groundwater at exit
h_w = depth of groundwater at a point
i = infiltration rate (L/T)
I = total amount of infiltration = snowmelt + rain
I_g = hydraulic gradient
K = coefficient of permeability
K_s = coefficient of permeability at saturation.
L = slope length
M =snowmelt
MT = potential snowmelt
N = model error
P(.)= probability
p = probability mass function
Q_f = recharge through fracture
Q_r = rainfall recharge
R = rainfall (L)
S = snow-water equivalent (L)
T_a = air temperature
t_o = return period
t = time
a = slope angle
α_e = evapotranspiration coefficient
β = catchment closing angle
θ = volumetric water content
θ_d = drainable volumetric water content
θ_s = saturated volumetric water content
γ = transverse slope angle
η = kinematic viscosity
ψ = suction
ψ_s = suction at saturation
Ω (.) = coefficient of variation.
σ = standard deviation.